Dist: A

AD-A284 171

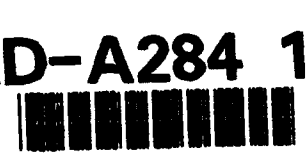

ATION PAGE

Form Approved
OMB No. 0704 0188

average 1 hour per response, including the time for reviewing instructions, searching existing data sources g the collection of information. Send comments regarding this burden estimate or any other aspect of this to Washington Headquarters Services, Directorate for information Operations and Reports, 1215 Jefferson Management and Budget, Paperwork Reduction Project (0704-0188), Washington, DC 20503

1. AGENCY USE ONLY (Leave blank)	2. REPORT DATE	3. REPORT TYPE AND DATES COVERED
		ANNUAL 15 Feb 93 TO 14 Feb 94

4. TITLE AND SUBTITLE

ELECTROCHEMICAL AND SPECTROSCOPY STUDIES OF SELECTED INORGANIC AND ORGANIC SYSTEMS IN MOLTEN HALIDES

5. FUNDING NUMBERS

F49620-93-1-0129
61102F
2303/AS

6. AUTHOR(S)

Dr Gleb Mamantov

7. PERFORMING ORGANIZATION NAME(S) AND ADDRESS(ES)

Dept of Chemistry
Univ of Tennessee
552 Buehler Hall
Knoxville, TN 37996-1600

8. PERFORMING ORGANIZATION REPORT NUMBER

AFOSR-TR- 94 0496

9. SPONSORING/MONITORING AGENCY NAME(S) AND ADDRESS(ES)

AFOSR/NL
110 DUNCAN AVE SUITE B115
BOLLING AFB DC 20332-0001

Maj Ersfeld

DTIC ELECTE SEP 07 1994 F

10. SPONSORING/MONITORING AGENCY REPORT NUMBER

11. SUPPLEMENTARY NOTES

12a. DISTRIBUTION/AVAILABILITY STATEMENT

Approved for public release;
distribution unlimited.

A

12b. DISTRIBUTION CODE

13. ABSTRACT *(Maximum 200 words)*

The research during the past year has concentrated on the photochemistry of anthracene and 9-methylanthracene in molten aluminum chloride-1-ethyl-3-methylimidazolium chloride (AlCl3/EMIC), looking in particular for photoinduced electron transfer reactions. Several such reactions have been found. Experiments demonstrate that this chemistry was initiated by electron transfer from the excited state of 9-methylanthracene to EMI+. The difference in behavior of anthracene and 9-methylanthracene in the basic melt can be attributed to the difference in the rate of electron transfer to EMI+: for anthracene, the electron transfer is endothermic and slow, while for 9-methylanthracene, the electron transfer is exothermic and fast. Irradiation of anthracene in oxygenated basic medium afforded several products including 9-chloranthracene. Although the formation of 9-chloranthracene can be envisioned to arise by electron transfer from the excited state of anthracene to O2, additional work will be required to prove that this assumption is correct.

14. SUBJECT TERMS

DTIC QUALITY INSPECTED 3

15. NUMBER OF PAGES

16. PRICE CODE

17. SECURITY CLASSIFICATION OF REPORT	18. SECURITY CLASSIFICATION OF THIS PAGE	19. SECURITY CLASSIFICATION OF ABSTRACT	20. LIMITATION OF ABSTRACT
(U)	(U)	(U)	

AFOSR GRANT F49620-93-1-0129

ELECTROCHEMICAL AND SPECTROSCOPIC STUDIES

of

SELECTED INORGANIC AND ORGANIC SYSTEMS IN MOLTEN HALIDES

The Department of Chemistry
University of Tennessee
Knoxville, TN 37996-1600

Technical Report for the First Year
(2/15/93 - 2/14/94)

Accesion For
NTIS CRA&I
DTIC TAB
Unannounced
Justification
By
Distribution /
Availability Codes
Dist | Avail and / or Special
A-1

Gleb Mamantov
Principal Investigator
June 15, 1994

4398 94-28983

DTIC QUALITY INSPECTED 3

94 9 06 055

21 JUN 1994

Introduction

This program involves several aspects of chemistry, electrochemistry, photochemistry, and spectroscopy of selected systems in molten halides. This report summarizes the research performed during the first year of the program. The following personnel were involved in this program during this period.

1. Professor Gleb Mamantov, principal investigator.
2. Professor Richard M. Pagni, coprincipal investigator
3. Dr. Guang-Sen Chen, postdoctoral research associate, supported by this program during the period 2/15/93 - 7/20/93.
4. Dr. Haiming Xiao, postdoctoral research associate, supported by this program during the period 11/10/93 - present.
5. Dr. Yvette Yang, part-time postdoctoral research associate, supported by this program during the period 2//15/93 - present.
6. Dr. Anna Edwards, part-time postdoctoral research associate, not supported by this program.
7. Ellen Hondrogiannis, Ph.D. student, not supported by this program.
8. Carlos Lee, Ph.D. student, partially supported by this program.
9. Sven Eklund, Ph.D. student, not supported by this program.
10. George Hondrogiannis, Ph.D. Student, partially supported by this program.

The status of projects investigated under this program is summarized below.

Results

1. Purification of Alkali Haloaluminate Melts.

Oxide impurities in molten chloroaluminates may have pronounced effects on the behavior of other solute species in these media. This problem is particularly serious for basic ($AlCl_3$/NaCl mole ratio < 1) alkali chloroaluminates containing refractory metal solute species such as Nb(V), Ta(V), and W(V). We have previously reported on the removal of oxide

impurities from $AlCl_3$-NaCl melts saturated with NaCl using phosgene(1). Phosgene, however, is a poisonous gas and must be handled with extreme caution. We have now been able to achieve complete conversion of oxide impurities to chlorides by treating the melt with carbon tetrachloride (2, Appendix 1). This procedure is also applicable to acidic alkali chloroaluminates and fluorochloroaluminates, such as the $NaAlCl_4$-NaF (90-10 mole%) melt.

2. Electrochemical and Spectroscopic Studies of Refractory Metal Species in Basic Alkali Haloaluminates.

Using haloaluminate melts purified with CCl_4, we have investigated the electrochemistry of tantalum in $AlCl_3$-$NaCl_{sat}$ and $NaAlCl_4$-NaF (90-10 mole %) melts in the temperature range 200-450°C (3, Appendix 2). We have also conducted spectroscopic and electrochemical studies of tungsten(VI) and tungsten(V) chloride and oxychloride complexes in the $AlCl_3$-$NaCl_{sat}$ melt at 175° (4, Appendix 3) and have reinvestigated the electrochemistry of niobium(V) in the $AlCl_3$-$NaCl_{sat}$ and related melts at 160-500°C (5, Appendix 4). In all cases (3-5) strong evidence for dimeric and cluster species was obtained resulting in very complicated chemistry. Formation of metals at high temperatures (>500°C) was also observed. We have initiated studies to compare electroplating of these elements (W, Nb, Ta) from basic haloaluminate melts with that from the LiF-NaF-KF eutectic (6). Our prior studies indicate that these metals cannot be plated using acidic ($AlCl_3$-rich) chloroaluminate melts.

3. Spectroelectrochemical Studies in Molten Alkali Chloroaluminates.

Spectroelectrochemistry - coupling of electrochemistry and spectroscopy - can be a very useful approach for investigating complex reactions in solutions(7).

Using Raman, UV-visible and electron spin resonance spectroscopies we reinvestigated the reduction of chloranil in $AlCl_3$-NaCl melts (8, Appendix 5). This material was previously investigated (9,10) because of its potential use as a cathode material for high-energy molten salt batteries. The spectroelectrochemical results (Appendix 5) show clearly that the reduction of chloranil in the basic $AlCl_3$-NaCl melt occurs not by a single two-electron process (as believed previously) but through the stepwise reduction of chloranil to the radical anion and the dianion.

The spectroelectrochemical approach was also quite useful in the studies of the reduction of Nb(V) (see Appendix 4) and of Re(IV) in $AlCl_3$-$NaCl_{sat}$. The rhenium system is being studied by Ellen Hondrogiannis (EH) as part of her doctoral dissertation. This work, supported by an AFOSR fellowship to EH, will be reported separately.

4. Photochemistry of Aromatic Hydrocarbons in Aluminum Chloride - 1-Ethyl-3-Methylimidazolium Chloride Ambient Temperature Melts (this aspect of the program is codirected by Professor R. M. Pagni).

The research during the past year has concentrated on the photochemistry of anthracene and 9-methylanthracene in molten aluminum chloride-1-ethyl-3-methylimidazolium chloride ($AlCl_3$/EMIC), looking in particular for photoinduced electron transfer reactions. Several such reactions have been found. Anthracene in deoxygenated basic medium ($AlCl_3$/MEIC mole ratio <1) afforded the 4+4 dimer exclusively (11, Appendix 6); no electron transfer from the excited state of anthracene to EMI^+ was observed under these conditions. Anthracene in deoxygenated acidic medium ($AlCl_3$/MEIC mole ratio >1), on the other hand, yielded a large number of monomeric and dimeric, reduced, neutral and oxidized products. Experiments showed that this unique chemistry was initiated by electron transfer from the excited state of anthracene to protonated anthracene which was formed by the reaction of anthracene with trace amounts of HCl, a strong acid in the acidic molten salt. Photolysis of the more easily oxidized 9-methylanthracene in deoxygenated basic melt afforded, in addition to the 4+4 dimer, two monomeric and two dimeric products, all of which were characterized by independent synthesis. Experiments demonstrate that this chemistry was initiated by electron transfer from the excited state of 9-methylanthracene to EMI^+. The difference in behavior of anthracene and 9-methylanthracene in the basic melt can be attributed to the difference in the rate of electron transfer to EMI^+: for anthracene, the electron transfer is endothermic and slow, while for 9-methylanthracene, the electron transfer is exothermic and fast. Irradiation of anthracene in oxygenated basic medium afforded several products including 9-chloroanthracene. Although the formation of 9-chloroanthracene can be envisioned to arise by electron transfer from the excited state of anthracene to O_2, additional work will be required to prove that this assumption is correct.

References

1. I.-Wen Sun, K. D. Sienerth, and G. Mamantov, J. Electrochem. Soc., 138, 2850 (1991).

2. G.-S. Chen, I.-W. Sun, K. D. Sienerth, A. G. Edwards, and G. Mamantov, J. Electrochem. Soc., 140, 1523 (1993).

3. G.-S. Chen, A. G. Edwards, and G. Mamantov, J. Electrochem. Soc., 140, 2439 (1993).

4. I-W. Sun, A. G. Edwards and G. Mamantov, J. Electrochem. Soc., 140, 2733 (1993).

5. K. D. Sienerth, E. M. Hondrogiannis, and G. Mamantov, J. Electrochem. Soc. (in press).

6. S. Senderoff and G. W. Mellors, Science, 153, 1475 (1966).

7. V. E. Norvell and G. Mamantov, in Molten Salt Techniques, Vol. 1, D. G. Lovering and R. J. Gale, eds., Plenum Press, 1983, pp. 151-176.

8. E. M. Hondrogiannis and G. Mamantov, Appl. Spectrosc., 48, 406 (1994).

9. G. Mamantov, R. Marassi, and J. Q. Chambers, Final Report, Contract DAAB07-73-7-0060 (1974), ECOM-0060-F.

10. P. A. Flowers and G. Mamantov, J. Electrochem. Soc., 136, 2944 (1989).

11. G. Hondrogiannis, C. W. Lee, R. M. Pagni, and G. Mamantov, J. Amer. Chem. Soc., 115, 9828 (1993).

Removal of Oxide Impurities from Alkali Haloaluminate Melts Using Carbon Tetrachloride

Guang-Sen Chen,* I-Wen Sun, Karl D. Sienerth, Anna G. Edwards, and Gleb Mamantov*

Department of Chemistry, The University of Tennessee, Knoxville, Tennessee 37996-1600

ABSTRACT

Small amounts of oxide impurities in alkali chloroaluminate and fluorochloroaluminate melts can complicate markedly the electrochemical and spectroscopic behavior of other solute species in these melts. A simple method for the removal of oxides from these melts has been developed in our laboratory. This method is based on the reaction of carbon tetrachloride with oxides to convert them to chlorides. Spectroscopic techniques (UV-visible and IR spectroscopy) have shown that addition of carbon tetrachloride results in the complete conversion of oxides to chlorides.

Oxide impurities in molten chloroaluminates[1] may have pronounced effects on the behavior of other solute species in these media;[2-4] these impurities are difficult to avoid. Recently we reported on the removal of oxide impurities from a sodium chloroaluminate melt saturated with NaCl with phosgene ($COCl_2$).[5] Prior studies on the determination and removal of oxide species from chloroaluminate melts are summarized briefly in that paper.[5]

Phosgene is a very poisonous gas and must be handled with extreme caution. In addition, we have found that the removal of oxide impurities from acidic sodium chloroaluminate melts ($AlCl_3$/NaCl mole ratio > 1) using $COCl_2$ is not complete.[6]

We report here a method for the removal of oxides from both acidic and basic alkali chloroaluminate melts, as well as fluorochloroaluminate melts. This method is based on the reaction of carbon tetrachloride with oxide species to convert these species to the corresponding chloride complexes. Using CCl_4 as a chlorinating reagent is advantageous compared to the $COCl_2$-treatment in that CCl_4 is much easier to handle.

Experimental

Aluminum chloride (Fluka, >99.0%) was purified by subliming it twice under vacuum in a sealed Pyrex tube. Sodium chloride (Mallinckrodt, reagent grade) was dried under vacuum (<50 mTorr) at 450°C for at least 48 h. High purity sodium fluoride (AESAR, puratronic, 99.995%), niobium pentachloride (AESAR, puratronic, 99.99%), and tungsten oxychloride ($WOCl_4$, Aldrich) were used without further purification. Carbon tetrachloride (water 0.001%) was purchased from Baxter Diagnostics, Inc.

$AlCl_3$-NaCl melts were prepared from purified aluminum chloride and vacuum dried sodium chloride. Any remaining base metal impurities in the melts were removed by adding aluminum metal (AESAR, 99.999%) in the process of preparing the melts.

Sodium fluorochloroaluminate melts[7] were prepared by mixing $AlCl_3$-$NaCl_{sat.}$ salts with high purity sodium fluoride in a suitable ratio, followed by premelting this mixture in a quartz tube. All handling of melts and solutes was performed in a nitrogen-filled dry box (moisture level <2 ppm). Pyrex cells and ampuls were torch-sealed under vacuum (<50 mTorr).

Ultraviolet-visible absorption spectra were obtained using 2 mm path length quartz cells and a Hewlett Packard 8452A diode array spectrophotometer with a water-cooled furnace. Infrared spectra were recorded with a Bio-Rad FTS-7 Fourier transform infrared (FTIR) spectrophotometer which was controlled by a microcomputer system.

The *in situ* infrared spectra of the molten salts were obtained using a cell similar to that described by Flowers and Mamantov.[8,9] The cell utilized silicon windows which were torch-sealed to the Pyrex body of the cell. AceThred adapters (Ace Glass Inc.) on the top of the cell provided access for loading and sample addition, and produced an airtight seal when closed. One AceThred adapter on the cell was covered with a septum. An appropriate amount of CCl_4 was added by injecting it through the septum using an airtight microsyringe (Baxter Diagnostics, Inc.). A furnace with diametrically opposed holes, which was constructed in house, allowed heating of the melt inside the sample chamber of the FTIR instrument.

Results and Discussion

$AlCl_3$-$NaCl_{sat.}$ melt at 200°C.—Figure 1 shows infrared absorption spectra in the region from 640 to 880 cm^{-1} for

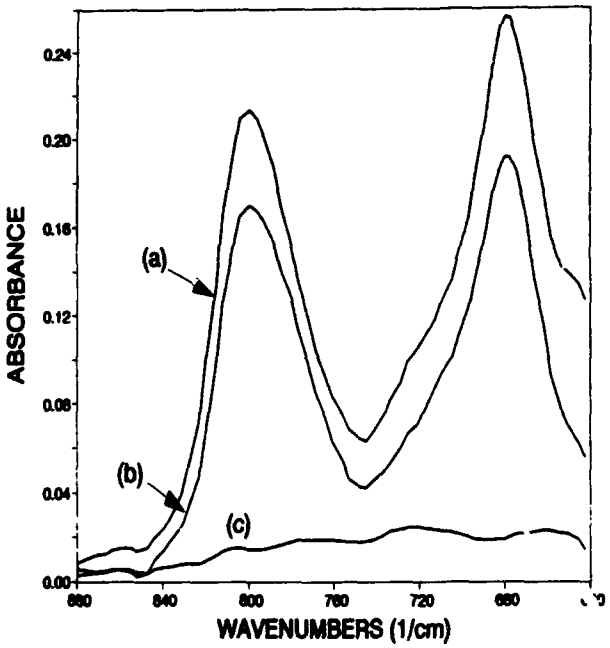

Fig. 1. Infrared absorption spectra of the aluminum oxychloride species in an $AlCl_3$-$NaCl_{sat.}$ melt containing 20.3 m*M* Na_2CO_3 at 200°C; (a) the initial melt; (b) 30 min after the introduction of 150 μliter CCl_4; and (c) 120 min after the introduction of 450 μliter CCl_4 total.

* Electrochemical Society Active Member.

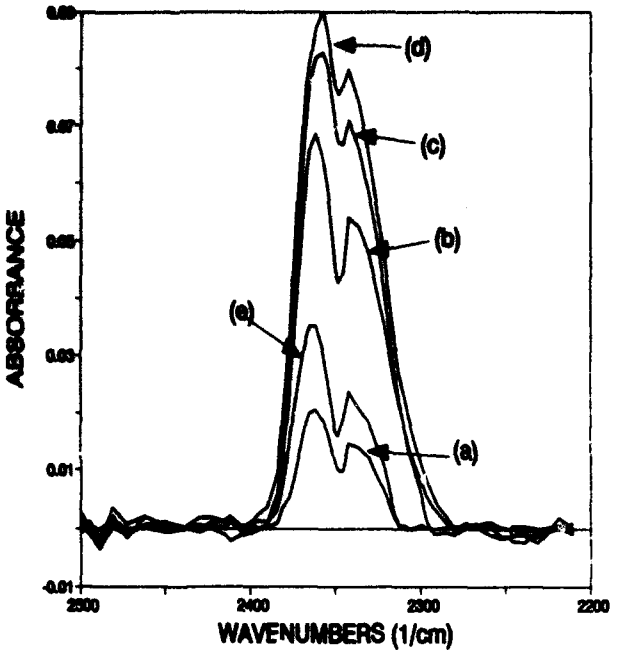

Fig. 2. Infrared absorption spectra of CO_2 in the $AlCl_3$-$NaCl_{sat.}$ melt containing 20.3 m*M* Na_2CO_3 at 200°C; (a) the initial melt; (b) 25 min after the addition of 50 μliter CCl_4; (c) 30 min, 150 μliter CCl_4; (d) 135 min, 450 μliter CCl_4; and (e) after 1 h of evacuation.

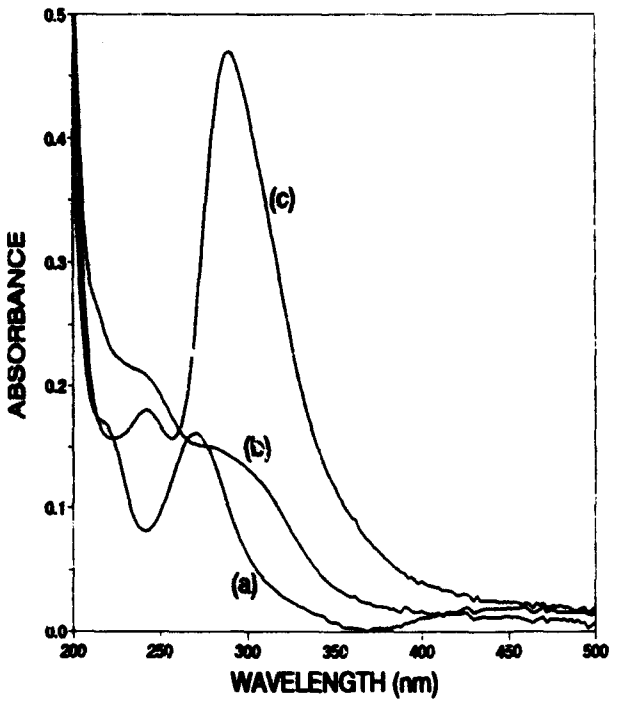

Fig. 3. UV-visible absorption spectra of niobium (V) species in a basic melt, $AlCl_3$-$NaCl_{sat.}$ (2.317 g), at 200°C; (a) the initial melt containing 0.17 m*M* $NbOCl_3$; (b) 16 min; and (c) 45 min after the introduction of 10 μliter CCl_4; the quartz cell path length was 2 mm.

the $AlCl_3$-$NaCl_{sat.}$ ($AlCl_3$/NaCl mol ratio = 0.99) melt containing 20.3 m*M* Na_2CO_3 at 200°C. The amount of Na_2CO_3 in this cell was 0.568×10^{-3} mol; this number of moles correspond to 138 μliter CCl_4 (at 25°C). Two absorption bands for aluminum oxychloride were observed at 680 and 800 cm^{-1}, which is in good agreement with the previous results reported by Flowers and Mamantov.[10] Thirty minutes after an addition of 150 μliter CCl_4, which was approximately equal to the molar amount of oxide in the melt, was made, the intensity of the absorption band at 800 cm^{-1} was decreased to *ca.* 80% of the initial absorption intensity; the signal further decreased to 75% after 60 min and remained unchanged for 2 h. Subsequently, an excess of CCl_4, 450 μliter in total, was added to the same cell. After 70 min, 70% of the oxide was converted to the corresponding chloride species. After 120 min, no infrared absorption bands for the aluminum oxychloride species were detected in the melt. It was apparent that all of the oxide impurities were eliminated in 2 h. The reaction of the oxide with CCl_4 was much faster than that with phosgene since 4 and 8 h were needed to remove 14 and 34 m*M* of the oxide, respectively, using $COCl_2$.[8]

A doublet occurring at 2342 and 2357 cm^{-1}, which is typical of the infrared spectrum of CO_2,[11-13] increased significantly with the introduction of CCl_4 into the melt (Fig. 2). The doublet bands were observed even in the absence of the sample cell; however, the band intensities were weaker than those after the addition of CCl_4. Prior to CCl_4 addition, these weak bands probably resulted from the trace amounts of CO_2 in the sample chamber of the FTIR instrument. From the results depicted in Fig. 2, we can conclude that the reaction of CCl_4 with O^{2-} formed CO_2 and Cl^- as follows

$$CCl_4 + 2\ O^{2-} = CO_2 + 4Cl^-$$

where O^{2-} and Cl^- represent the oxide species and free chloride ions or the chloride species, respectively.

The spectrum obtained for this melt after evacuation for 1 h is shown in Fig. 2. It is evident that the CO_2 absorption bands were reduced markedly. After 1 h more of evacuation, these bands were decreased further to the level observed before the introduction of CCl_4. These results indicate that the by-product (CO_2) formed by the reaction of CCl_4 with the oxide impurities was removed by evacuation.

An alternative way to measure oxide impurities is to examine the UV-visible spectra of Nb (V) in the melts. This

Table I. UV-visible spectroscopic data for niobium (V) species.

Species	Solvent	λ/nm (ε/M^{-1} cm^{-1})	Ref.
$NbCl_6$	gas at 100°C,	240 (1.0×10^4), 285 (1.0×10^4),	16
$NbCl_6^-$	CH_3CN	242 (8.1×10^3), 294 (3.4×10^4), 318 (1.4×10^4), 355 (sh, 2.5×10^3)	17
Et_4NNbCl_6	CH_3CN	242 (6.4×10^3), 290 (2.9×10^4), 315 (sh, 1.1×10^4), 355 (sh, 2.0×10^3)	18
$NbCl_6^-$	$AlCl_3$-MEIC (44.4/44.6 m/o)	291 (3.2×10^4), 316 (1.7×10^4) 360 (sh, 4.1×10^3)	19
$NbCl_6$	$AlCl_3$-$NaCl_{sat.}$	240 (1.1×10^4), 288 (1.3×10^4)	20
$NbCl_6^-$	$AlCl_3$-$NaCl_{sat.}$ (CCl_4-treated, at 200°C)	242 (5.3×10^3), 290 (1.4×10^4) 316 (sh, 9.1×10^3), 350 (sh, 3.4×10^3)	This work
$NbOCl_5^{2-}$	12*M* HCl	228 (3.6×10^3), 280 (1.1×10^4) 320 (sh, 1.3×10^3)	19
$NbOCl_5^{2-}$	$AlCl_3$-MEIC	278 (1.3×10^4), 317 (sh, 1.2×10^3)	19
$NbOCl_5^{(3-n)-}$	$AlCl_3$-$NaCl_{sat.}$ at 200°C	220 (6.9×10^3), 270 (4.7×10^3)	This work
$NbOCl_5^{2-}$	$NaAlCl_4$-NaF (90-10 m/o) at 480°C	278 (s)	This work

Table II. UV-visible spectroscopic data for tungsten (VI) species.

Species	Solvent	λ/nm (ε/M^{-1} cm^{-1})	Ref.
WCl_6	CCl_4	334 (8.0×10^3), 379 (3.0×10^3) 447 (8.0×10^2), 514 (?, 1.7×10^2) 585 (?, 60), 720 (?)	21
WCl_6	vapor	220 (s), 275 (sh), 330 (s), 375 (sh) 430 (w)	14
$WOCl_4$	toluene	355 (s)	22
$WOCl_4$	vapor	220 (s), 250 (sh), 270 (sh), 355 (s) 460 (w)	14
$WOCl_4$	$AlCl_3$-NaCl (63.37 m/o) at 200°C	228 (4.3×10^3), 266 (sh, 2.1×10^3), 284 (sh, 1.4×10^3), 360 (3.8×10^3)	This work
WCl_6	$AlCl_3$-NaCl (63-37 m/o) (after CCl_4 treatment at 200°C	332 (9.7×10^3), 378 (sh, 4.6×10^3), 434 (sh, 1.9×10^3), 484 (8.4×10^2)	This work

approach may be more sensitive for detecting a very low concentration of oxide species in the melts than the infrared spectral approach. A UV-visible absorption spectrum using niobium (V) species as a probe at 200°C is shown in Fig. 3. The concentration of the initial niobium oxychloride, which was added as $NbOCl_3$, was 0.17 m*M*. The results are summarized in Table I along with the literature data. The spectrum obtained before the introduction of CCl_4 (Fig. 3a) showed two main bands at 220 and 270 nm, which were similar to those for $NbOCl_3^{2-}$ in HCl and in basic room temperature melts[19] (Table I). We also observed results similar to the literature data for niobium oxychloride in $NaAlCl_4$-NaF [90-10 *mole percent (m/o)*] at 480°C at a higher concentration of 1 m*M*.

With the addition of CCl_4 to this cell, a significant change in the UV-visible spectrum was observed (Fig. 3b). After 45 min, the spectrum exhibited a much higher absorbance in the 250-350 nm region than that observed for the oxychloride species. Several absorbance maxima were observed at 242, 290, 316 (sh) and 350 nm (sh), which are in excellent agreement with those for $NbCl_6^-$ in other solvents (Table I). These results indicate clearly that using CCl_4 can reduce the oxide impurities to an extremely low level.

$AlCl_3$-NaCl (63-37 m/o) melt.—The oxide contamination in acidic chloroaluminates also complicates the electrochemical and spectroscopic behavior of some solutes of interest in these melts.[14] However, removal of oxide impurities from acidic chloroaluminate melts has not been reported previously. As mentioned above, phosgene cannot eliminate the oxide completely from these melts.[6] Therefore, we attempted to remove the oxide impurities from an acidic melt, $AlCl_3$-NaCl (63-37 m/o), using CCl_4. The efficiency was monitored by measuring the UV-visible spectra of melts containing a W(VI) species, which was employed as the probe.

Figure 4 shows the change in the UV-visible spectrum of tungsten(VI) species in the acidic melts with the addition of CCl_4 at 200°C. The features of these spectra are summarized in Table II together with the literature data. From these results we conclude that the tungsten(VI) species in the initial melt was $WOCl_4$. A significant change in the spectrum was observed *ca.* 2 h after the introduction of CCl_4. The new spectrum was characteristic of WCl_6 (Table II). The use of CCl_4 can remove all the oxide impurities in these melts. The reaction in the acidic melts was slower than that in $AlCl_3$-$NaCl_{sat.}$ melts.

$NaAlCl_4$-NaF (90-10 m/o) melt.—The electrochemistry and spectroscopy of solutes of sodium fluorochloroaluminate melts can be investigated over a large temperature region, *ca.* 200 to 800°C or higher.[15] There exists a large quantity of liquid phase for the $NaAlCl_4$-NaF (90-10 m/o) at temperatures ≥200°C, although the liquidus temperature at which the melt is completely molten, is 395°C.

We first attempted to remove the oxide impurities at a relatively low temperature (200-250°C) using CCl_4. However, CCl_4 only partly converted the oxides to the chlorides. This was due probably to the presence of the solid precipitate which prevented complete conversion.

As the temperature was increased to the liquidus temperature, 395°C or higher, the complete conversion of the oxides to chlorides by CCl_4 was obtained in less than 5 min as indicated by the UV-visible spectral changes of Nb(V) species contained in the melt (Table I). We noticed that the chloride species transformed again to the oxide species *ca.* 45 min after the introduction of 10 μliter CCl_4 to 2.38 g of the fluorochloroaluminate melt with 1 m*M* Nb(V) species in a quartz UV cell (2 mm in path length). This may be caused by the slight reaction of the melt with the quartz cell.

In summary, an oxide-free fluorochloroaluminate melt can be obtained by the following procedure: (*i*) increase the temperature to 400°C or higher for $NaAlCl_4$-NaF (90-10 m/o); (*ii*) add an excess of CCl_4 to the cell after the melt becomes molten; (*iii*) keep the cell at the high temperature for *ca.* 30 min; (*iv*) cool the cell to 300°C or lower; (*v*) evacuate the excess CCl_4 and CO_2 at this temperature for *ca.* 2 h; and (*vi*) cool the melt to room temperature.

Conclusion

Spectroscopic techniques (IR and UV-visible spectroscopies) indicate that the addition of carbon tetrachloride removes all traces of oxide impurities from both basic and acidic sodium chloroaluminate melts, as well as from fluorochloroaluminate melts. This method has an obvious advantage over using other chlorinating reagents, such as $COCl_2$ and HCl, since CCl_4 is easier to handle. This method

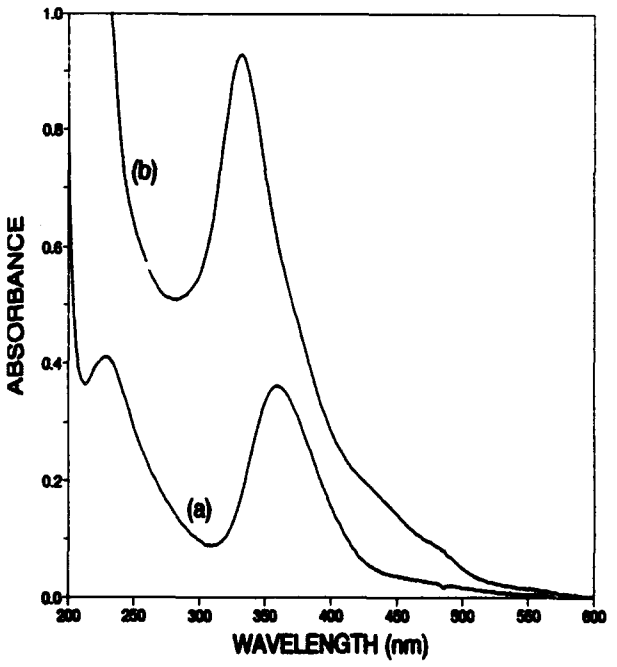

Fig. 4. UV-visible absorption spectra of tungsten (VI) species in an acidic melt, $AlCl_3$-NaCl (63-37 m/o, 2.781 g), at 200°C; (a) the initial melt containing 0.478 m*M* $WOCl_4$; (b) 120 min after the introduction of 20 μliter CCl_4; the quartz cell path length was 2 mm.

also may be suitable for the removal of oxide impurities from other alkali chloride melts such as LiCl-KCl and KCl-NaCl.

Acknowledgment

This work was supported by the Air Force Office of Scientific Research, Grant No. 88-0307.

Manuscript submitted Nov. 30, 1992; revised manuscript received Feb. 26, 1993.

The University of Tennessee assisted in meeting the publication costs of this article.

REFERENCES

1. T. M Laher, L. E. McCurry, and G. Mamantov, *Anal. Chem.*, **57**, 500 (1985).
2. B. Gilbert and R. A. Osteryoung, *J. Am. Chem. Soc.*, **100**, 2725 (1978).
3. K. Zachariassen, R. W. Berg, and N. S. Bjerrum, *This Journal*, **134**, 1153 (1987).
4. I-W. Sun, E. H. Ward, and C. L. Hussey, *Inorg. Chem.*, **26**, 4309 (1987).
5. I-W. Sun, K. D. Sienerth, and G. Mamantov, *This Journal*, **138**, 2850 (1991).
6. I-W. Sun, K. D. Sienerth, and G. Mamantov, Unpublished results.
7. B. Gilbert, S. D. Williams, and G. Mamantov, *Inorg. Chem.*, **27**, 2359 (1988).
8. P. A. Flowers and G. Mamantov, *This Journal*, **136**, 2944 (1989).
9. P. A. Flowers and G. Mamantov, *Anal. Chem.*, **61**, 190 (1989).
10. P. A. Flowers and G. Mamantov, *ibid.*, **59**, 1062 (1987).
11. J. H. Taylor, W. S. Benedict, and J. Strong, *J. Chem. Phys.*, **20**, 1884 (1952).
12. A. H. Nielsen and R. J. Lageman, *ibid.*, **22**, 36 (1954).
13. N. B. Colthup, L. H. Daly, and S. E. Wiberley, *Introduction to Infrared and Raman Spectroscopy*, pp. 43-45, Academic Press, New York (1975).
14. J.-P. Schoebrechts, P. A. Flowers, G. W. Hance, and G. Mamantov, *This Journal*, **135**, 3057 (1988).
15. G.-S. Chen, A. G. Edwards, and G. Mamantov, *ibid.*, Submitted.
16. R. F. W. Bader and A. D. Westland, *Can. J. Chem.*, **39**, 2306 (1961).
17. B. J. Brisdon, G. W. A. Fowles, D. J. Tidmarsh, and R. A. Walton, *Spectrochim. Acta*, **25A**, 999 (1969).
18. M. Volloton and A. E. Merbach, *Helv. Chim. Acta*, **57**, 2345 (1974).
19. I-W. Sun and C. L. Hussey, *Inorg. Chem.*, **28**, 2731 (1989).
20. E. Hondrogiannis and G. Mamantov, Unpublished results.
21. C. K. Jorgesen, *Mol. Phys.*, **2**, 309 (1959).
22. E. Thorn-Csanyi and H. Timm, *J. Mol. Cat.*, **28**, 37 (1985).

Reprinted from JOURNAL OF THE ELECTROCHEMICAL SOCIETY
Vol. 140, No. 6, June 1993
Printed in U.S.A.
Copyright 1993

Reprinted from JOURNAL OF THE ELECTROCHEMICAL SOCIETY
Vol. 140, No. 9, September 1993
Printed in U.S.A.
Copyright 1993

Electrochemical Studies of Tantalum in Fluorochloroaluminate Melts at 200-450°C

Guang-Sen Chen,* Anna G. Edwards, and Gleb Mamantov*

Department of Chemistry, University of Tennessee, Knoxville, Tennessee 37996-1600

ABSTRACT

The electrochemistry of tantalum(V) species in sodium fluorochloroaluminate melts (10 mole percent NaF) has been investigated in the temperature range of 200 to 450°C using cyclic, normal pulse, and square wave voltammetries, exhaustive electrolysis, Raman and electronic spectroscopies, and x-ray diffraction methods. The electrochemical behavior of tantalum(V) is strongly dependent on temperature. Three main reduction waves are observed at a temperature of 300°C or higher. The first and second reduction waves merge into one wave at temperatures below 300°C The first reduction wave is associated with the reduction of tantalum(V) to tantalum(IV) species followed by a dimerization reaction which occurs very slowly at lower temperatures. The second reduction wave is believed to be the reduction of the tantalum(IV) dimer, Ta_2^{8+}, to a tantalum(III) species (probably Ta_2^{6+}). The tantalum(III) species decomposes resulting in the formation of the cluster, $Ta_6Cl_{12}^{3+}$. The last reduction wave is assigned to the reduction of the trivalent tantalum species to a divalent tantalum species, which is highly unstable and decomposes to form the tantalum cluster, $Ta_6Cl_{12}^{2+}$, and metallic tantalum. The clusters are slowly reduced to metallic tantalum.

The electrochemistry of tantalum is complicated by the existence of various compounds with different oxidation states, such as Ta^{5+}, Ta^{4+}, Ta^{3+}, Ta_6^{15+}, Ta_6^{14+}, Ta^{0} [1-4] in $AlCl_3$-NaCl melts.[5,6] McCarley *et al.*[2,3] reported that anhydrous low-valent tantalum halides can be synthesized by the reduction of tantalum(V) halides with aluminum metal at appropriate temperatures. The electrolytic reduction and oxidation of tantalum and other refractory metal species in molten halide salts,[7-13] organic solvents,[14] and room temperature melts[15] have received considerable attention, since these metals generally have very high melting points and high corrosion resistance.

We are interested in the electrochemistry and electroplating of refractory metals such as Nb, Ta, and W in alkali chloroaluminate and fluorochloroaluminate melts. von Barner *et al.*[5] have recently reported electrochemical and spectroscopic studies of tantalum species in $AlCl_3$-NaCl melts at 160-300°C. Tantalum(V) forms two different species, $TaCl_6^-$ and $TaCl_5$, in basic ($AlCl_3$/NaCl mole ratio <1) and moderately acidic $AlCl_3$-NaCl melts.[5,16] In addition, $TaOCl_4^-$ is formed in basic melts in the presence of small amounts of oxide ions.[5] The reduction of tantalum(V) in an acidic $AlCl_3$-NaCl [51-49 mole percent (m/o)] melt at 175°C is believed to follow the sequence, $Ta^{5+} + e^- = Ta^{4+}$, $2\ Ta^{4+} = Ta_2^{8+}$, $Ta_2^{8+} + 2e^- = Ta_2^{6+}$, $5\ Ta_2^{6+} = Ta_6^{14+} + 4\ Ta^{4+}$. This reduction leads to the formation of a tantalum cluster. Formation of metallic tantalum was not observed in the electrolysis at 175°C in the sodium chloroaluminate melts.

McCurry[17] investigated the electrochemical behavior of tantalum(V) in $AlCl_3$-NaCl melts saturated with NaCl, noted $AlCl_3$-$NaCl_{sat}$ melts, as a function of the oxide concentration in these melts. These studies resulted in a voltammetric method employing tantalum(V) as a probe to determine small amounts of dissolved oxide impurities in molten $AlCl_3$-$NaCl_{sat}$.[6]

Several researchers[18-20] have described spectroscopic studies of the chlorobromoaluminate and chloroiodoaluminate melts. The various mixed ions $AlCl_xX_{4-x}^-$ (X = Br, I) were reported when $AlCl_4^-$ was mixed with $AlBr_4^-$ or AlI_4^-. Gilbert *et al.*[21] investigated the Raman spectroscopy of fluoride-containing chloroaluminate melts at 580-820°C. It was observed that fluoride replaced chloride progressively, depending on the molar ratio of NaF to $NaAlCl_4$, to form the species $AlCl_3F^-$, $AlCl_2F_2^-$, $AlClF_3^-$, and AlF_4^-.

Sodium fluorochloroaluminate melts are interesting media because the electrochemistry and spectroscopy of solutes can be examined over a large temperature range (from *ca.* 200 to 800°C or higher). The attack of Pyrex and quartz cells by these melts is much smaller than that by alkali fluoride melts.[21] The cathodic limit of the fluorochloroaluminate melts occurs at more negative potentials than that of sodium chloroaluminate melts at high temperatures (see below). There is sufficient molten phase in the $NaAlCl_4$-NaF (90-10 m/o) system at temperatures well below its liquidus temperature (395°C)[22] for the electrochemical studies. In this paper, we describe the electrochemical studies of tantalum(V) in oxide-free fluorochloroaluminate melts, $NaAlCl_4$-NaF (90-10 m/o), at 200-450°C.

Experimental

Aluminum chloride (Fluka, >99.0%) was purified by subliming it twice under vacuum in a sealed Pyrex tube.[5,6] Sodium chloride (Mallinckrodt, reagent grade) was dried under vacuum (<50 mTorr) at 450°C for at least 48 h. High purity sodium fluoride (AESAR, puratronic, 99.995%) and tantalum chloride (AESAR, puratronic, 99.99%) were used without further purification. Carbon tetrachloride (water, 0.001%) was purchased from Baxter Diagnostics, Incorporated.

$AlCl_3$-$NaCl_{sat}$ melts were prepared from purified aluminum chloride and vacuum-dried sodium chloride. The melts were saturated with NaCl at 175°C. Any remaining base metal impurities in the melts were removed by adding aluminum metal (AESAR, 99.999%) in the process of preparing the melts.

It is very important to eliminate small amounts of oxide species in the melts since the presence of the oxide species will complicate the electrochemical behavior of Ta, Nb, and W in these melts.[15,23-25] Recently, we reported the use of phosgene, $COCl_2$, to convert oxide species to the chloride species in basic alkali chloroaluminate melts.[24] Very recently, we have found that carbon tetrachloride can also remove oxides effectively. The treatment with CCl_4 has several advantages compared to the $COCl_2$-treatment including the ease of handling CCl_4. The details of this new method will be reported elsewhere.[26]

Sodium fluorochloroaluminate melts were prepared by mixing CCl_4-treated $AlCl_3$-$NaCl_{sat}$ salts with high purity

sodium fluoride in a suitable ratio, followed by premelting this mixture in a quartz tube.[21]

The electrochemical studies were performed in a Pyrex cell using a glassy carbon plate as a counterelectrode, a tungsten wire (0.5 mm in diam), platinum wire (0.5 mm in diam) or a glassy carbon rod as a working electrode, and a platinum wire directly immersed in the melts as a quasi-reference electrode. The reference electrode was a silver wire dipped in $AlCl_3$-$NaCl_{sat}$ melt containing 6.28 m/o AgCl and placed in a thin Pyrex bulb. The silver electrode was found to be very stable and reproducible even at high temperatures, while an aluminum reference electrode was not steady at high temperatures. The potential difference of the Ag/Ag(I) reference *vs.* Al in $AlCl_3$-$NaCl_{sat}$ at 175°C was found to be 1.090 ± 0.005 V. The platinum quasi-reference electrode was used as the reference electrode for the electrochemical measurements, since the resistance across the Pyrex membrane was very high. The potential differences between the platinum quasi-reference and the silver reference electrodes were measured using a high impedance multimeter (Keithley 173A) before taking any voltammograms. In this report, the potentials given are with respect to the silver reference electrode.

The exhaustive electrolyses were performed using a large surface area glassy carbon crucible as a working electrode. An aluminum coil sealed in a glass tube and separated by a beta-alumina diaphragm was used as a counterelectrode. We found that a beta-alumina diaphragm was suitable for the exhaustive electrolysis of a species with high vapor pressure since it is a good sodium ion conductor and is gas tight.

All handling of melts and solutes was done in a nitrogen filled dry box (moisture level <2 ppm). Cells and ampuls were torch sealed under vacuum (<50 mTorr).

An EG&G Princeton Applied Research (PAR) potentiostat/galvanostat (Model 273) connected to an IBM computer (PS/2 Model 70 386) utilizing the PAR M270 software package was used to obtain cyclic, normal pulse, and square wave voltammograms.

Raman spectroscopic measurements were performed as described previously.[21,27] A furnace of the proper optical design was constructed in-house and enabled the detection of Raman signals at 90° to the excitation beam. Fairly high power levels, typically 400 mW, were required because of losses at the windows of the furnace. The monochromator slits were set for a bandpass of 3 cm^{-1}.

Ultraviolet-visible absorption spectra were recorded at room temperature (25°C) in 10 mm path length quartz cells, using a Hewlett Packard 8452A diode array spectrophotometer or a Varian Cary 219 spectrophotometer.

The chemical analyses were performed by Schwarzkopf Microanalytical Laboratory, Incorporated.

Results

Characterization of the fluorochloroaluminate melts.— In this study, we focused our attention on the electrochemical behavior of tantalum(V) in sodium fluorochloroaluminate melt, $NaAlCl_4$-NaF (90-10 m/o). Sato *et al.*[22] investigated the phase properties of fluoride-containing sodium chloroaluminate systems using differential thermal analysis. Their results indicated that the system $NaAlCl_4$-NaF (90-10 m/o) exhibited two-phase transition temperatures, 395 and 152°C. Although some solid material precipitated from the solution at temperatures ≥200°C, the amount of liquid phase was sufficiently large to permit the use of this melt over a large temperature range.

Since it is important to know the composition of the liquid and solid phases of the fluorochloro melts at temperatures lower than the liquidus point, the liquid phase was analyzed by Raman spectroscopy and chemical analysis, and the solid phase was characterized by x-ray diffraction. Figure 1 shows the Raman spectra of the liquid phase of $NaAlCl_4$-NaF (89.86-10.14 m/o) melt at several temperatures. First, the sample was gradually heated to 550°C, at which temperature it was completely molten, and then the spectrum was acquired after 30 min of equilibration. Next, the temperature of the sample was gradually lowered and equilibrated at the lower level for at least 30 min prior to data acquisition. The frequencies of the observed bands are presented in Table I. The frequency of band 4 was obtained by deconvolution of band 3 and band 4 using a nonlinear least squares curve fitting technique. The deconvoluted bands were integrated to determine their areas. Bands 1, 2, and 3 were assigned to $AlCl_4^-$ species and band 4 to the fluorochloro species, $AlCl_3F^-$.[21] It is important to note that the band for the fluorochloro species, $AlCl_3F^-$, is observed at lower temperatures (even at 200°C). The ratio of $[AlCl_3F^-/AlCl_4^-]$ in the liquid phase was approximately constant in the temperature range studied since the area ratio of S_{Band4}/S_{Band3} was nearly independent of the temperature. It appeared that only a relatively small amount of the fluoride species precipitated at lower temperatures. This conclusion was supported by the chemical analysis of the liquid phases at 350 and 250°C, which contained 1.3 w/o and 0.86 w/o F, respectively, [the theoretical F content is 1.06 w/o in the $NaAlCl_4$-NaF (89.86-10.14 m/o) melt].

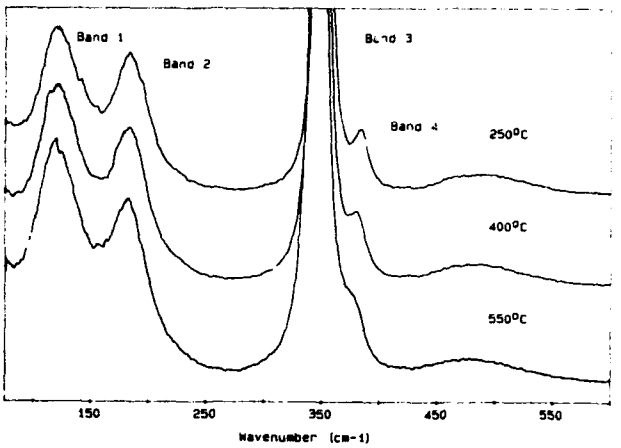

Fig. 1. Typical Raman spectra of the liquid phase of $NaAlCl_4$-NaF (89.86-10.14 m/o) melt at different temperatures (550, 400, and 250°C). Excitation wavelength, 488.0 nm; excitation power, 400 mW; bandpass, 3 cm^{-1}.

The results from Raman spectroscopy were in good agreement with the x-ray diffraction studies of the precipitate from the same melts at 250°C since the main compound in the precipitate was identified as NaCl. From these results, it is reasonable to conclude that the sodium chloroaluminate melts containing 10.14 m/o NaF, at temperatures below the liquidus point are fluorochloroaluminate melts saturated with NaCl.

The voltammetric characteristics of the fluorochloroaluminate melt differed from $AlCl_3$-$NaCl_{sat}$ melt at different temperatures. Typical cyclic voltammograms at a tungsten electrode at 450°C in these melts are shown in Fig. 2 and the cathodic limits are listed in Table II. The cathodic limit

Table I. Raman spectral data for the liquid phase of the $NaAlCl_4$-NaF (89.86-10.14 m/o) system.

t (°C)	Band 1 (cm^{-1})	Band 2 (cm^{-1})	Band 3 (cm^{-1})	Band 4 (cm^{-1})	S_{Band4} S_{Band3}
550	119.8	182.8	346.5	376.6	0.062
450	119.4	184.0	347.9	379.2	0.061
400	121.2	184.6	348.7	380.7	0.060
350	119.2	183.6	349.3	382.3	0.057
300	121.0	183.8	349.9	383.1	0.059
250	119.6	183.0	350.3	384.4	0.059
200	119.9	183.3	351.0	385.1	0.059

S_{Band4}/S_{Band3} is the area ratio of band 4 over band 3. The areas were obtained by integrating the deconvoluted band 3 and band 4, respectively.

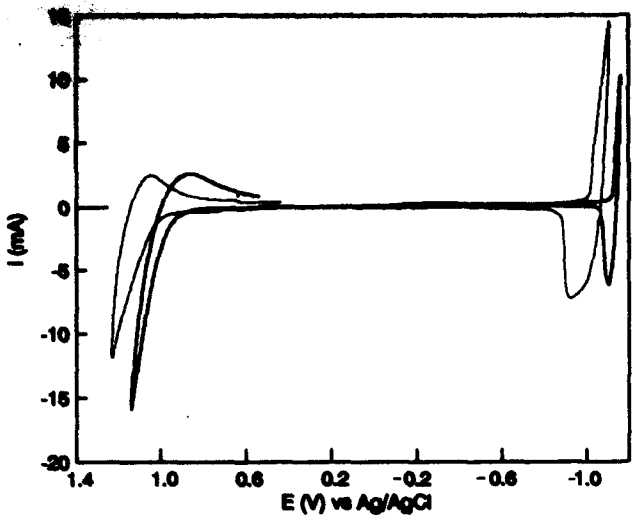

Fig. 2. Cyclic voltammograms at a tungsten electrode (0.175 cm^2) in $AlCl_3$-$NaCl_{sat}$ melt (----) and $NaAlCl_4$-NaF (90-10 m/o) melt (——) at 0.1 V/s and 450°C.

shifted to more positive values in both melts as the temperature was increased. The cathodic limit of the melt containing NaF was more negative at high temperatures than that of the melt without NaF added. This fact is important in studying the electrochemical behavior of Ta species, since the most negative reduction wave is very close to the cathodic limit (see below). An additional advantage of the fluorochloro melts over the saturated chloro melts is that the fluorochloro melts contain enough Cl^- ions to complex the Ta^{5+} species as $TaCl_6^-$ in the $TaCl_5$ concentration range studied (<0.3 mol/kg).[27]

The anodic limit in the fluorochloro melt occurred at less positive potentials than in the chloro melt at high temperatures. This is believed to be due to the higher free Cl^- activity in the former melt.

The electrochemical behavior of a glassy carbon electrode in this melt was identical to that of a tungsten electrode, while the behavior of a Pt electrode was complicated at high temperatures (>300°C) by the formation of Al-Pt alloys.

Cyclic voltammetry.—Several electrochemical techniques, including cyclic voltammetry, normal pulse voltammetry, square wave voltammetry, and exhaustive electrolysis were used to study the electrochemical behavior of tantalum species.

Figure 3 shows typical voltammograms of tantalum(V) obtained in the $AlCl_3$-$NaCl_{sat}$ melt (Fig. 3a) and in the fluorochloroaluminate melt, $NaAlCl_4$-NaF(90-10 m/o) (Fig. 3b) at 250°C. For convenience, the last cathodic wave is referred to as wave 3c since a new peak appears at high temperatures at a potential between the first and the second waves observed at low temperatures. It may be seen that the electrochemical behavior of the tantalum(V) species in the chloro melt is similar to that in the fluorochloro melt. It is noted that the peak potentials of waves 1c and 3c in the

Table II. Comparison of the cathodic limits of the $AlCl_3$-$NaCl_{sat}$ melt (E'_{0Cl}) and $NaAlCl_4$-NaF (90-10 m/o) melt (E'_{0F}).

t (°C)	E'_{0Cl} (V)	E'_{0F} (V)	E'_{0F}-E'_{0Cl}
200	−1.214	−1.171	0.043
250	−1.191	−1.196	−0.005
300	−1.130	−1.192	−0.062
350	−1.090	−1.188	−0.098
400	−1.069	−1.182	−0.113
450	−1.020	−1.130	−0.110

E'_0, the potentials at $i_c = 0$, were determined by extrapolating the Al(III) reduction current to zero. Scan rate 0.1 V/s.

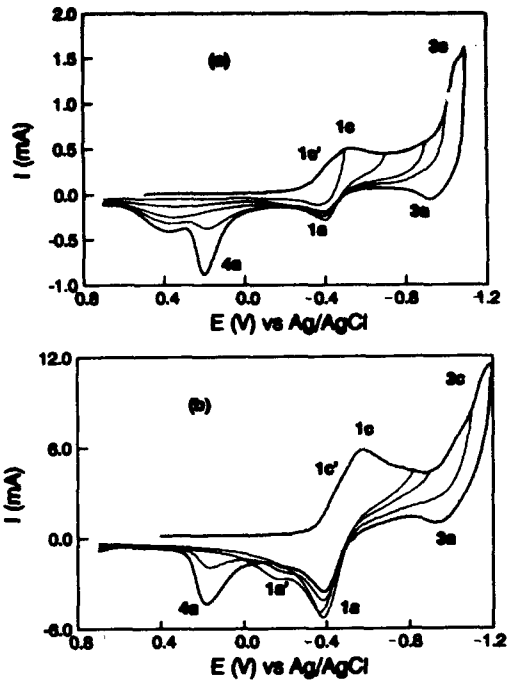

Fig. 3. Typical cyclic voltammograms of tantalum(V) at a tungsten electrode (0.175 cm^2) at 250°C, (a) in the $AlCl_3$-$NaCl_{sat}$ melt with 5.65×10^{-3} mol/kg $TaCl_5$ at 0.1 V/s; (b) in the $NaAlCl_4$-NaF (90-10 m/o) melt with 37.6×10^{-3} mol/kg $TaCl_5$ at 0.5 V/s.

NaCl-saturated chloro melts are slightly more positive than the corresponding waves in the fluorochloro melts at the same $TaCl_5$ concentration. The cyclic voltammetric behavior seems to be more complicated in the chloro melts at high $TaCl_5$ concentrations (>*ca.* 50 m*M*) because $TaCl_5$ and $TaCl_6^-$ coexist in the chloro melt according to our recent Raman studies of the melt with a higher $TaCl_5$ concentration. These results indicate that as the concentration of $TaCl_5$ in the melt is increased the relative concentration of $TaCl_5$ to $TaCl_6^-$ increases as the concentration of Cl^- decreases due to complexation with $TaCl_5$. In the fluorochloro melts, only $TaCl_6^-$ was observed in the $TaCl_5$ concentration range studied, <0.3 mol/kg. Therefore, the electrochemistry of tantalum(V) species in the fluorochloro melt (10 m/o NaF) is the primary emphasis of this paper and the following discussion deals with studies in the fluorochloro melt unless otherwise specified.

Two main reduction waves were observed at lower temperatures. The first one (1c) was well defined while the second one (3c) was poorly defined. The anodic behavior was strongly dependent on the reversal potential. One oxidation wave (1a) was observed, which corresponded to wave 1c when the reversal potential was more positive than that of the onset of wave 3c. Two new anodic waves (3a and 4a) were observed when the potential was reversed at potentials corresponding to wave 3c. It is interesting to note that the small anodic wave (3a) was associated with wave 3c while the anodic wave 4a appeared at a much more positive potential than that of wave 1a. Wave 4a had the appearance of an anodic stripping wave of an insoluble species on the electrode surface.

The cyclic voltammetric behavior of the first redox couple (1c and 1a) of tantalum(V) at a tungsten electrode was found to be a function of the scan rate and temperature (200 and 250°C) as depicted in Fig. 4. As the scan rate was increased and the temperature was decreased, a cathodic shoulder (1c′) became more prominent. At lower scan rates (<0.5 V/s at 250°C), the shoulder almost disappeared. As shown in Table III, the cathodic peak potentials of wave 1c shifted to more negative values with an increase in the scan rate, while the half-peak potentials were essentially independent of the scan rate. It was noted that the ratio $I_{pc}/v^{1/2}$, decreased as the scan rate increased.

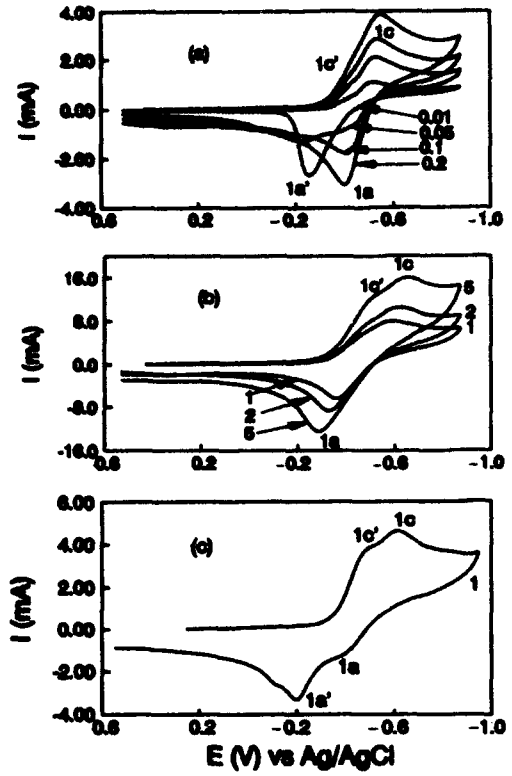

Fig. 4. The scan rate and temperature dependence of cyclic voltammograms of tantalum(V) species for the first redox couple in the fluorochloro melt with 34 × 10^{-3} mol/kg $TaCl_5$ (a) and (b) at 250°C, (c) at 200°C. A tungsten electrode (0.175 cm^2) was used. (a) 0.01, 0.05, 0.1, 0.2 V/s; (b) 1, 2, 5 V/s; (c) 1 V/s.

The anodic behavior (1a and 1a') also changed with the scan rate. At high scan rates (>0.1 V/s), only one well-defined wave (1a) was observed while two anodic waves (1a and 1a') appeared at 0.05 V/s. Wave 1a' became the main anodic wave at 0.01 V/s and 250°C. At a relatively low temperature (200°C), the reaction associated with wave 1a' dominated the anodic behavior even at 1 V/s (Fig. 4c).

The cathodic shoulder (1c') was not observed at a higher $TaCl_5$ concentration (75.4 × 10^{-3} mol/kg). Both the peak potential and the half-peak potential of wave 1c tended to shift to more positive values as the $TaCl_5$ concentration was increased (Table IV). The slope of E_{pc} or $E_{(p/2)c}$ *vs.* ln (c) was determined to be in the range of 19 to 25 mV, which agreed with the expected value of 22.5 mV at 250°C for an EC reaction.[28,29]

The overall cyclic voltammograms of tantalum(V) at a tungsten electrode were influenced by the temperature. Typical cyclic voltammograms of tantalum(V) species at temperatures ranging from 300 to 450°C are shown in Fig. 5.

Table III. Cyclic voltammetric data for the first reduction wave of tantalum(V) (34 × 10^{-3} mol/kg) in the $NaAlCl_4$-NaF (90-10 m/o) melt.

v(V/s)	E_{pc}(V)	$E_{(p/2)c}$(V)	$I_{pc}/v^{1/2}$
0.01	−0.538	−0.453	10.43
0.05	−0.537	−0.446	8.96
0.10	−0.544	−0.441	8.54
0.20	−0.554	−0.441	8.11
0.50	−0.578	−0.440	7.83
1.00	−0.595	−0.437	7.45
2.00	−0.631	−0.447	6.86
5.00	−0.667	−0.449	6.71

I_{pc} in mA.
Tungsten electrode area: 0.175 cm^2.
Temperature: 250°C.

Table IV. The tantalum(V) concentration dependence of E_{pc} and $E_{(p/2)c}$ for the first reduction wave in the fluorochloro melt at 250°C and 0.1 V/s.

$TaCl_5$ (×10^{-3} mol/kg)	E_{pc}(V)	$E_{(p/2)c}$(V)
12.3	−0.551	−0.406[a]
34.0	−0.544	−0.441
37.6	−0.544	−0.445
79.5	−0.527	−0.432
138.8	−0.517	−0.427

[a] In the case of the lowest $TaCl_5$ concentration, wave 1c is significantly affected by the shoulder (1c').

Three main reduction waves (1c, 2c, and 3c) were observed when the temperature was 350°C or higher. A small shoulder (3c') also appeared. A new wave (2c) was observed at high temperatures (Fig. 5) and it became more pronounced as the temperature was increased. In other words, the first reduction wave observed at lower temperatures split into two waves at higher temperatures. The first wave (1c) seemed to change only slightly while the last two waves (2c and 3c) increased greatly as the temperature was increased.

The oxidation waves coresponding to waves 1c and 2c were ill-defined at higher temperatures in the overall cyclic voltammograms (Fig. 5) while waves 4a and 4a' at positive potentials (between *ca.* 0 and *ca.* 0.4 V) were very pronounced. It was found that the anodic behavior was dependent on the reversal potential and the delay time (Fig. 6). When the cyclic voltammogram was reversed at a potential corresponding to wave 1c, only wave 1a was observed. This indicated that the reduced species corresponding to wave 1c was relatively stable at 450°C. A large anodic wave (4a) appeared if the reversal potential was extended to Wave 2c and a delay time was used (Fig. 6b). The corresponding anodic waves (1a and 2a) almost vanished. When

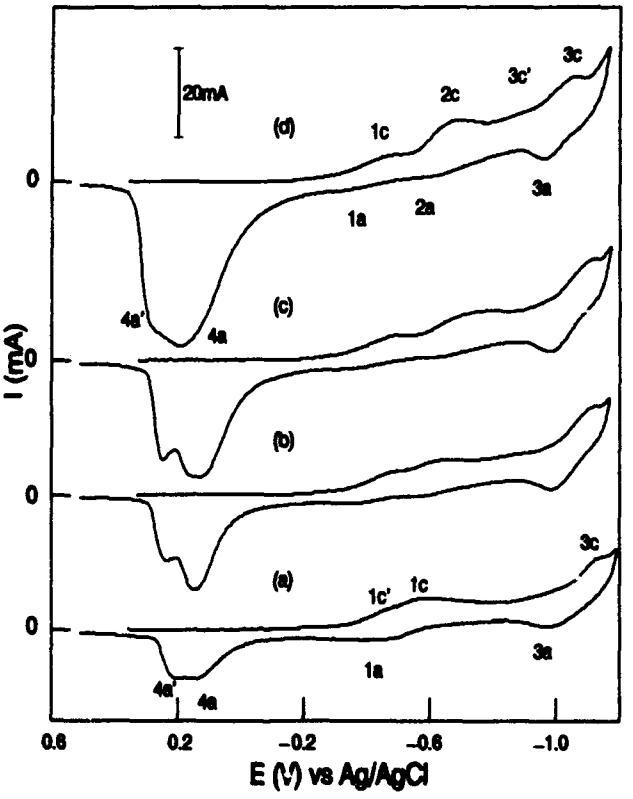

Fig. 5. The temperature dependence of the cyclic voltammograms of tantalum(V) at a tungsten electrode (0.175 cm^2) in the fluorochloro melt with 37.6 × 10^{-3} mol/kg $TaCl_5$ at (a) 300°C, (b) 350°C, (c) 400°C, and (d) 450°C. The scan rate was 0.5 V/s.

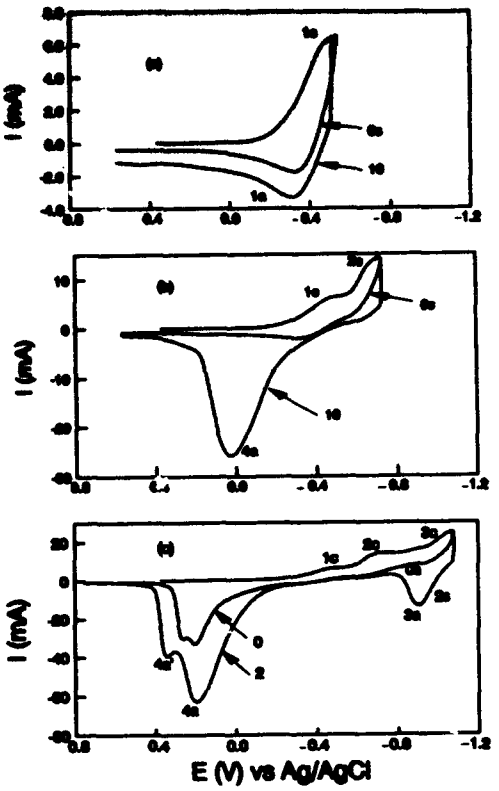

Fig. 6. Effects of the delay time at the reversal potential on the cyclic voltammograms of tantalum(V) (37.4×10^{-3} mol/kg) at a tungsten electrode (0.175 cm^2) at 450°C. The scan rate was 0.5 V/s. The delay times were (a) and (b): 0 s and 10 s; (c) 0 s and 2 s.

the reversal potential was extended to the third cathodic wave, the large anodic wave was composed of two waves (4a and 4a') (Fig. 6c). A relatively small stripping wave (3a) was found in the cyclic voltammogram with a short delay time (2 s). During the electrolyses or electrodeposition using a small electrode, an insoluble black deposit was formed at potentials corresponding to the second or third wave. The black deposit was found to dissolve in ethanol forming yellow or green solutions. The spectra of these solutions are discussed below.

Normal pulse voltammetry.—Typical normal pulse voltammograms of Ta(V) at a tungsten electrode at different temperatures are shown in Fig. 7. It was evident that these voltammograms were strongly dependent upon temperature. At lower temperatures (<300°C), two main cathodic waves (waves 1 and 3) were observed. As the temperature was increased to 350°C or higher, another wave (wave 2) was observed; this wave became more pronounced at 400 and 450°C. The third wave (wave 3) grew significantly with temperature. This wave exhibited a maximum at a lower temperature (<350°C) when a short pulse width (0.1 s) was applied (Fig. 7). The maximum was diminished at a long pulse width (>0.5 s). The second wave was steeper than the first wave although the ratios of the second limiting current over the first limiting current were close to unity at 350 to 450°C (Table V).

According to Flanagan *et al.*,[30] no visible anomaly is present in the normal pulse voltammograms when only the reduced species are adsorbed. For a CE or EC process, plots of E *vs.* ln $[(I_d - I)/I]$ have the same slope as that for a simple redox reaction without a preceding or following chemical reaction.[31] Therefore, we can use the plots of E *vs.* ln $[(I_d - I)/I]$ to evaluate the n-values of waves 1 and 2 although these two waves may involve a following or a preceding chemical reaction.

The plots of E *vs.* ln $[(I_d - I)/I]$ for wave 1 at both 200-300°C and 400-450°C gave excellent linear curves. Typical results are summarized in Table V. It was found that the slopes of these plots for wave 1 agreed well with the theoretical values of (RT/nF) for $n = 1$ in a wide temperature range. A reasonable plot for wave 1 at 350°C could not be obtained since wave 2 is too close to wave 1. Linear relations of E *vs.* ln $[(I_d - I)/I]$ for wave 2 were also found at 400 to 450°C. An n-value of *ca.* 2 was found while the limiting current ratios of wave 2 over wave 1 were approximately 1 as mentioned above.

The plots of E *vs.* ln $[(I_d - I)/I]$ for wave 3 were not linear. The formation of a large amount of solid material on the electrode surface was observed at these potentials. The limiting current ratio of wave 3 over wave 1 was about three at 400-450°C, while it was approximately one at 350°C.

Square wave voltammetry.—Ramaley and Krause[32,33] developed the theory of square wave voltammetry for the hanging mercury drop electrode; however, the treatment was limited to small step heights (and consequently, slow scan rates). Osteryoung and coworkers[34-38] have made significant contributions to the theory of the square wave voltammetry including systems with coupled chemical reactions. Square wave voltammetry has previously been applied to studies of molten salt solutions.[39]

In the square wave voltammetry used in this work, the currents are sampled at the end of both the forward and reverse halves of the cycle. The net current is the difference of the forward current and the reverse current. For a simple reversible reaction, the net current-potential curve is bell shaped and symmetrical about the half-wave potential, and the peak height is proportional to concentration. The shape of the net current voltammogram is relatively insensitive to a variety of common complications in voltammetric experiments. The theoretical relationships for a reversible reaction are as follows for a pulse height of E_{sw} = 25 mV[35]

$$W_{1/2} = 3.91RT/nF \quad [1]$$

$$W_{1/2f} = 1.95RT/nF \quad [2]$$

where $W_{1/2}$ and $W_{1/2f}$ represent the total peak width and the front peak width at half height. These two equations may be used to estimate the n-values of reversible electron-transfer reactions preceded or followed by a chemical reaction since the peak width is not significantly dependent on

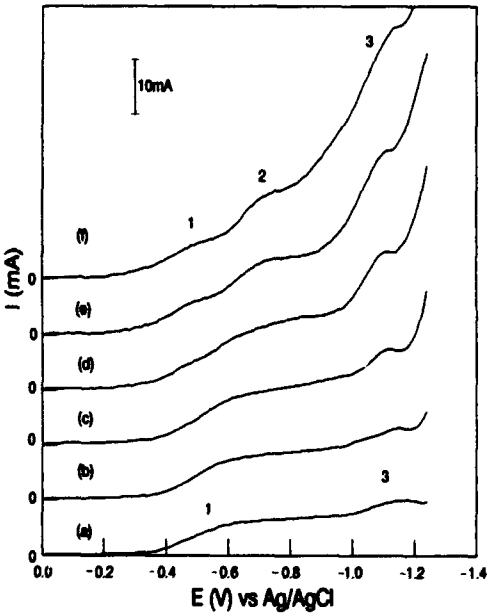

Fig. 7. Normal pulse voltammograms of tantalum(V) species in the $NaAlCl_4$-NaF (90-10 m/o) melt at (a) 200, (b) 250, (c) 300, (d) 350, (e) 400, and (f) 450°C. Tungsten electrode: 0.175 cm^2; $TaCl_5$ concentration: 37.6×10^{-3} mol/kg: pulse width: 0.1 s; step time: 0.5 s.

Table V. Normal pulse voltammetric data for the reduction of tantalum(V) (37.6×10^{-3} mol/kg) in the fluorochloro melt.

t (°C)	puw/s st/s	SL_1/mV n	$E_{1/2,1}$ (V)	SL_2/mV n	$E_{1/2,2}$ (V)	I_2/I_1	I_3/I_1
200	0.1	45.5	−0.481				0.40
	0.5	0.90					
200	1.0	40.6	−0.470				0.71
	5.0	1.01					
250	0.1	45.4	−0.488				0.53
	0.5	0.99					
250	1.0	41.9	−0.486				0.50
	5.0	1.07					
300	0.1	46.9	−0.471				0.79
	0.5	1.06					
300	1.0	48.4	−0.505				1.19
	5.0	1.02					
350	1.0	83.5	−0.565				0.82
	5.0	0.64					
400	0.1	55.8	−0.409	29.5	−0.639	1.11	2.9
	0.5	1.05		1.97			
400	1.0	58.3	−0.416	31.4	−0.640	1.30	3.17
	5.0	0.99		1.85			
450	0.1	59.2	−0.407	31.9	−0.649	1.30	3.33
	0.5	1.05		1.95			

puw: pulse width; st: step time; SL: the slope of E vs. $\ln[(I_d - I)/I]$; n: number of electrons.

the characteristics of the coupled chemical reactions and is close to the theoretical value for a simple reversible electron transfer reaction although the peak potential shifts negatively or positively.[37]

Figure 8A shows typical net-current square wave voltammograms of tantalum(V) at a tungsten electrode at temperatures from 200 to 450°C. These voltammograms were strongly dependent on temperature in agreement with the cyclic and normal pulse voltammograms discussed above. Only one well-defined wave (wave 1) appeared at 200°C. As the temperature was increased to 300°C or higher, a new wave (wave 2) appeared, and this wave became much better defined at temperatures higher than 350°C. This wave shifted to a more negative potential with temperature. Although wave 3 was ill-defined at temperatures lower than 300°C, it became well-defined at higher temperatures.

The peak heights and peak widths of wave 1 can be directly determined from the experimental results. For the case of wave 2, it is necessary to separate wave 2 from wave 1. Since the net-current voltammograms are bell-shaped and symmetric, the "back side" curve of wave 1 may be obtained by a symmetric extension. The "front side" of wave 2 is obtained by subtracting the back side of wave 1 from the experimental curve at the corresponding potentials. A typical result is shown in Fig. 8B. The peak height and width of wave 2 can be determined from the resulting wave.

The peak potentials and widths are presented in Table VI. It is obvious that wave 3 shifted to more positive potentials,

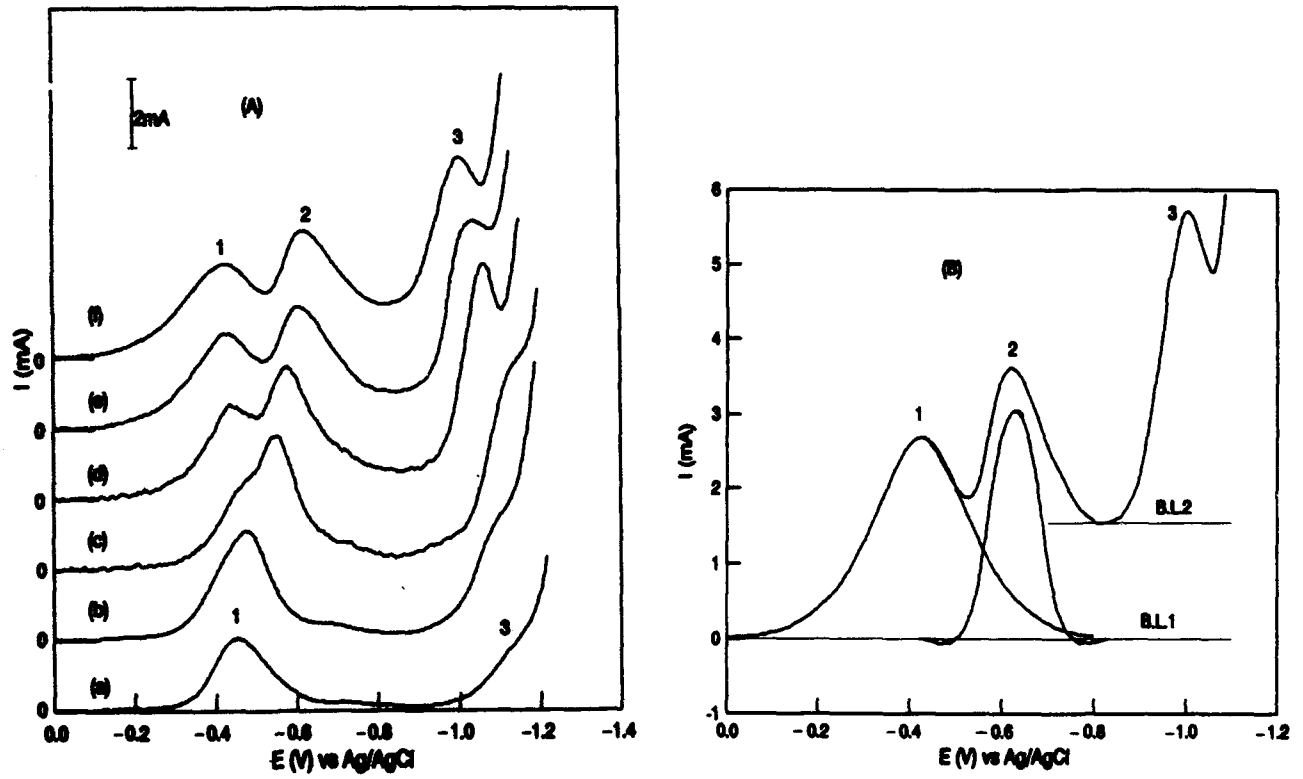

Fig. 8. (A) Net-current square wave voltammograms of tantalum(V) (37.6×10^{-3} mol/kg) in the $NaAlCl_4$-NaF(90-10 m/o) melt at (a) 200, (b) 250, (c) 300, (d) 350, (e) 400, and (f) 450°C. Tungsten electrode area: 0.175 cm^2; step potential: 2 mV; pulse amplitude (E_{sw}): 25 mV; frequency: 10 Hz. (B) Typical separation of wave 1 and wave 2. This voltammogram was obtained at 450°C and 100 Hz; step potential: 2 mV; E_{sw}: 25 mV; B. L. represents the base lines.

Table VI. Flat-current square wave voltammetric data for tantalum(V) (37.6×10^{-3} mol/kg) in the fluorochloro melt.

t(°C)	Frq/Hz	$E_{p/2}$(V)	$W_{(1/2)1}$/(mV)	n_1	$E_{p/2}$(V)	$W_{(1/2)2}$(mV)	n_2	I_{p2}/I_{p1}
200	100	−0.461	83.0	0.95				
200	10	−0.452	70.0	1.13				
250	100	−0.453	84.0	1.04				
250	10	−0.452	68.0	1.29				
300	100	−0.420	110	0.87				
350	100	−0.443	97.0	1.08	−0.555			
350	10	−0.434	72.0	1.45	−0.578	54.0	1.94	1.18
400	100	−0.446	110	1.03	−0.628	56.0	2.02	0.86
400	10	−0.422	90.0	1.25	−0.610	57.0	1.98	1.13
450	100	−0.425	120	1.01	−0.631	59.0	2.06	0.89
450	10	−0.426	120	1.01	−0.628	60.0	2.02	1.17

t(°C)	Frq./Hz		$E_{p/2}$(V)	$W_{1/2}$/(mV)	n_2	I_{p2}/I_{p1}
350	10	B.L.1	−1.058	58.0	1.80	2.47
		B.L.2	−1.058	51.0	2.05	2.17
400	100	B.L.1	−1.080	79.0	1.43	2.32
		B.L.2	−1.08	73.0	1.55	2.08
400	10	B.L.1	−1.040	75.0	1.51	2.19
		B.L.2	−1.038	65.0	1.74	1.85
450	100	B.L.1	−1.023	73.0	1.66	2.31
		B.L.2	−1.023	62.0	1.96	1.84
450	10	B.L.1	−1.002	81.0	1.50	2.13
		B.L.2	−1.002	63.0	1.93	1.63

E_{sw} = 25 mV; ΔE = 2 mV.
n-values were calculated from $W_{1/2} = 1.95\ RT/nF$
$W_{1/2}$: the front peak widths.
B. L.: Base line (see Fig. 8B).

while wave 2 moved in the opposite direction as the temperature was increased. The position of wave 1 was changed only slightly. The peak height ratios of wave 2 over wave 1, I_{p2}/I_{p1}, are close to one although they were slightly higher than one at a low frequency (10 Hz). The ratio of wave 3 to wave 1, I_{p3}/I_{p1}, was found to be between 1.6 and 2.5; it decreased slightly with an increase in temperature. The calculated n-values are given in Table VI. The n-value for wave 1 was close to unity although errors may be produced due to the shoulder observed in the cyclic voltammograms at a lower temperature (<300°C). The number of electrons involved in wave 2 was found to be two and that for wave 3 was between 1.5 and 2.05. These results are in good agreement with those obtained from normal pulse voltammograms (Table V).

Figure 9 shows typical square wave voltammograms for the forward and reverse currents. Three anodic waves were observed corresponding to the three cathodic reduction waves even at a higher temperature while these anodic waves were poorly defined in the cyclic voltammograms (Fig. 5 and 6). This may be due to the fact that the time between reduction and oxidation in square wave voltammetry was so short that only a small amount of the reduced species was consumed by the following chemical reactions. The chemical reaction following the electron charge transfer in wave 2 became faster at a higher temperature (450°C) as indicated by the fact that the anodic wave (wave 2a) almost disappeared at low frequencies (compare Fig. 9c and d).

Exhaustive and controlled-potential electrolyses of Ta(V).—It is clear that the electrochemistry of Ta(V) in these melts is complicated by coupled chemical reactions. Exhaustive coulometry provides additional information on the reduction process since the n-value for each reduction wave can be determined. The electrolyses were conducted both at a lower temperature (*ca.* 200°C) and a higher temperature (450°C) at different potentials. Typical results are summarized in Table VII.

For the first reduction wave at a lower temperature (see Fig. 3), the n-value was found to be approximately 2 when the electrolysis was performed at −0.75 V and 210°C. This result was quite surprising since the value of n = 1 was found from normal pulse and square wave voltammograms as mentioned above. The product dissolved in ethanol or distilled water to give an essentially colorless solution. Only a very weak band with an absorption maximum at *ca.* 330 nm was observed using UV-visible spectroscopy.

The electrolysis at −1.0 V and 205°C was carried out to investigate the last reduction wave (see Fig. 3). The voltammetric changes were monitored by interrupting the electrolysis and using a tungsten working electrode in this cell to record the voltammograms [cyclic voltammograms (CV) and square wave voltammograms (SWV)]. The cyclic voltammograms before the exhaustive electrolysis were identical to those shown in Fig. 3b. The electrolysis current decreased markedly from 70 to 3.6 mA in the first 2 h. It was also noticed that the first reduction wave at the tungsten electrode decreased with time and disappeared after 1.8 h of electrolysis. The n-value at this point was found to be 2.73 which was close to the n-value of 2.67 for reducing Ta(V) to the Ta_6^{14+} cluster. The voltammograms showed a significant change. Typical square wave voltammograms at the tungsten electrode after 1.8 h are shown in Fig. 10a. These voltammograms were very similar to those for a $Ta_6Cl_{12}^{2+}$ cluster coating on a glassy carbon electrode in $AlCl_3$-$NaCl_{sat}$ melt (Fig. 10b). At this point the electrolysis current had decreased to 3.6 mA, and the electrolysis became very slow. We also found that the current of the square wave voltammograms at the tungsten electrode for the tantalum cluster gradually decreased (Fig. 10c). The final n-value was observed to be approximately five. When the electrolysis was completed, the waves for the tantalum cluster disappeared, and the melt became almost colorless.

At a higher temperature, 450°C, the n-values were found to be 1, 5, and 5 for the first, second, and third reduction waves, respectively, from the exhaustive electrolyses at −0.5, −0.75, and −1.0 V *vs.* Ag/AgCl. The melt became greenish and finally colorless in the case of the electrolyses at −0.75 and −1.0 V; the glassy carbon electrodes (crucibles) were coated by a shiny metallic film. This shiny film was identified as metallic tantalum by means of x-ray diffraction.

Additional information for the second reduction wave was extracted from the square wave voltammogram of the melt which had been exhaustively electrolyzed at −0.5 V. The forward width was determined to be 60.2 mV, from which the n-value of 2.02 was obtained. This result was in excellent agreement with that given for this reduction wave in Table VI.

Thick black deposits were formed on small Ni or Pt electrodes by controlled-potential electrolyses in the potential

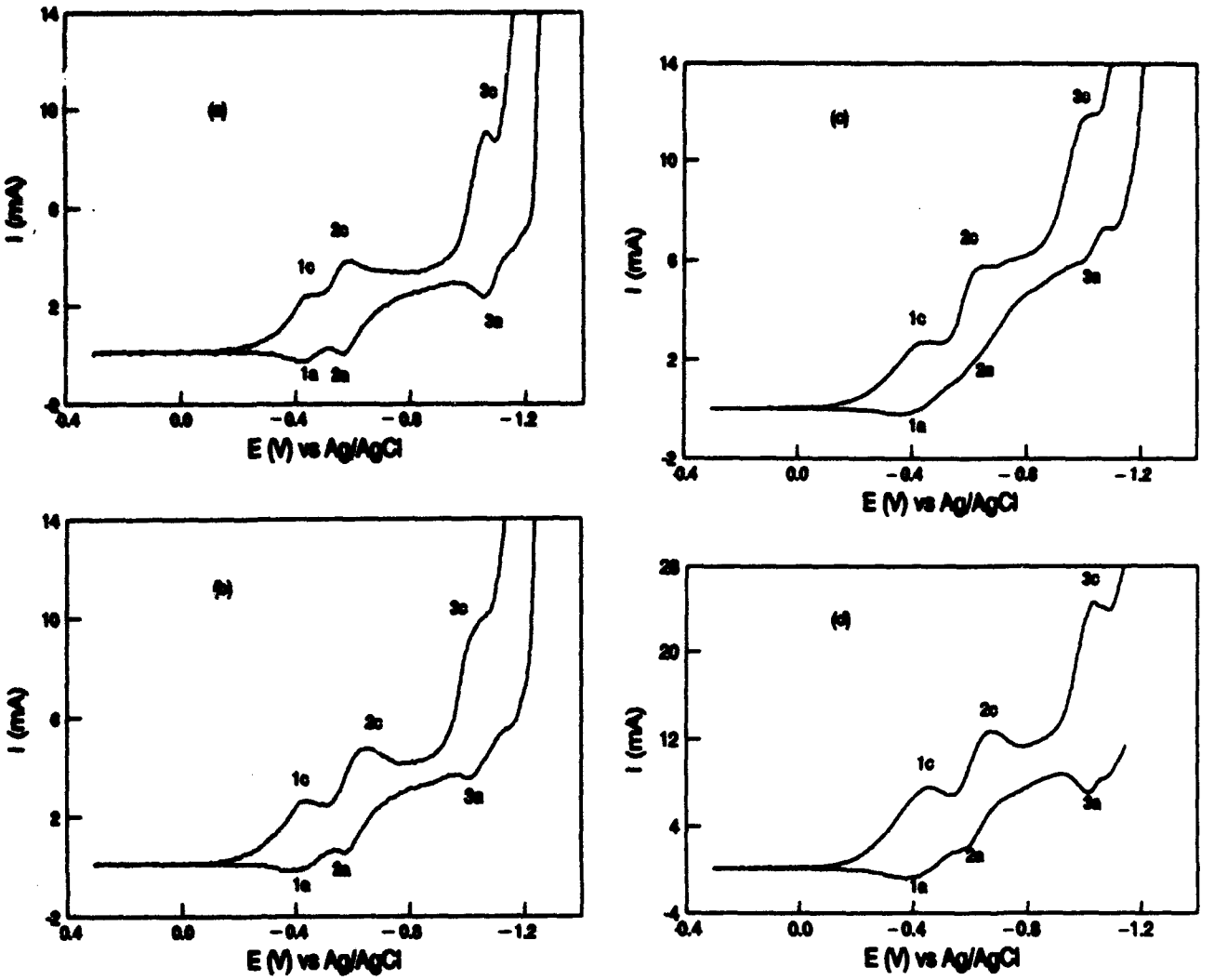

Fig. 9. The forward and reverse current square wave voltammograms of tantalum(V) (37.6×10^{-3} mol/kg) in the $NaAlCl_4$-NaF (90-10 m/o) melt. Tungsten electrode: 0.175 cm^2; step potential: 2 mV; pulse amplitude (E_{sw}): 25 mV. (a) 350°C, 10 Hz; (b) 400°C, 10 Hz; (c) 450°C, 10 Hz; (d) 450°C, 100 Hz.

region of the second and third cathodic waves at a temperature of 450°C. The black deposit which was formed in the third cathodic wave region at 200-450°C, was identified by x-ray diffraction to contain a tantalum cluster (Ta_6Cl_{14}) mixed with the melt. Green aqueous and ethanol solutions were obtained by dissolving this black deposit in distilled water in air and in ethanol under an inert nitrogen atmosphere. Both of these solutions gave the same UV-visible spectrum. Several well-defined absorption maxima were observed at 282, 330, 398, 470, 638, and 748 nm. These data were in excellent agreement with Kahn and McCarley's[2] and our previous results[3] for $Ta_6Cl_{12}^{2+}$ in aqueous solution, indicating that the black deposit formed at the potential region of the third wave contained the $Ta_6Cl_{12}^{2+}$ cluster.

Table VII. Exhaustive electrolysis data for Ta(V) in the $NaAlCl_4$-NaF (90-10 m/o) melt.

Temperature (°C)	E(V) vs. Ag/AgCl	n-value
210	−0.75 (wave 1c)	2.05
205	−1.0 (wave 3c)	2.73,[a] 5.07[b]
450	−0.5 (wave 1c)	0.98
450	−0.75 (wave 2c)	4.95
450	−1.0 (wave 3c)	4.98

[a] This n-value corresponds to the time when no reduction wave of Ta(V) could be observed in the cyclic and square wave voltammograms at a Pt electrode in the same cell.
[b] This n-value was the final value when no waves for the $Ta_6Cl_{12}^{2+}$ cluster from square wave voltammograms were observed.

A black deposit was also formed on small electrodes at the potential region of the second reduction wave at 450°C. When this black deposit was dissolved in ethanol under a nitrogen atmosphere, a greenish yellow solution was produced. These spectra were quite different from that for a $Ta_6Cl_{12}^{2+}$ solution. Several well-defined absorption maxima were obtained at 238, 282, 348, 424, 640, 760, and 826 nm. The main absorption bands were in very good agreement with the results of McCarley *et al.*[2,3] for $Ta_6Cl_{12}^{2+}$ in ethanol: 235, 274, 344, 431, 735, and 826 nm. The small absorption maximum of 640 nm may indicate that the greenish yellow solution also contained a small concentration of $Ta_6Cl_{12}^{3+}$. Therefore, we may conclude that the black deposit formed at the potentials of the second cathodic wave consisted primarily of $Ta_6Cl_{12}^{3+}$ cluster species.

Thin metallic tantalum deposits were also found using ESCA on the surfaces of the small electrodes which were obtained in the potential region of waves 2 and 3 after dissolving the thick black deposits.

Discussion

Based on the results obtained in this work, it appears that the electrochemical reduction of tantalum(V) in fluorochloroaluminate melts is critically dependent on temperature and is complicated by following chemical reactions.

Waves 1, 1c, and 2, 2c.—As seen above, the first and second reduction waves, which are observed at a higher temperature, merge into one reduction wave at lower tempera-

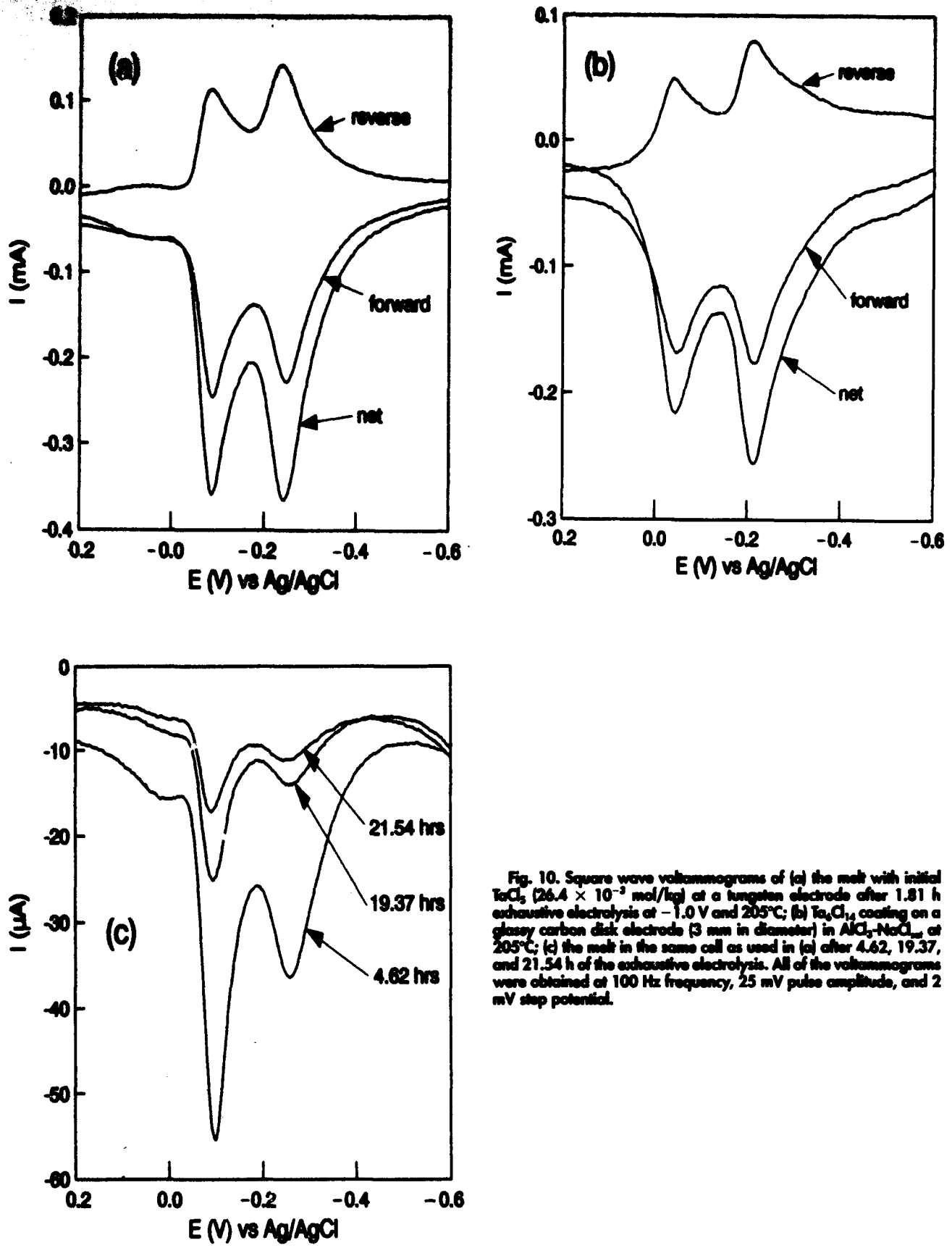

Fig. 10. Square wave voltammograms of (a) the melt with initial $TaCl_5$ (26.4×10^{-3} mol/kg) at a tungsten electrode after 1.81 h exhaustive electrolysis at −1.0 V and 205°C; (b) Ta_6Cl_{14} coating on a glassy carbon disk electrode (3 mm in diameter) in $AlCl_3$-$NaCl_{sat}$ at 205°C; (c) the melt in the same cell as used in (a) after 4.62, 19.37, and 21.54 h of the exhaustive electrolysis. All of the voltammograms were obtained at 100 Hz frequency, 25 mV pulse amplitude, and 2 mV step potential.

tures. Therefore, we discuss these two waves in the same section.

The first reduction wave of tantalum(V) was reasonably well defined in the temperature range 200–450°C, regardless of the voltammetric method. The n-value involved in this reduction wave was determined to be one for the voltammetric time scale at 200–450°C from normal pulse voltammetry (Table V) and square wave voltammetry (Table VI). Also, $n = 1$ was observed for a relatively long time scale at a higher temperature (450°C) based on exhaustive electrolysis (Table VII). Therefore, we conclude that the electron transfer reaction involved in this wave is

the reduction of a Ta^{5+} species (believed to be $TaCl_6^-$) to a Ta^{4+} species

$$Ta^{5+} + e^- = Ta^{4+} \quad [3]$$

for short time scales at 200-450°C and for long time scales at higher temperatures (>300°C).

The presence of a following chemical reaction is indicated by the shift of the peak potential of wave 1c in the positive direction with increasing tantalum(V) concentration. Additional evidence is provided by normal pulse voltammetry. In the normal pulse voltammograms at temperatures >350°C, the height ratios of wave 2 to wave 1 are close to one (see Table V). However, the n-value for wave 2 is determined to be two from both normal pulse and square wave voltammograms. The limiting current of a normal pulse wave should be proportional to n and the reactant concentration.[40] The above results may indicate that the concentration of the product is only about half that of the reactant. Therefore, the following chemical reaction of Ta^{4+} is probably the dimerization reaction of the product as follows

$$2Ta^{4+} = Ta_2^{8+} \quad [4]$$

which occurs slowly at <300°C.

At temperatures lower than 300°C, the differences of the n-value, one in the voltammetric time scale, while two in a long time scale (exhaustive electrolysis, Table VII), also support the existence of the following chemical reaction.

Wave 2 or 2c appeared only as the temperature was increased to 300°C for square wave voltammetry and to 350°C for cyclic and normal pulse voltammetries. The n-value from the slope of the linear relationship of E *vs.* ln $[(I_d - I)/I]$ was found to be two (Table V). Square wave voltammetry also produced an n-value very close to two (Table VI). Based on these results, it is reasonable to suggest that the electron-transfer reaction in the second catnodic wave is a two-electron reduction. A well-defined corresponding oxidation wave (2a) was observed in the square wave voltammograms (Fig. 9) while it was not apparent in the cyclic voltammograms (Fig. 5 and 6). These results indicated that the intermediate product (Ta_2^{6+}) was only stable for a very short time. The trivalent tantalum species was also previously observed to be unstable in the $AlCl_3$-EMIC room temperature melt,[15] and acetonitrile.[14] This wave involved a following chemical reaction, since a large anodic stripping wave (4a) appeared when a delay time was applied at the reversal potential of the second wave (Fig. 6). The presence of a preceding chemical reaction (the dimerization of Ta^{4+}) for the second reduction wave was indicated by the change in the peak height ratios of wave 2 over wave 1 with frequency in the net-current square wave voltammograms; the ratio was greater at 10 Hz than at 100 Hz. These results supported the above assumption about the dimerization reaction of Ta^{4+} (reaction 4). $Ta_6Cl_{12}^{3+}$ cluster species was found in the black deposit from the potential-controlled electrolysis at the potentials of the second wave at 450°C using a small electrode. According to these results, the reaction sequence is proposed to be as follows

$$Ta_2^{6+} + 2e^- = Ta_2^{6+} \quad [5]$$

$$9Ta_2^{6+} = 6Ta^{4+} \text{ (or } 3Ta_2^{8+}) + 2Ta_6^{15+} \quad [6]$$

The trivalent tantalum species (Ta_2^{6+}) became less stable as the temperature was increased as indicated by square wave voltammetry (Fig. 9), *i.e.*, the corresponding anodic wave (2a) was less pronounced with an increase in the temperature and at a lower frequency (10 Hz and 450°C).

The cluster species was slowly reduced to metallic tantalum, since a five-electron transfer was observed (Table VII) and a shiny metallic tantalum film was formed on the glassy carbon crucible (with a large surface area) from exhaustive electrolysis.

At temperatures lower than 300°C the first and the second reduction waves merged together when the temperature was decreased from 450 to 200°C in CV, NPV, and SWV studies. Thus, it is reasonable to propose that the first reduction wave observed at a temperature <300°C is an ECEC process which consists of reactions 3, 4, 5 and 6. In this process, reaction 3 is the main reaction while the occurrence of the remaining reactions is limited due to the slow following reactions 4 and 6. This reaction sequence explains reasonably well the results both from CV, NPV and SWV (short time scale) and the exhaustive electrolysis (long time scale). A similar reduction process was previously proposed to explain the electrochemical behavior of Ta(V) in acidic $AlCl_3$-NaCl melts[5] at temperatures <200°C. However, we also notice that the electrochemical behavior of Ta(V) in $AlCl_3$-$NaCl_{sat}$ and $NaAlCl_4$-NaF (90-10 m/o) melts is different from that in acidic melts. By comparing our present and previous results, two well-separated reduction waves are observed in acidic melts[5] while only one reduction wave appears in basic melts at low temperatures. As mentioned in the introduction, the electrochemical behavior of a tantalum chloride species can be examined only after complete removal of the oxide impurities using $COCl_2$ or CCl_4.

A shoulder (wave 1c') appeared in the cyclic voltammograms at lower temperatures (200 and 250°C) and higher scan rates (Fig. 3 and 4). This shoulder became less significant at lower scan rates or as the tantalum(V) concentration or the temperature was increased. This shoulder may be assigned tentatively to the adsorption of the reduced species according to the theoretical treatments.[41,42]

Wave 3, 3c.—Unlike the second reduction wave which only appeared at temperatures >300 or 350°C, this wave was observed in the whole temperature range studied although the peak height was significantly enhanced as the temperature was increased. The product of the cathodic charge transfer reaction of this wave seemed to be highly unstable since the corresponding oxidation wave (3a) was very small in the cyclic and square wave voltammograms (Fig. 5 and 9). Instead, a large anodic stripping wave composed of waves 4a and 4a' was observed at much more positive potentials (between 0 and 0.4 V). The n-value involved in wave 3 or 3c' was approximately equal to two from square wave voltammograms (Table VI). The electron transfer reaction may be written as follows

$$Ta_2^{6+} + 2e^- = Ta_2^{4+} \quad [7]$$

The smaller and ill-defined voltammetric wave at a lower temperature (<300°C) resulted from the limited formation of Ta_2^{6+} species by the slow following chemical reaction (reaction 4).

The product of this step, the divalent tantalum species, decomposes quickly to form the tantalum cluster Ta_6^{14+} (or $Ta_6Cl_{12}^{2+}$) and metallic tantalum, as indicated by the UV-visible spectra of the black deposit dissolved in ethanol or distilled water and the electron spectroscopy for chemical analysis of the electrodeposited electrode surface. The results of exhaustive electrolysis (Fig. 10) also show the formation of the cluster. The following chemical reaction is proposed

$$7Ta_2^{4+} = 2Ta_6^{14+} + 2Ta^0 \quad [8]$$

The exhaustive electrolysis results in the transfer of five electrons (Table VII) and the formation of metallic tantalum film. Figure 10c also shows further reduction of the tantalum cluster. These results indicate that the Ta_6^{14+} cluster is slowly reduced to metallic tantalum.

Waves 4a and 4a'.—From the discussion above, it is obvious that these two anodic stripping waves are associated with the electrochemical oxidation of the tantalum clusters, Ta_6Cl_{15} and Ta_6Cl_{14}, formed in the second and third reduction waves (Fig. 5 and 6).

Acknowledgments

This work was supported by the U.S. Air Force Office of Scientific Research, Grants No. 88-0307 and No. F49620-93-1-0129.

Manuscript submitted Feb. 18, 1993; revised manuscript received May 12, 1993.

The University of Tennessee assisted in meeting the publication costs of this article.

REFERENCES

1. R. J. H. Clark and D. Brown, *The Chemistry of Vanadium, Niobium and Tantalum*, Pergamon Press, New York (1973).
2. P. J. Kahn and R. E. McCarley, *Inorg. Chem.*, **4**, 1482 (1965).
3. P. B. Fleming and R. E. McCarley, *ibid.*, **9**, 1347 (1970).
4. J. G. Converse, J. B. Hamilton, and R. E. McCarley, *ibid.*, **9**, 366 (1970).
5. J. H. von Barner, L. E. McCurry, C. A. Jørgensen, N. J. Bjerrum, and G. Mamantov, *ibid.*, **31**, 1034 (1992).
6. T. M. Laher, L. E. McCurry, and G. Mamantov, *Anal. Chem.*, **57**, 500 (1985).
7. G. W. Mellors and S. Senderoff, *This Journal*, **112**, 266 (1965).
8. S. Senderoff, G. W. Mellors, and W. J. Reinhart, *ibid.*, **122**, 840 (1965).
9. S. Senderoff and G. W. Mellors, *Science*, **153**, 1475 (1966).
10. V. I. Konstantinov, E. G. Polyakov, and P. T. Stangrit, *Electrochim. Acta*, **23**, 713 (1978).
11. T. Suzuki, *ibid.*, **15**, 127 (1970).
12. F. Lantelme, A. Barhoun, G. Li, and J. P. Besse, *This Journal*, **139**, 1249 (1992).
13. R. A. Bailey, E. N. Balko, and A. A. Nobile, *J. Inorg. Nucl. Chem.*, **37**, 971 (1975).
14. D. E. Lighter, Jr., J. R. Kirk, and V. Katovic, *J. Coord. Chem.*, **19**, 223 (1988).
15. P. A. Barnard and C. L. Hussey, *This Journal*, **137**, 913 (1990).
16. R. Huglen, F. W. Poulsen, G. Mamantov, and G. M. Begun, *Inorg. Chem.*, **18**, 2551 (1979).
17. L. E. McCurry, Ph.D. Dissertation, University of Tennessee, Knoxville, TN (1978).
18. R. W. Berg, E. Kemnitz, H. A. Hjuler, R. Fehrmann, and N. J. Bjerrum, *Polyhedron*, **4**, 457 (1985).
19. R. G. Kidd and D. R. Truax, *J. Am. Chem. Soc.*, **90**, 6867 (1968).
20. D. E. H. Jones, *J. Chem. Soc., Dalton Trans.*, 567 (1972).
21. B. Gilbert, S. D. Williams, and G. Mamantov, *Inorg. Chem.*, **27**, 2359 (1988).
22. N. Sato, K. D. Sienerth, and G. Mamantov, In preparation.
23. G. Ting, Ph.D. Dissertation, University of Tennessee, Knoxville, TN (1973).
24. I. W. Sun, K. D. Sienerth, and G. Mamantov, *This Journal*, **138**, 2650 (1991).
25. H. Linga, Z. Stojek, and R. A. Osteryoung, *J. Am. Chem. Soc.*, **103**, 3754 (1981).
26. G.-S. Chen, I. W. Sun, K. D. Sienerth, A. G. Edwards, and G. Mamantov, *This Journal*, **140**, 1523 (1993).
27. V. Taranenko, K. D. Sienerth, N. Sato, A. G. Edwards, and G. Mamantov, *Mater. Sci. Forum*, **73-75**, 595 (1991).
28. J. M. Saveant and E. Vianello, *Electrochim. Acta*, **12**, 1545 (1967).
29. C. P. Andrieux, L. Nadjo, and J. M. Saveant, *J. Electroanal. Chem.*, **26**, 147 (1970).
30. J. B. Flanagan, K. Takahashi, and F. C. Anson, *ibid.*, **81**, 261 (1977).
31. Southampton Electrochemistry Group, *Instrumental Methods in Electrochemistry*, p. 220, Ellis Horwood Limited, Chichester (1985).
32. L. Ramaley and M. S. Krause, Jr., *Anal. Chem.*, **41**, 1362 (1969).
33. M. S. Krause, Jr., and L. Ramaley, *ibid.*, **41**, 1365 (1969).
34. J. G. Osteryoung and R. A. Osteryoung, *ibid.*, **57**, 101A (1985).
35. J. H. Christie, J. A. Turner, and R. A. Osteryoung, *ibid.*, **49**, 1899 (1977).
36. J. A. Turner, J. H. Christie, M. Vukovic, and R. A. Osteryoung, *ibid.*, **49**, 1904 (1977).
37. J. J. O'Dea, J. G. Osteryoung, and R. A. Osteryoung, *ibid.*, **53**, 695 (1981).
38. J. Zeng and R. A. Osteryoung, *ibid.*, **58**, 2766 (1986).
39. D. L. Manning and G. Mamantov, *Electrochim. Acta*, **19**, 177 (1974).
40. A. J. Bard and L. R. Faulkner, *Electrochemical Methods*, John Wiley & Sons, Inc., New York (1980).
41. R. H. Wopschall and I. Shain, *Anal. Chem.*, **39**, 1514 (1967).
42. M. H. Hulbert and I. Shain, *ibid.*, **42**, 162 (1970).

Reprinted from JOURNAL OF THE ELECTROCHEMICAL SOCIETY
Vol. 140, No. 10, October 1993
Printed in U.S.A.
Copyright 1993

Spectroscopic and Electrochemical Studies of Tungsten(VI) and Tungsten(V) Chloride and Oxychloride Complexes in a Sodium Chloride Saturated Sodium Chloroaluminate Melt

I.-Wen Sun,* Anna G. Edwards, and Gleb Mamantov*

Department of Chemistry, The University of Tennessee, Knoxville, Tennessee 37996-1600

ABSTRACT

Raman and UV-visible absorption spectroscopies indicate that the addition of WCl_6 or $KWCl_6$ to a sodium chloride saturated sodium chloroaluminate melt at 175°C produces the tungsten(V) hexachloride anion $[WCl_6]^-$. The production of $[WCl_6]^-$ from WCl_6 may be attributed to the chemical reduction of the latter by the free chloride ion in this melt. $[WCl_6]^-$ can be oxidized to WCl_6 via a reversible one-electron charge-transfer process with a voltammetric half-wave potential of 2.077 V referenced to aluminum in a pure sodium chloride saturated sodium chloroaluminate melt. With fast scan rate voltammetry, $[WCl_6]^-$ can be reduced to $[WCl_6]^{2-}$ and $[WCl_6]^{3-}$ via two consecutive one-electron reduction processes with half-wave potentials of 1.578 and 0.818 V, respectively. Both $[WCl_6]^{2-}$ and $[WCl_6]^{3-}$ form precipitates in this melt at this temperature. Using slow scan rate voltammetry, the reduction processes are complicated by coupled chemical reactions. Tungsten(VI) oxychloride, $WOCl_4$, is stable in this melt, and can be reduced to tungsten(V) oxychloride via a reversible one-electron reduction process with a half-wave potential of 1.746 V. Absorption spectroscopy shows that the tungsten(V) chloride is $[WOCl_5]^{2-}$. Fast scan rate voltammetry indicates that tungsten(V) oxychloride exhibits a two-electron reduction process to produce a W(III) species. At slow scan rates, the reduction appears to be complicated by coupled chemical reactions. Definitive characterization of the reduction mechanisms is prevented by film formation on the electrode surface during these reductions.

Tungsten exhibits a wide variety of oxidation states, ranging from +6 to 0; some of these states involve cluster species such as W_6Cl_{12}. A few years ago we reported the results of electrochemical and spectroscopic studies of tungsten hexachloride in $AlCl_3$-NaCl [63 mole percent (*m/o*) $AlCl_3$] melt at temperatures of 150 and 175°C.[1] W(VI) was involved in an equilibrium between two electroactive species, the hexachloride, WCl_6, and the oxide tetrachloride, $WOCl_4$. Several reduction steps were observed for WCl_6 before the cathodic limit of the solvent; only the first step resulting in the formation of WCl_5 was investigated in detail.[1]

It is well known that the chemistry and the electrochemistry of some elements, including tungsten, are influenced significantly by the modified Lewis acidity of the chloroaluminate solvent system.[2] It has been realized in recent years that even the purest alkali chloroaluminates contain millimolar quantities of complexed oxides which may result from the interaction of some melts with Pyrex glass. Therefore, we have developed methods for the removal of oxide from alkali chloroaluminate melts based on the treatment of melts with phosgene, $COCl_2$, and carbon tetrachloride, CCl_4.[3,4]

In prior studies of W(VI) electrochemistry and spectroscopy in basic $AlCl_3$-NaCl ($AlCl_3$/NaCl mole ratio < 1) melts, oxide contamination could not be entirely avoided.[5,6] Therefore, we have reexamined the chemistry of W(VI) and of the lower oxidation states of tungsten in $AlCl_3$-NaCl melts saturated with NaCl which have been treated with either $COCl_2$[3] or CCl_4.[4] The results of this work are reported below.

Of direct relevance to this study is the work of Scheffler and Hussey[7] who have shown that when either WCl_6 or $KWCl_6$ is dissolved in basic aluminum chloride-1-methyl-3-ethylimidazolium chloride ($AlCl_3$-MEIC), $[WCl_6]^-$ is obtained, and this species can be reduced to $[WCl_6]^{2-}$ and $[WCl_6]^{3-}$ via two consecutive reversible one-electron reduction processes. The metal-bonded tungsten(III) dimer, $[W_2Cl_9]^{3-}$, is also stable in this melt and can be oxidized to $[W_2Cl_9]^{2-}$, which disproportionates slowly to $[WCl_6]^{2-}$ and a tungsten(III) species, which in turn is oxidized to $[WCl_6]^{2-}$ at the same potential as that for the oxidation of $[W_2Cl_9]^{3-}$. The addition of oxide to this melt did not cause any change in the observed electrochemical behavior of the tungsten species studied.

Other work on tungsten species in $AlCl_3$-NaCl melts has involved the formation of the cluster species $W_6Cl_8^{4+}$ by the reduction of WCl_6 with aluminum metal at approximately 450°C in acidic ($AlCl_3$-rich) melts[8] and the formation of a reduced cluster (oxidation state between +2 and 0) by the electroreduction of W_6Cl_{12} in acidic $AlCl_3$-NaCl melts.[9]

Relatively few studies of the electrochemistry of tungsten chlorides in other molten salt systems have been reported. Several investigations of the electrochemical behavior of different tungsten chlorides in molten LiCl-KCl[10-14] have been published. For example, Zuckerbrod[13] reported that W(V) can be reversibly reduced to W(IV), which can be reduced further to W(II) in the LiCl-KCl eutectic, while Sequeira[14] claimed that W(V) was reduced to W(III) in the same melt. Katagiri *et al.*[15] have obtained coherent metallic tungsten deposits from the $ZnCl_2$-NaCl melt through the reduction of WCl_6 at 450°C.

Experimental

Dry box system.—Because of the air- and moisture-sensitive nature of the tungsten compounds and of the molten salts used, these materials were handled under a nitrogen atmosphere inside a Vacuum Atmospheres dry box equipped with a dry train/oxygen removal column. The

* Electrochemical Society Active Member.
* Present address: National Cheng Kung University, Taiwan, China.

moisture level inside this dry box was typically less than 2 ppm.

Chemicals.—The aluminum chloride was obtained from Fluka (anhydrous, 99%) and purified twice by sublimation at 210°C. The sodium chloride was obtained from Fisher Scientific and was dried under vacuum at 450°C for 4 days. The chloroaluminate melts were prepared by mixing the appropriate amounts of aluminum chloride and sodium chloride. Pieces of aluminum metal (AESAR, 99.999%) were added to the melt to remove the base metal impurities in the melt. Finally, the melts were treated with $COCl_2$ [3] or with CCl_4 [4] to remove oxide impurities.

Tungsten hexachloride, WCl_6, and tungsten oxide tetrachloride, $WOCl_4$, were obtained from Aldrich (99+%) and purified by sublimation at 180 and 110°C, respectively. WCl_4 was obtained from Aldrich (97%) and used without further purification. Potassium hexachlorotungstate(V), $KWCl_6$, potassium hexachlorotungstate(IV), K_2WCl_6, and tripotassium nonachloroditungstate(III), $K_3W_2Cl_9$, were synthesized following the procedures described previously.[5]

Electrochemical measurements.—The electrochemical cell contained four electrodes. A glassy carbon disk (with a geometric area of 0.071 cm^2) served as the working electrode. The counterelectrode was an aluminum spiral which was immersed in a pure $AlCl_3$-$NaCl_{sat}$ melt separated from the bulk solution with a fine porosity frit. The use of an aluminum spiral as the counterelectrode was critical for exhaustive controlled potential electrolysis experiments; the use of other metals such as platinum or tungsten led to unsatisfactory results. A small hole at the top of the counterelectrode above the melt balanced the pressure between the counterelectrode compartment and the bulk cell compartment. The reference electrode consisted of an aluminum wire immersed in an $AlCl_3$-$NaCl_{sat}$ melt and sealed in a thin Pyrex bulb. A platinum wire directly immersed in the bulk melt was used as a quasi-reference electrode. During the electrochemical experiments, the potentials were referenced to the platinum quasi-reference electrode, since the resistance across the Pyrex membrane of the reference electrode was very high. After each experiment, the potential was corrected with respect to the aluminum reference electrode by measuring the open-circuit potential between the aluminum reference electrode and the platinum quasi-reference electrode. The entire electrochemical cell was heated in a furnace and the temperature was controlled at 175°C unless otherwise specified.

Electrochemical experiments were performed with Princeton Applied Research (PAR) Model 273 potentiostat/galvanostat controlled with an IBM PC and PAR M270 software.

Raman spectra.—Raman spectra were acquired with a scanning Jobin-Yvon 2000M 1 m focal length double monochromator. Scanning was controlled by an Instruments S. A. (ISA) 980015 Controller. The excitation wavelength was the 488.0 or 514.5 nm line from a Coherent Innova Model I100-15 argon ion laser. The tungsten compounds produced highly colored solutions which were somewhat difficult to analyze by conventional 90° scattering. Although the laser beam path was 90° to the collection lens of the monochromator, scattering from the front surface of the square cell, taking care to direct the specular reflectance away from the collection lens, produced the best signals. The laser power was typically set to 200 mW. The monochromator slits were set to give a bandpass of 3 cm^{-1}. Raman signals were detected by an RCA C31034A photomultiplier tube mounted in a Products for Research thermoelectrically cooled photomultiplier tube (PMT) housing. The PMT output was connected to a Pacific Instruments amplifier/discriminator for pulse shaping for photon counting by a Pacific Instruments Model 126 Photometer. A trigger on the ISA controller controlled data acquisition by a Keithley Metrabyte CDAS-8PGA plugged into an IBM PS/2 Model 55SX computer. The software was written by Professor Bernard Gilbert at the University of Liege.

Spectroscopic measurements.—Absorption spectra in the UV-visible region were recorded with a Hewlett Packard 8452A diode array spectrophotometer. While $COCl_2$ or CCl_4 treatment helped to minimize the oxide level in the chloroaluminate melts, millimolar oxide concentration remained even after the treatment. Therefore, a sufficient amount of the appropriate tungsten compound was added to the melt to ensure that the relative concentration of oxotungstate species produced was much lower than the concentration of the analyte. The resulting solutions required narrow spectroscopic cells. The shorter paths were achieved by placing a 0.9 mm wide quartz insert into a 1 mm pathlength quartz cell.

Results and Discussion

WCl_6 and $KWCl_6$.—The addition of either WCl_6 or $KWCl_6$ to the $AlCl_3$-$NaCl_{sat}$ melt at 175°C produced a yellow solution. Upon cooling, the frozen solutions turned blackish green, a color similar to that of solid $KWCl_6$. Raman spectra of these solutions are illustrated in Fig. 1. The observed band frequencies of the stronger bands of the tungsten species are listed in Table I. The Raman spectrum for the pure melt in Fig. 1d exhibits bands at 120, 184, 350, and 490 cm^{-1}. Figure 1b shows the Raman spectrum of 98.9 m*M* $KWCl_6$ in $AlCl_3$-$NaCl_{sat}$. In addition to melt bands, only one major band at 394 cm^{-1} is present. This band can be assigned to the ν_1 vibration of $[WCl_6]^{1-}$. [16] The Raman spectrum of 100.3 m*M* WC_6 in $AlCl_3$-$NaCl_{sat}$ is shown in Fig. 1a. Two bands at 394 and 410 cm^{-1} are observed along with the solvent bands. Tanemoto *et al.* [6] previously reported a band for WCl_6 in $AlCl_3$-$NaCl_{sat}$ at 410 cm^{-1} which was attributed to the ν_1 vibration of WCl_6. These results were supported by the results of other Raman studies of WCl_6.[17] However, the concentration of W(VI) examined in this study was lower than the solution concentration studied by Tanemoto *et al.* [6]

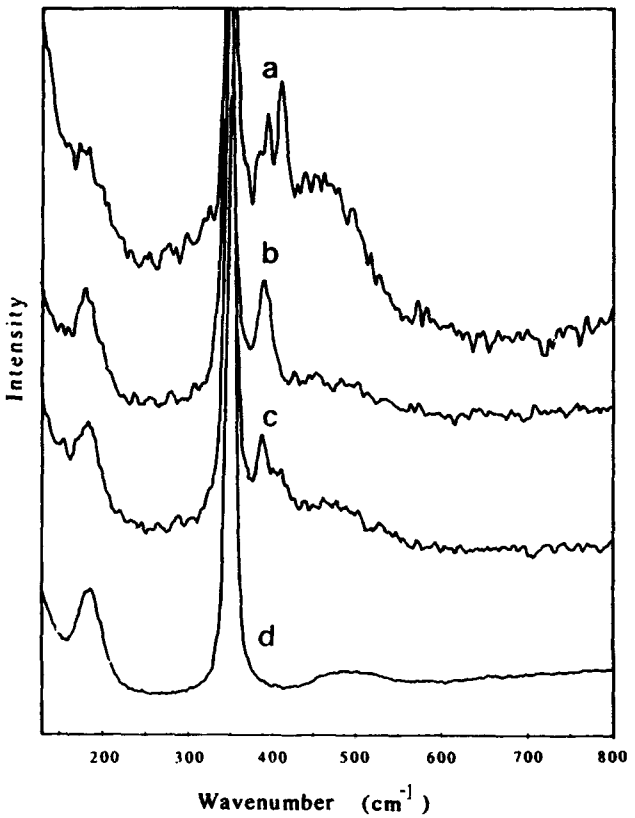

Fig. 1. Raman spectra of tungsten chlorides dissolved in the $AlCl_3$-$NaCl_{sat}$ melt at 175°C: (a) 100.3 m*M* of WCl_6, (b) 98.9 m*M* of $KWCl_6$, (c) 98.1 m*M* of WCl_6 with excess amount of NaCl, and (d) pure $AlCl_3$-$NaCl_{sat}$ melt.

Table I. Raman spectroscopic data for the strong bands of tungsten complexes.

Species	Wave numbers	Ref.
WCl_6 in $AlCl_3$-NaCl (63-37 m/o) 238°C	410 s (ν_1)	6
WCl_6 solid	410 s (ν_1)	17
WCl_6 in CH_3NO_2	437 s (ν_1)	22
WCl_6 in $AlCl_3$-$NaCl_{sat}$	394 m, 410 s	this work[a]
WCl_6 in $AlCl_3$-$NaCl_{sat}$ with excess NaCl	394 m	this work[b]
$KWCl_6$ in $AlCl_3$-$NaCl_{sat}$	394 m	this work[c]
$[WCl_6]^-$	382 m (ν_1)	16
$WOCl_4$	411 m (ν_1)	this work

[a] Figure 1a.
[b] Figure 1c.
[c] Figure 1b.
Abbreviations: s, strong; m, medium.

Table II. Absorption Spectroscopic Data for Tungsten Complexes.

Solute	Solvent	λ_{max}, nm	Ref.
WCl_6	vapor	225(m), 275(sh), 330(s), 375(sh), 430(w)	1
WCl_6	basic $AlCl_3$-MEIC	275(sh), 299(s), 347(m), 390 (sh)	7
$KWCl_6$	basic $AlCl_3$-MEIC	275(sh), 298(s), 350(m), 390(sh)	7
$KWCl_6$	CH_3CN	246(m), 275(sh), 297(s), 347(m), 390(sh)	7
WCl_6	$AlCl_3$-$NaCl_{sat}$	288(s), 338(m)	this work
$KWCl_6$	$AlCl_3$-$NaCl_{sat}$	288(s), 338(m)	this work
$WOCl_4$	vapor	220(s), 250(sh), 270(sh), 355(s), 460(w)	1
$WOCl_4$	toluene	355(s)	23
$WOCl_4$	$AlCl_3$-NaCl (63-37 mol%)	228(s), 360(s)	4
$WOCl_4$	$AlCl_3$-$NaCl_{sat}$	230(s), 360(s), 460(w)	this work
Cs_2WOCl_5	$HCl_{(aq)}$	225(s), 269(s), 305(sh), 397(w), 704(vw)	21
$KWCl_6$	$AlCl_3$-$NaCl_{sat}$ excess Na_2CO_3	268(s), 306(sh)	this work

Abbreviations: s, strong; sh, shoulder; w, weak; vw, very weak.

The most likely species giving rise to the band at 394 cm^{-1} is $[WCl_6]^{1-}$ by comparison with the results for $KWCl_6$ in solution. These results suggest that WCl_6 must have reacted with the melt to produce $[WCl_6]^{1-}$. It is likely that WCl_6 was reduced by the free Cl^- ions in the melt. Consequently, the conversion of WCl_6 to $[WCl_6]^{1-}$ depends upon the concentration of available Cl^- ion in the melt. In a typical $AlCl_3$-$NaCl_{sat}$ melt, the Cl^- concentration is normally about 30 m*M*, [18] and thus not all of the WCl_6 that was added to the melt in Fig. 1a can be reduced to $[WCl_6]^{1-}$. When an $AlCl_3$-$NaCl_{sat}$ melt containing 98.1 m*M* WCl_6 was treated with an excess amount of NaCl to ensure that sufficient Cl^- was available, and kept molten at 200°C for 72 h, the Raman spectrum shown in Fig. 1c was obtained. The decrease in the intensity of the 410 cm^{-1} band along with an increase in the 394 cm^{-1} band with the addition of excess chloride supports the argument that chloride ion reacted in solution with WCl_6 to produce $[WCl_6]^{1-}$. It is apparent from this figure that the band at 410 cm^{-1} was reduced significantly while the band at 394 cm^{-1} was increased.

UV-visible absorption spectra were obtained for solutions prepared by dissolution of either WCl_6 or $KWCl_6$ in $AlCl_3$-$NaCl_{sat}$ melt. These spectra are shown in Fig. 2. The wavelengths and relative intensities observed in this figure are compiled in Table II. The spectra of the WCl_6 and $KWCl_6$ solutions are essentially identical to one another. Furthermore, they are similar to the spectra reported for $[WCl_6]^{1-}$ ion dissolved in the basic $AlCl_3$-MEIC room-temperature melt.[7] The spectra for wavelengths shorter than 240 nm are not included for these solutions, since the UV cutoff of the melt occurs near this wavelength. Nevertheless, these results strongly support the Raman results; *i.e.*, WCl_6 dissolved in $AlCl_3$-$NaCl_{sat}$ exists as ionic $[WCl_6]^{1-}$ instead of molecular WCl_6, provided that there is sufficient Cl^- ion in the melt. The conversion of WCl_6 to $[WCl_6]^{1-}$ has been reported previously in the basic $AlCl_3$-MEIC melt.[7] In addition, this type of chemical reduction has been observed for molybdenum(VI) compounds in the $AlCl_3$-$NaCl_{sat}$ melt.[19]

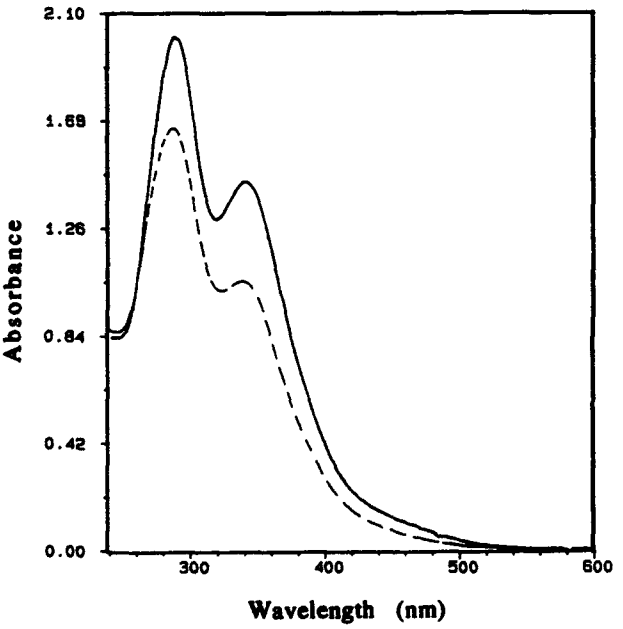

Fig. 2. Absorption spectra of tungsten(V) in $AlCl_3$-$NaCl_{sat}$ melt at 175°C: (—) 18.7 x 10^{-3} M $KWCl_6$ (vs. pure melt); (- - -) 11.0 × 10^{-3} M WCl_6.

Slow scan rate cyclic voltammograms of solutions prepared by the dissolution of WCl_6 in $AlCl_3$-$NaCl_{sat}$ were obtained at a glassy carbon disk electrode. These voltammograms are essentially the same as those obtained for solutions of $KWCl_6$ under the same conditions. The similarity of these voltammograms again supports the contention that addition of WCl_6 to the $AlCl_3$-$NaCl_{sat}$ melt produces the $[WCl_6]^{1-}$ ion. Illustrated in Fig. 3 is a typical cyclic voltammogram for an $AlCl_3$-$NaCl_{sat}$ melt containing $[WCl_6]^-$. The rest potential of the glassy carbon working electrode immersed in this solution is *ca.* 1.850 V. When the cyclic voltammogram is slowly scanned in the positive direction from the rest potential, one oxidation wave, Wave 1a, with a peak potential of 2.125 V is observed. This oxidation wave exhibits a reverse reduction wave, Wave 1c. The average peak potential separation, ΔE_p, of this wave over the range of scan rates from 0.02 to 0.5 V/s is 0.092 V at 175°C. This value is in excellent agreement with the theoretical value of approximately 0.089 V expected for a reversible, one-electron electrode reaction at this temperature. In addition, the peak current ratio, i_p^c/i_p^a, which was calculated using Nicholson's empirical method,[20] varies from 1.0 to 0.98 over this range of scan rates. The peak current function, $i_p^a/v^{1/2}$, where v is the scan rate, was essentially constant for a series of voltammograms that were recorded over this same range of scan rates. The half-wave potential, $E_{1/2}$, which was calculated using the equation $E_{1/2} = (E_p^a + E_p^c)/2$, for these voltammograms, was basically constant with an average value of 2.076 V. The limiting oxidation current, i_l, from the normal pulse voltammetric data in Fig. 4a was used to prepare a plot of log $[(i_l - i)/i]$ *vs.* E. A linear plot was produced. The $E_{1/2}$ determined from the intercept of this plot was 2.079 V, and the n value calculated from the slope of this plot was 1.04. These results suggest that oxidation Wave 1a corresponds to the reversible one-electron charge-transfer process

$$[WCl_6]^{1-} \rightleftarrows WCl_6 + e^-$$

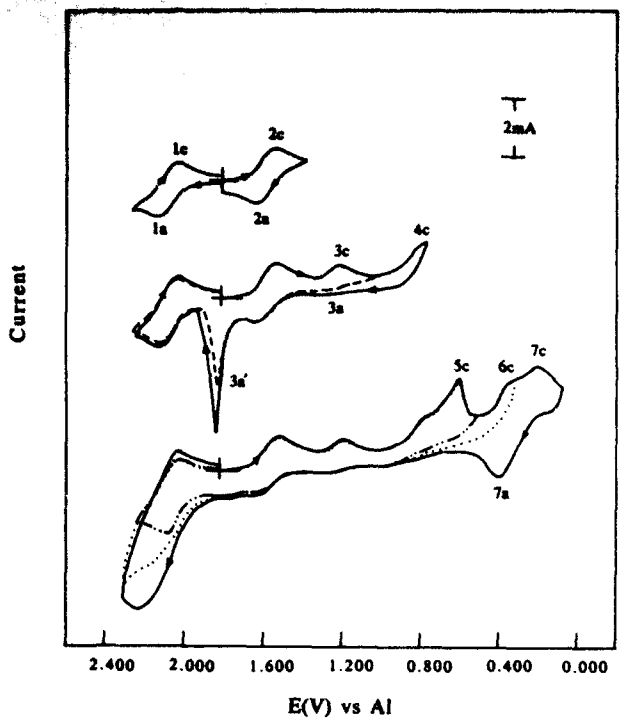

Fig. 3. Cyclic voltammograms of 18.1 × 10^{-3}M WCl_6 at a glassy carbon electrode in $AlCl_3$-$NaCl_{sat}$ melt at 175°C. Scan rate was 0.020 V/s.

where the product WCl_6 is stable on the voltammetric time scale but reacts slowly with the melt to produce $[WCl_6]^{1-}$.

Figure 3 shows that when cyclic voltammograms were scanned in the negative direction from the rest potential, one reduction wave (Wave 2c), with a peak potential of 1.527 V, and three closely spaced reduction waves at 1.198 V (Wave 3c), 0.766 V (Wave 4c) and 0.606 V (Wave 5c) followed by a shoulder (Wave 6c) on a large wave (Wave 7c) at 0.185 V were observed.

The reduction Wave 2c is associated with a reverse oxidation wave (Wave 2a). Analysis of this reduction wave suggests that it corresponds to a one-electron reversible charge-transfer process on the voltammetric time scale;

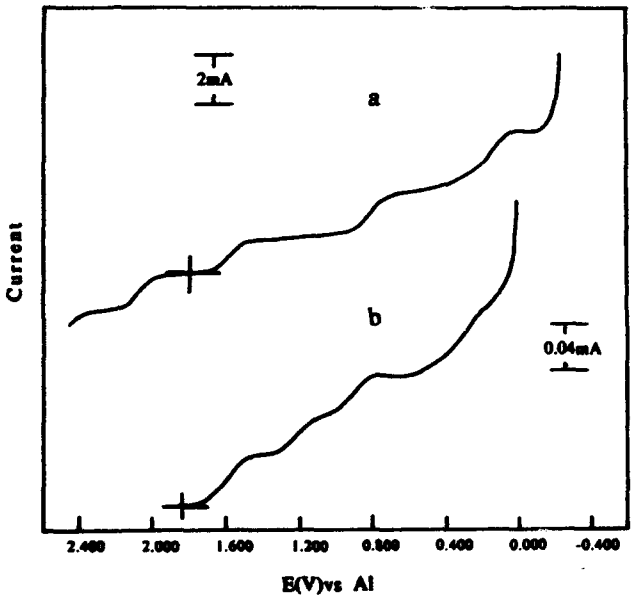

Fig. 4. Normal pulse voltammograms of 18.1 × 10^{-3}M WCl_6 at a glassy carbon electrode in $AlCl_3$-$NaCl_{sat}$ melt at 175°C: (a) pulse width was 0.02 s; (b) pulse width was 5 s.

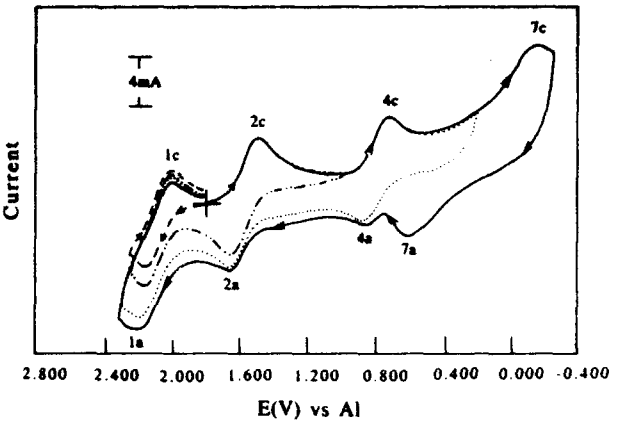

Fig. 5. Cyclic voltammogram of 18.1 × 10^{-3}M WCl_6 at a glassy carbon electrode in $AlCl_3$-$NaCl_{sat}$ melt at 175°C. Scan rate was 40.0 V/s.

i.e., the average ΔE_p is about 0.089 V, i_p^a/i_p^c is essentially 1.0, the cathodic peak current is linearly proportional to the square root of the scan rate, and $E_{1/2}$ is constant with an average value of 1.576 V over the scan rate range 0.02 V/s to 0.5 V/s. In addition, plots of log $[(i_l - i)/i]$ *vs.* E for the first reduction wave in Fig. 4a and 4b were linear giving an average $E_{1/2}$ value of 1.580 V and an n-value of 0.97. Therefore, reduction Wave 2c appears to arise from the following reaction

$$[WCl_6]^{1-} + e^- \rightleftarrows [WCl_6]^{2-}$$

Exhaustive controlled potential reduction experiments were performed with solutions of $[WCl_6]^{1-}$ at an applied potential of 1.400 V at a glassy carbon plate electrode in an attempt to determine if $[WCl_6]^{2-}$ was completely stable in the $AlCl_3$-$NaCl_{sat}$ melt. Based on the initial number of moles of $[WCl_6]^{1-}$ present in the solution and on the total charge consumed during the electrolysis, the n-value for this reduction was essentially one. This result is in agreement with cyclic voltammetric and normal pulse voltammetric data. At the end of the electrolysis, a dark purple precipitate was present on the bottom of the electrochemical cell along with a faint pink solution. When the solution was allowed to sit overnight, the pink color disappeared. This result indicates that the $[WCl_6]^{2-}$ complex ion is either insoluble or unstable in the melt. The attempted dissolution of K_2WCl_6 or WCl_4 in the $AlCl_3$-$NaCl_{sat}$ melt also produces a dark purple precipitate.

At slow scan rates the reduction Waves 3c to 7c in Fig. 3 become complicated. The electrochemical behavior of these waves depends upon the switching potentials and scan rates. If the direction of the potential scan is switched right after Wave 3c, a small reverse oxidation Wave 3a and a symmetric sharp stripping oxidation wave, Wave 3a', are observed. This anodic stripping wave disappears if the cathodic potential scan is switched after Wave 5c. The reduction Wave 5c also exhibits a peak-shaped character. It was observed that when the scan rate was increased, the peak currents for Waves 3c, 5c, and 3a' decreased but the peak current for Wave 4c increased. These results suggest that at slow scan rates, the reduction product of Wave 2c undergoes a chemical reaction to give some compound which is reduced at Wave 3c. The product of Wave 3c may be deposited (or adsorbed) on the electrode surface and this deposit could be reoxidized at Wave 3a' or further reduced at Wave 5c. As the scan rate is increased, the chemical reaction following Wave 2c becomes less favorable, thus resulting in the decrease in the peak currents of Waves 3c, 3a', and 5c. The reduction Wave 4c may be due to the reduction of the product of Wave 2c. At scan rates higher than 10 V/s, the voltammograms are greatly simplified; *i.e.*, Waves 3c, 3a', and 5c essentially disappear, and Wave 4c becomes much more prominent. Figure 5 shows the cyclic voltammogram obtained at a scan rate of 40 V/s, the practical scan

limit of our experimental system. It can be seen that Wave 4c is associated with an anodic Wave 4a. The peak current of Wave 4c is approximately equal to that of Wave 2c and/or Wave 1a. Also, the peak potential separation between Waves 4c and 4a is essentially equal to that between Waves 2c and 2a. The larger peak potential separation for the cyclic voltammograms obtained at these high scan rates may arise from the uncompensated IR drop. Although the peak potential separation increases with scan rate, $E_{1/2}$, calculated over the scan rate range of 10 to 40 V/s is essentially constant with an average value of 0.810 V. Figure 4a shows that normal pulse voltammogram for a solution containing $[WCl_6]^-$ at a short pulse width. In this figure the magnitude of the limiting current of Wave 4c is essentially the same as that of Wave 2c. The plot of log $[(i_l - i)/i]$ *vs.* E, which utilized the data obtained from this figure for Wave 4c, is linear. The slope of this plot gives an n value of 0.99 and the intercept of this plot gives an $E_{1/2}$ of 0.826 V. Taken together, these results indicate that at high scan rates, Wave 4c is due to a reversible, one-electron charge-transfer process. This reaction may be expressed as

$$[WCl_6]^{2-} + e^- \rightleftarrows [WCl_6]^{3-}$$

Exhaustive controlled potential reduction experiments were performed for $AlCl_3$-$NaCl_{sat}$ melts containing $[WCl_6]^-$ at a glassy carbon plate electrode with the potential controlled at 0.75 V. The charge consumed by this reduction revealed an n-value of two indicating that $[WCl_6]^-$ was reduced to $[WCl_6]^{3-}$. When the reduction was completed, the solution turned clear and a dark precipitate was observed on the bottom of the cell indicating that $[WCl_6]^{3-}$ was converted to an insoluble species. We were unable to dissolve the green $K_3W_2Cl_9$ in the $AlCl_3$-$NaCl_{sat}$ melt to obtain a W(III) solution.

The last two reduction waves, Waves 6c and 7c in Fig. 3, extensively overlap with each other. If the potential scan is reversed right after Wave 6c, no significant reverse oxidation wave associated with Wave 6c can be observed. If the potential scan is reversed after Wave 7c, a reverse oxidation Wave 7a appears. The product of the reduction Wave 7c may form an insoluble film on the electrode surface since the current was not reproducible and increased each time after this wave was traversed unless the electrode surface was cleaned by stepping the potential to 2.00 V for several seconds. Furthermore, a large oxidation wave occurred at approximately the same potential as Wave 1a and was associated with Wave 7c. During a bulk controlled potential electrolysis experiment, conducted at 0.0 V, the current did not decay with time. Consequently, the n-value could not be determined from these experiments. A major difficulty for the study of this wave comes from the fact that this wave occurs too close to the cathodic limit of the melt. Wave 7c in Fig. 3 is similar to the cyclic voltammogram observed for W_6Cl_{12} dissolved in an acidic $AlCl_3$-NaCl melt.[5] Thus, Wave 7c in Fig. 3 may be due to the reduction of W(II) chloride. However, we could not obtain enough evidence to prove this postulate because the solubility of W_6Cl_{12}, like that of K_2WCl_6, in the $AlCl_3$-$NaCl_{sat}$ melt was very low.

The complexity of the electrochemistry of the $[WCl_6]^-$ species in this melt can be illustrated using the normal pulse voltammogram with longer pulse width shown in Fig. 4b. Conclusions similar to those obtained from the cyclic voltammetric data can be drawn from normal pulse voltammetry.

$WOCl_4$.—The dissolution of $WOCl_4$ in the $AlCl_3$-$NaCl_{sat}$ melt at 175°C produces a reddish orange solution. A UV-visible spectrum of this solution is shown in Fig. 6 with the relative intensities and wavelengths of each absorption peak collected in Table II. The absorption bands are essentially identical to those reported for $WOCl_4$ in the gas phase and those in the acidic $AlCl_3$-NaCl [1] melt indicating that $WOCl_4$ is indeed stable in the $AlCl_3$-$NaCl_{sat}$ melt at this temperature. However, $WOCl_4$ is fairly volatile at 175°C, and reddish orange $WOCl_4$ crystals can be seen on the cell walls above the melt.

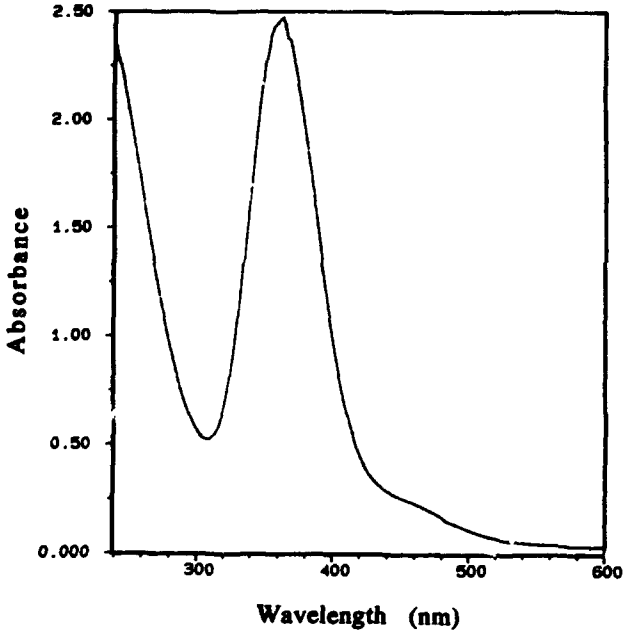

Fig. 6. Absorption spectrum of 18.6 × 10^{-3}M $WOCl_4$ in $AlCl_3$-$NaCl_{sat}$ melt at 175°C.

Cyclic voltammograms obtained at a glassy carbon electrode for a solution of $WOCl_4$ in the $AlCl_3$-$NaCl_{sat}$ melt at 175°C are shown in Fig. 7. The rest potential for this solution at a glassy carbon electrode was 2.030 V. When the cyclic voltammogram was scanned anodically from the rest potential, no oxidation wave was observed until the anodic limit of the melt. When the cyclic voltammogram was scanned in the negative direction, a well-defined reduction wave with a peak potential of 1.692 V followed by five closely spaced reduction waves at peak potentials of 0.951 V (Wave 2c), 0.798 V (Wave 3c), 0.650 V (Wave 4c), 0.331 V (Wave 5c), and 0.176 V (Wave 6c) were observed.

The reduction Wave 1c in Fig. 7 is associated with the reverse oxidation Wave 1a. Data collected from the voltammograms for this redox process recorded at scan rates ranging from 0.01 to 0.5 V/s exhibit the criteria for a re-

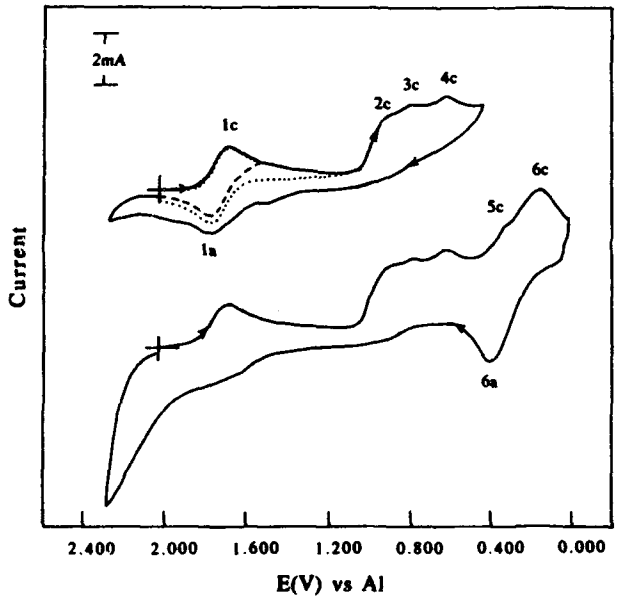

Fig. 7. Cyclic voltammograms of 19.1 × 10^{-3}M $WOCl_4$ at a glassy carbon electrode in $AlCl_3$-$NaCl_{sat}$ melt at 175°C. Scan rate was 0.050 V/s.

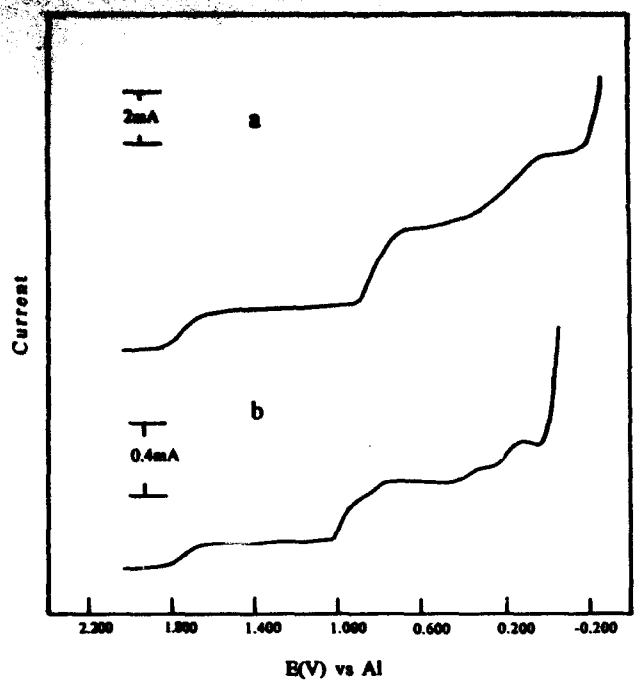

Fig. 8. Normal pulse voltammograms of 19.1 × 10^{-3}M $WOCl_4$ at a glassy carbon electrode in $AlCl_3$-$NaCl_{sat}$ melt at 175°C: (a) pulse width was 0.02 s; (b) pulse width was 3 s.

versible, one-electron charge-transfer reaction; *i.e.*, constant peak potential separation with an average value of 0.095 V, a unit peak current ratio, and a linear relationship between the cathodic peak current and the square root of the scan rate. The values for $E_{1/2}$ calculated from these voltammograms are essentially constant with an average value of 1.743 V. Typical normal pulse voltammograms for $WOCl_4$ solution are presented in Fig. 8a and 8b. The plots of $\log [(i_l - i)/i]$ *vs.* E, constructed from the data in these figures for Wave 1c, give an n value of 1 and an $E_{1/2}$ value of 1.748 V, which is in good agreement with the value obtained from cyclic voltammetry data.

Although the oxidation state of tungsten in $WOCl_4$ is the same as in WCl_6, $WOCl_4$ is not reduced by the Cl^- in the $AlCl_3$-$NaCl_{sat}$ melt. The stability of $WOCl_4$ in this melt can be understood by comparing the half-wave potentials of these two tungsten complexes. The $E_{1/2}$ of $WOCl_4$ is more negative than that of WCl_6, and is sufficiently far from the oxidation potential of Cl^- that Cl^- does not reduce $WOCl_4$.

Exhaustive controlled potential electrolysis experiments were conducted at a potential of 1.600 V to determine if the reduced $WOCl_4$ was stable in the melt. However, the $WOCl_4$ vaporizes from the melt and contaminates the counterelectrode melt by entering the pressure-balancing hole for the counterelectrode. During the electrolysis, the reduction current rapidly decayed toward zero, and the total charge consumed experimentally was much less than the theoretical value for a one-electron reduction. After the reduction was completed, the solution turned bluish-green while the counterelectrode compartment turned reddish orange. Consequently, the experimentally determined charge for the reduction of $WOCl_4$ was less than the expected value. Cyclic voltammograms were recorded for the reduced $WOCl_4$ solution, and the same redox couples that were present in the $WOCl_4$ solution were still present in this solution. However, the one-electron reduction product of $WOCl_4$ was now the principal electroactive species present in this solution.

The tungsten(V) oxychloride complex also can be obtained by the reaction of oxide with $[WCl_6]^-$. When excess oxide as Na_2CO_3 was introduced into a solution of $[WCl_6]^-$ in $AlCl_3$-$NaCl_{sat}$ melt at 175°C, the yellow solution slowly turned bluish green. An absorption spectrum in the UV-visible region recorded for this solution is depicted in Fig. 9.

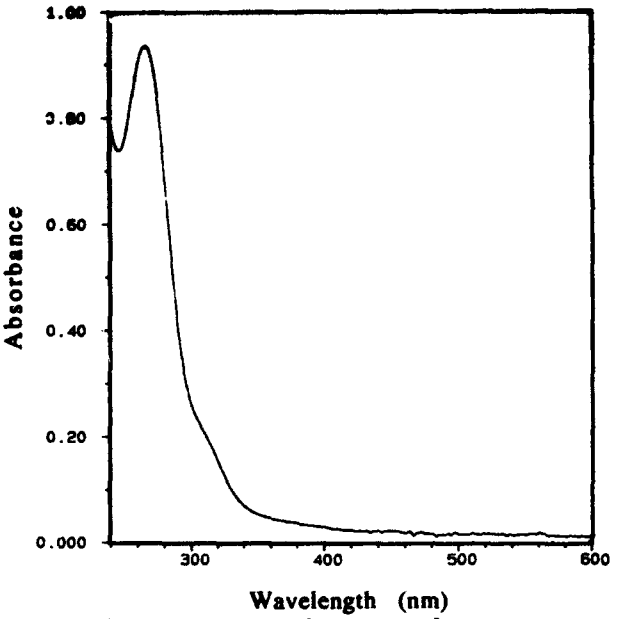

Fig. 9. Absorption spectrum of 19.2 × 10^{-3}M W(V) in a $AlCl_3$-$NaCl_{sat}$ melt upon the addition of excess Na_2CO_3 at 175°C.

The data collected from this figure are summarized in Table II. These data agreed well with those reported for the $[WOCl_5]^{2-}$ complex.[21]

The reduction Waves 2c, 3c, 4c, 5c, and 6c (Fig. 7) appear to involve coupled chemical reactions. At present, the reaction sequence for these reductions cannot be determined; however, the following observations about these reduction waves are provided. Although Waves 2c, 3c, and 4c are distinguishable at slow scan rates (<2 V/s), these three waves collapsed into a single wave at high scan rates. Figure 10 shows the cyclic voltammogram obtained at a scan rate of 40 V/s. Waves 2c, 3c, and 4c have merged into one wave, which exhibits a peak potential of *ca.* 0.650 V and a peak current approximately twice the magnitude of the peak current observed for Wave 1c. However, there is no reverse oxidation wave associated with this wave suggesting that some coupled chemical reaction is involved. The normal pulse voltammogram, shown in Fig. 8a, with shorter pulse width exhibits three major reduction waves. The limiting current ratios of these waves are approximately 1.0 : 2.0 : 2.0. These results together with the results from the fast scan cyclic voltammograms suggest that the second reduction wave (the reduction wave at 0.650 V in Fig. 10) may be due to the reduction of W(V) oxychloride to W(III) oxychloride species at the short voltammetric time scale. The third reduction wave (Fig. 10) is probably a combination of two reduction processes as judged from its shape. A normal pulse voltammogram obtained at a longer pulse width is

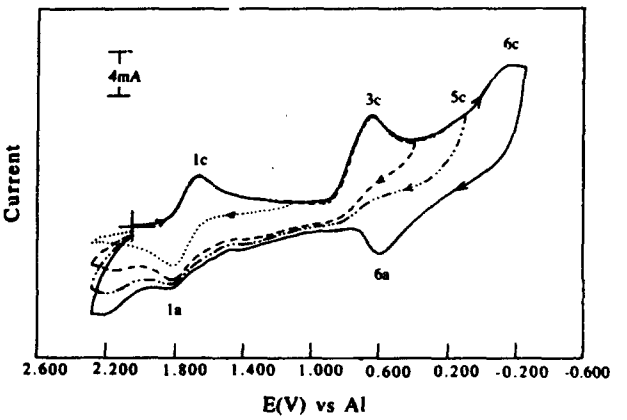

Fig. 10. Cyclic voltammogram of 19.1 × 10^{-3}M $WOCl_4$ at a glassy carbon electrode in $AlCl_3$-$NaCl_{sat}$ melt at 175°C. Scan rate was 40.0 V/s.

shown in Fig. 8b. It appears to be more complicated possibly due to film formation. These results are essentially the same as those obtained from the slow scan cyclic voltammograms shown in Fig. 7.

When the cyclic voltammograms of $WOCl_4$ (Fig. 7 and 10) are compared to the cyclic voltammograms of WCl_6^- (Fig. 3 and 4), within experimental error, Waves 5c and 6c observed in the cyclic voltammograms of $WOCl_4$ are essentially the same as Waves 6c and 7c in the cyclic voltammograms of $[WCl_6]^-$. This observation suggests that Waves 5c an 6c in the cyclic voltammograms of $WOCl_4$ and Waves 6c and 7c in the cyclic voltammograms of $[WCl_6]^-$ may be due to the same reduction processes. Thus, it is possible that tungsten oxychlorides with oxidation states lower than +3 are unstable in the $AlCl_3$-$NaCl_{sat}$ melt at the operating temperature (175°C) and are converted to tungsten chlorides. With this assumption, the final reduction products of WCl_6^- and $WOCl_4$ in this melt may be the same.

Conclusion and Summary

This study shows that WCl_6 is reduced by $AlCl_3$-$NaCl_{sat}$ melt to $[WCl_6]^-$; the reduction is related to the Cl^- concentration in the melt. Using fast scan rate cyclic voltammetry, $[WCl_6]^-$ can be reduced electrochemically to $[WCl_6]^{2-}$ and $[WCl_6]^{3-}$ through two successive one-electron charge-transfer processes. Both $[WCl_6]^{2-}$ and $[WCl_6]^{3-}$ form precipitates in the melt on a long time scale. The solubilities of K_2WCl_6 and $K_3W_2Cl_9$ as well as W_6Cl_{12} were found to be very low in this melt. $WOCl_4$ is stable in the melt and can be reduced to tungsten(V) oxychloride through a reversible one-electron reaction. The addition of oxide to $[WCl_6]^-$ in melt also produces tungsten(V) oxychloride complex, which is identified as $[WOCl_5]^{2-}$. The formation of tungsten(V) oxychloride in $AlCl_3$-$NaCl_{sat}$ melt is different from the results reported for basic $AlCl_3$-MEIC melts.[7] Tungsten oxychlorides with oxidation states lower than +3 apparently are converted to tungsten chlorides.

There was no evidence of tungsten metal formation in this study. However, additional work in our laboratory shows that electrodeposition of metallic tungsten may be achieved in a sodium tetrachloroaluminate-sodium fluoride ($NaAlCl_4$-NaF) melt at temperatures higher than 650°C.[24] The temperature effect on the electrochemical behavior of these tungsten complexes will be studied further. Experiments based on the use of spectroelectrochemical techniques, may be necessary to resolve the reduction sequence of these tungsten complexes fully.

Manuscript submitted March 17, 1993; revised manuscript received June 10, 1993.

The University of Tennessee assisted in meeting the publication costs of this article.

REFERENCES

1. J-P. Schoebrechts, P. A. Flowers, G. W. Hance, and G. Mamantov, *This Journal*, **135**, 3057 (1988).
2. G. Mamantov and R. A. Osteryoung, in *Characterization of Solutes in Nonaqueous Solvents*, G. Mamantov, Editor, p. 223, Plenum Press, New York (1978).
3. I-W. Sun, K. D. Sienerth, and G. Mamantov, *This Journal*, **138**, 2850 (1991).
4. G. S. Chen, I-W. Sun, K. D. Sienerth, A. G. Edwards, and G. Mamantov, *ibid.*, **140**, 1523 (1993).
5. D. L. Brotherton, Ph. D. Dissertation, University of Tennessee, Knoxville, TN (1974).
6. K. Tanemoto, G. Mamantov, and G. M. Begun, *Inorg. Chim. Acta*, **76**, L79 (1983).
7. T. B. Scheffler and C. L. Hussey, *Inorg. Chem.*, **23**, 1926 (1984).
8. W. C. Dorman and R. E. McCarley, *ibid.*, **13**, 491 (1974).
9. A. G. Cavinato, G. Mamantov, and X. B. Cox III, *This Journal*, **132**, 1136 (1985).
10. E. N. Balko, Ph.D. Dissertation, Rensselaer Polytechnic Institute, Troy, NY (1973).
11. K. E. Johnson and J. R. Mackenzie, *Anal. Chem.*, **41**, 1483 (1969).
12. R. O. Johnston, Ph.D. Dissertation, University of Illinois at Champaign-Urbana, Urbana, IL (1974).
13. D. Zuckerbrod, Ph.D. Thesis, Rensselaer Polytechnic Institute, Troy, NY (1982).
14. C.A. C. Sequeira, *Mater. Sci. Forum*, **73**, 569 (1991).
15. A. Katagiri, M. Suzuki, and Z. Takehara, *This Journal*, **138**, 767 (1991).
16. J. A. Creighton and T. J. Sinclair, *Spectrochim. Acta*, **35A**, 507 (1979).
17. W. van Bronswyk, R. J. H. Clark, and L. Maresca, *Inorg. Chem.*, **8**, 1395 (1969).
18. G. Torsi and G. Mamantov, *ibid.*, **10**, 1900 (1971).
19. J. Phillips and R. A. Osteryoung, *This Journal*, **124**, 1465 (1977).
20. R. S. Nicholson, *Anal. Chem.*, **38**, 1406 (1966).
21. E. A. Allen, B. J. Brisdon, D. A. Edwards, G. W. A. Fowles, and R. G. Williams, *J. Chem. Soc.*, 4649 (1963).
22. T. L. Brown, W. G. McDugle, Jr., and L. G. Kent, *J. Am. Chem. Soc.*, **92**, 3645 (1970).
23. E. Thorn-Csanyi and H. Timm, *J. Mol. Cat.*, **28**, 37 (1985).
24. I-W Sun and G. Mamantov, Unpublished results.

...due mainly to a higher porosity. The rate-determining step for the redox reaction is characterized by employing a finite diffusion control model instead of a semi-infinite model. The apparent diffusion coefficient of Li^+ through the WO_3 film is 1.2×10^{-9} cm^2 s^{-1}, which is two orders of magnitude higher than that of literature values for vacuum-deposited WO_3 films.

Manuscript submitted Oct. 20, 1993; revised manuscript received March 14, 1994.

REFERENCES

1. B. W. Faughnan and R. S. Crandall, *Topics in Applied Physics, Display Devices*, J. I. Paukove, Editor, Vol. 40, p. 181, Springer-Verlag Berlin (1980).
2. R. D. Rauh, S. F. Cogan, and M. A. Parker, *Proc. SPIE*, **502**, 38 (1984).
3. P. K. Shen, J. Syed-Bokhari, and A. C. C. Tseung, *This Journal*, **138**, 2778 (1991); A. C. C. Tseung, P. K. Shen, and J. Syed-Bokhari, *PCT Int. Appl.* WO 92 16,027, Sept. 17, 1992; *GB Appl.* 91/4,377, Mar. 1, 1991.
4. K. Nassau, *The Physics and Chemistry of Color*, p. 320, John Wiley & Sons, New York (1983).
5. L. H. Dao, A. Guerfi, and M. T. Nguyen, in *Electrochromic Materials*, M. K. Carpenter and D. A. Corrigan, Editors, PV 90-2, p. 30, The Electrochemical Society Proceedings Series, Pennington, NJ (1990).
6. P. K. Shen and A. C. C. Tseung, *J. Mater. Chem.*, **2**, 1141 (1992).
7. P. K. Shen, H. T. Huang, and A. C. C. Tseung, *This Journal*, **139**, 1840 (1992).
8. P. V. Ashrit, G. Bader, F. E. Girouard, and V.-V. Truong, in *Electrochromic Materials*, M. K. Carpenter and D. A. Corrigan, Editors, PV 90-2, p. 45, The Electrochemical Society Proceedings Series, Pennington, NJ (1990).
9. P. K. Shen, H. T. Huang, and A. C. C. Tseung, *J. Mater. Chem.*, **2**, 497 (1992).
10. J. Q. Chambers, *J. Electroanal. Chem.*, **130**, 381 (1981).
11. N. Leventis and Y. C. Chung, *J. Mater. Chem.*, **3**, 833 (1993).
12. P. K. Shen and A. C. C. Tseung, *This Journal*, Submitted 1993.
13. D. G. Peters and S. L. Burden, *Anal. Chem.*, **38**, 530 (1966).
14. A. J. Bard, *ibid.*, **35**, 340 (1963).
15. P. E. Sturrock, G. Privett and A. R. Tarpley, *J. Electroanal. Chem.*, **14**, 303 (1967).
16. W. T. deVries, *ibid.*, **17**, 31 (1968).
17. B. S. Hobbs and A. C. C. Tseung, *This Journal*, **119**, 580 (1972).
18. B. W. Faughnan, R. S. Crandall, and P. M. Heyman, *RCA Rev.*, **36**, 177 (1975).
19. B. Reichman and A. J. Bard, *This Journal*, **126**, 583 (1979).
20. C. Ho, I. D. Raistrick, and R. A. Huggins, *ibid.*, **127**, 343 (1980).
21. M. A. Habib and D. Glueck, *Sol. Energy Mater.*, **18**, 127 (1989).
22. M. Green, *Thin Solid Films*, **50**, 145 (1978).
23. A. J. Bard and L. R. Faulkner, *Electrochemical Methods*, p. 143, John Wiley & Sons, New York (1980).
24. *Handbook of Chemistry and Physics*, 67th ed., p. B-141, CRC Press, Boca Raton, FL (1986-1987).
25. S. K. Deb, *Philos. Mag.*, **27**, 801 (1973).
26. N. Yoskiike, M. Ayusawa, and S. Kondo. *This Journal*, **131**, 2600 (1984).

Appendix 4

A Reinvestigation of the Electrochemical Behavior of Nb(V) in $AlCl_3$-$NaCl_{SAT}$ and Related Melts

K. D. Sienerth

Department of Chemistry, Virginia Military Institute, Lexington, Virginia 24450

E. M. Hondrogiannis* and G. Mamantov**

Department of Chemistry, University of Tennessee, Knoxville, Tennessee 37996-1600

ABSTRACT

The electrochemistry and spectroelectrochemistry of Nb(V) in molten sodium chloroaluminate saturated with NaCl at 178°C were re-examined. It was determined that previous studies involved solutions of high oxide content. The reduction of $NbCl_5$ in oxide-free melts was found to proceed via four steps at short times and low concentrations. At higher concentrations and long times, the reduction sequence was complicated by a chemical reaction which follows the initial reduction step. The effect of temperature on the electrochemistry of Nb(V) in sodium chloroaluminates and fluorochloroaluminates was examined; temperature had a marked effect on the behavior of Nb(V) in these melts, but no significant differences were observed between melts with and those without fluoride. Attempts to produce electrolytically niobium metal from Nb(V) in these melts met with limited success.

Prior to the early 1970s, the possible influence of dissolved oxide species on solutes in molten salts was not considered in most investigations. Beginning with the latter part of that decade, researchers began to realize that the presence of even fairly low levels of oxide species in the melts could have a marked effect on solute chemistry and electrochemistry,[1-11] especially when work at low solute concentrations was attempted. Polyakov and coworkers[1,2] investigated the electrochemistry of K_2NbF_7 in KCl-KF [55–45 mole percent (m/o)], and found that in the absence of oxide, Nb(V) was reduced to niobium metal in two well-defined, reversible steps [Nb(V)/Nb(IV) and Nb(IV)/Nb(0)]. The addition of oxide in the form of Nb_2O_5 produced more complicated results. Initial small quantities of oxide caused the two waves due to the reduction of $[NbF_7]^{2-}$ to decrease, and resulted in a new wave. When the K_2NbF_7:Nb_2O_5 ratio reached 3:1, the original two waves had disappeared completely, and only the new wave was noted. Analysis of this wave revealed that it corresponded to the five-electron reduction of Nb(V) to the metal. These researchers proposed that this wave was due to the reduction of the niobium oxyfluoride complex $[NbOF_4]^{3-}$.

Lantelme *et al.*[3] studied the effect of oxide added to a LiCl-KCl solution of Nb(V), where they initially observed two waves [Nb(V)/Nb(IV) and Nb(IV)/Nb(III)]. Upon the addition of oxide, both waves decreased in height, and finally completely disappeared when the O^{2-}/Nb(V) ratio had reached approximately two.

Sun and Hussey[4] examined the electrochemistry of niobium chloride and oxychloride in basic $AlCl_3$-1-methyl-3-

* Electrochemical Society Student Member.
** Electrochemical Society Active Member.

ethylimidazolium chloride ($AlCl_3$-MEICl) room temperature melts. They found that $[NbCl_6]^-$ could be reduced in two one-electron reversible steps to $[NbCl_6]^{2-}$ and $[NbCl_6]^{3-}$, with $E_{1/2}$'s of 0.17 and −0.93 V, respectively, *vs.* Al(III)/Al. Upon the addition of oxide to the melt, $[NbCl_6]^-$ was converted to $[NbOCl_4]^{2-}$, and this oxychloride moiety was reduced to $[NbOCl_2]^{3-y}$ in a one-electron quasi-reversible reaction with a formal potential of −0.521 V. These workers found that the oxychlorides could be converted to their respective chlorides in this melt by reaction with phosgene.

Ting *et al.* in our laboratory[5,6] studied the electrochemical behavior of Nb(V), added as $NbCl_5$, in the $AlCl_3$-$NaCl_{SAT}$ melt. The results of that study indicated that Nb(V) was first reduced in a one-electron step to Nb(IV), followed by three further reduction steps resulting in subvalent niobium chloride cluster species which were quite stable, preventing reduction to metallic niobium. These results were evaluated in terms of the reduction of $NbCl_5$, and a reduction sequence involving only niobium chloride species was proposed; the studies were conducted at a time when the importance of oxide impurities in molten salts was not fully understood. It has recently been demonstrated[8] that our prior results[5,6] were erroneous in that the melts utilized in the studies probably contained quite high levels of oxide impurities.

Our group has found phosgene to be effective also in the removal of oxide impurities from the $AlCl_3$-$NaCl_{SAT}$ melt.[9] Recently, we have reported[10] that the removal of oxides from this melt can be accomplished with ease by treatment with carbon tetrachloride. The development of oxide removal methods has made feasible the reinvestigation of the electrochemistry of Nb(V) in oxide-free melts. We report here the results of studies of the electrochemical and spectroelectrochemical behavior of Nb(V) in oxide-free sodium chloroaluminate and chlorofluoroaluminate melts.

Experimental

Due to the hygroscopic nature of the melts and solutes used, all work was conducted in an inert-atmosphere drybox (water level <2 ppm) or in sealed Pyrex or quartz cells.

Chemicals.—Sodium chloride (Mallinkrodt, analytical reagent grade) was dried under vacuum (<50 mTorr) at 450°C in a Pyrex tube for >48 h. Anhydrous aluminum chloride (Fluka, puriss grade, >99%) was purified by distillation as described in Ref. 11. Sodium fluoride (Alfa, puratronic, 99.995%) was used as received. Carbonyl chloride (Matheson Gas, 99.0%) and carbon tetrachloride (Mallinkrodt, 99.9%) were used as received. Niobium pentachloride (Alfa, 99.9%) was purified by sublimation as described previously.[6,10] Sodium carbonate (Mallinkrodt, analytical reagent grade) was dried under vacuum at 300°C for >48 h, and then was transferred to the drybox and stored until used.

Melts were prepared as described previously,[10] and were treated either in bulk or *in situ* (in the electrochemical cell) with phosgene[8,9] or CCl_4.[8,10]

Electrode materials.—Voltammetric working electrodes were constructed from tungsten or platinum wire. Counterelectrodes were made from glassy carbon rod or from platinum foil. Platinum wire quasi-reference electrodes were used, and were monitored with respect to an AgCl (saturated, in $AlCl_3$-$NaCl_{SAT}$)/Ag reference electrode enclosed in a thin glass bulb. All potentials reported herein are given *vs.* the Ag(I)/Ag reference.

For controlled potential coulometry, the working electrode was a glassy carbon cup; the counterelectrode was an aluminum coil, separated from the bulk melt by a medium-porosity frit; and the reference electrode was an aluminum wire in $AlCl_3$-$NaCl_{SAT}$, separated from the bulk melt by a fine-porosity frit.

The thin layer working electrode for the spectroelectrochemistry was constructed from platinum gauze (Aesar, 52 mesh woven from 0.1 mm diam wire, 99.9%).

Cathodes in the electrodeposition experiments were constructed using either nickel plates or tungsten foil. Niobium metal anodes, either coiled wire or plates, were used.

Instrumentation.—Electrochemical measurements were conducted using a Princeton Applied Research Model (PAR) potentiostat-galvanostat, PAR Model 273, with control from an IBM PS/2-70A computer and the PAR Model 270 electrochemical software. A Hewlett-Packard Model 8452A diode array spectrophotometer was used to obtain UV-visible spectra. High-temperature spectra were obtained with the use of a water-cooled furnace which was designed and constructed inhouse. A Perkin-Elmer PHI5000 ESCA and a Siemens D-500 x-ray diffractometer were used for analysis of electrodeposition products.

Results Obtained at 178°C

In prior studies conducted in our laboratory[5,6] four waves were observed during voltammetric reduction of Nb(V), added as $NbCl_5$ in $AlCl_3$-$NaCl_{SAT}$ at 178°C; these waves exhibited cyclic voltammetric (CV) peak potentials of −0.09, −0.24, −0.46, and −0.75 V, respectively. In the present studies, the voltammetric response observed at 178°C for $NbCl_5$ solutions in $AlCl_3$-$NaCl_{SAT}$ which had been treated with phosgene or CCl_4 differed significantly from that reported previously,[5,6] especially with respect to the peak potential of the initial reduction wave. A typical CV is shown in Fig. 1a (solid line); the four main waves have peak potentials of 0.114, −0.293, −0.482, and −0.809 V. However, when an excess of oxide had been added to the melt, in the form of Na_2CO_3, CVs nearly identical to those reported by Ting[5,6] were obtained (see Fig. 1b); the peak potential of the initial reduction wave in Fig. 1b is −0.081 V. No change in the melt potential limits was observed; the Ag(I)/Ag reference electrode was clearly not affected by the addition of oxide.

The UV-visible spectrum for a solution of 15 m*M* $NbCl_5$ in the $AlCl_3$-$NaCl_{SAT}$ melt, prepared using a $COCl_2$-treated melt, at 200°C, gave two main bands with maxima at 238 and 284 nm, and a shoulder at 320 nm, indicating that $NbCl_5$ was the main species present in the melt along with some $[NbCl_6]^-$.[4,11b] It has also been demonstrated using UV-visible spectroscopy[8] that the dominant initial species in the melts used by Ting[5,6] was probably a niobium oxychloride moiety formed by the reaction of $NbCl_5$ with oxide contaminants, which likely existed in the melt at fairly high levels.

Cyclic voltammetry (CV) at 178°C.—Solutions of $NbCl_5$ in $AlCl_3$-$NaCl_{SAT}$ at 178°C were investigated at concentrations ranging from 5 to 30 m*M* using various voltammetric methods. In general, the solutions were treated *in situ* with CCl_4 after each addition of $NbCl_5$ to ensure the elimination of any inadvertently introduced oxide impurities.

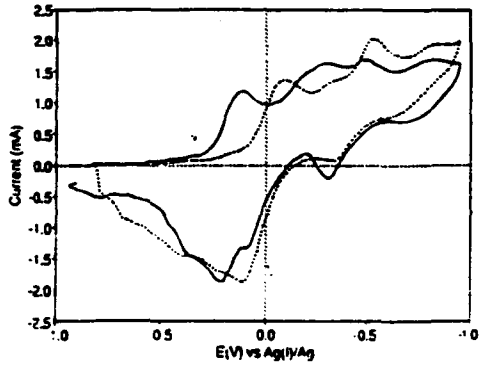

Fig. 1. Cyclic voltammogram of Nb(V) obtained in $AlCl_3$-$NaCl_{SAT}$ using a tungsten wire (0.24 cm^2) working electrode. The Nb(V) concentration was 2.91×10^{-2} *M*, the temperature was 178°C, and the scan rate was 0.20 V/s. (a) (—) Obtained in a melt treated with CCl_4 (no oxide) and (b) (---) obtained in same melt, after the addition of excess oxide (as Na_2CO_3).

[illegible] data for the CV of the first reduction wave of $NbCl_5$.

Concentration of $NbCl_5$ (mM)	Scan rate (V/s)	n	i_p^a/i_p^c
8.1	0.05	0.92	1.04
	0.10	0.95	1.05
	0.50	0.88	1.00
	5.0	0.93	1.05
	50.00	0.96	—
18.8	0.05	0.96	0.92
	0.10	0.91	0.94
	0.50	0.86	0.95
	5.0	0.88	0.99
	50.00	0.86	1.02

Table I lists some pertinent data for the initial CV reduction wave, which exhibits a maximum at 0.114 V in Fig. 1a. The values of i_p^a/i_p^c vary little, and remain near unity for all scan rates in the range studied (three decades, from 0.05 to 50 V/s); these values were obtained using Nicholson's criterion as described in Ref. 12 (pp. 229-230). The average value for n, as determined using CV,[a] was found to be 0.93, indicating that the initial reduction involves the transfer of one electron. Further evidence for the reversibility of the process was given by application of the Randles-Sevcik equation[b]

$$i_p = 0.4463nFA(Da)^{1/2}C^*$$

with

$$a = (nF\upsilon)/(RT) \qquad [1]$$

which predicts, for a diffusion-controlled process, a linear relationship between the peak current and the square root of the scan rate, and a similar relationship between the peak current and the solute concentration. Throughout the range of $NbCl_5$ concentrations studied, plots of i_p *vs.* $\upsilon^{1/2}$ were found to be linear, and a linear relationship between i_p and $NbCl_5$ concentration was observed for all waves.

Table II summarizes some results regarding the initial reduction process obtained using various voltammetric methods. In all cases, a high degree of reversibility was indicated. Chronoamperometric experiments closely followed the Cottrell equation (Ref. 12, p. 143). Plots of E *vs.* $\log[(i_d - i)/i]$ using normal pulse voltammetric data were linear, as predicted by the theory for a reversible reaction (Ref. 12, pp. 160-162). Cyclic voltammetric results were presented above, and square wave voltammetry experiments are discussed below.

The data given in Table II show that the number of electrons involved in the charge-transfer for the first reduction wave was near unity. The values for $E_{1/2}$ and D are in reasonable agreement among the indicated methods.

In solutions of low concentration (<20 mM), only four reduction waves were observed in the CV of $NbCl_5$; the shoulder which precedes the second wave (see Fig. 1a) only becomes significant at concentrations higher than 20 mM.

[a] Values for the number of electrons (n) were determined using the equation $(E_p^c - E_{p/2}) = 2.2\,RT/nF$.

[b] In Eq. 1, n is the number of electrons, F is Faraday's constant, A is the electrode area, D is the diffusion coefficient of the species reduced, C^* is the bulk concentration of the species reduced, R is the gas constant, and T is the temperature in Kelvins.

Table II. Summary of results for first reduction process at 178°C.

Method	n	$E_{1/2}$ (V)	D (cm^2/s)
Cyclic voltammetry (CV)	0.93	0.167	1.8×10^{-4}
Chronoamperometry (CA)	—	—	1.9×10^{-4}
Normal pulse voltammetry (NPV)	0.96	0.171	—
Square wave voltammetry (SWV)	—	0.170	—
Controlled potential coulometry (CPC)	0.97	—	—

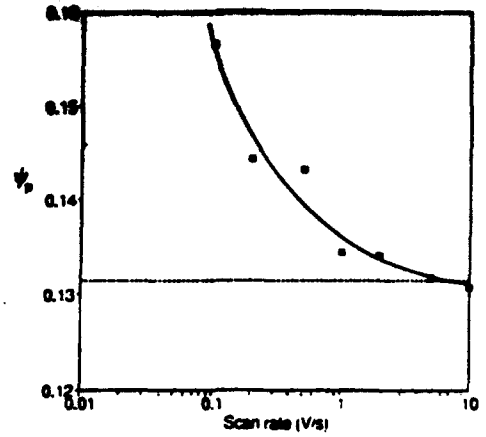

Fig. 2. Plot of the dimensionless current function (ψ_p) *vs.* the scan rate for the first reduction wave obtained by CV for Nb(V) in $AlCl_3$-$NaCl_{sat}$. The Nb(V) concentration was $2.91 \times 10^{-2}M$, the working electrode was a tungsten wire, the temperature was 178°C, and the scan rate ranged from 0.1 to 10 V/s. The dotted line represents the theoretical current expected for this concentration, using $D = 1.8 \times 10^{-6}$ $cm^2\,s^{-1}$.

Furthermore, even at high concentrations, the shoulder essentially disappears at high scan rates. A similar dependence upon experimental rate (step time) was observed in normal pulse voltammetry.

The behavior of the shoulder preceding the second wave indicates that it involves some reaction which is only significant at long times and high concentrations. In the treatment of the voltammetric data as discussed above, no variation from theory was observed that might indicate that the first reduction wave ($E_p = 0.114$ V) was complicated by a following chemical reaction. However, such methods are not always sensitive to small deviations from ideality. More sensitive probes for such behavior are described in the literature;[13] these methods consider the dependence of certain parameters related to i_p and $E_{p/2}$ on scan rate. Figure 2 shows a plot of the dimensionless current function given in Eq. 2 *vs.* the scan rate. The shape of the curve

$$\psi_p = i_p(nFAD^{1/2}C^*a^{1/2})^{-1} \qquad [2]$$

in Fig. 2 is indicative of a following chemical reaction which regenerates the initial redox species (Case VII in Ref. 16). Figure 3 shows a plot of $(\Delta E_{p/2})/(\Delta \log \upsilon)$ *vs.* the scan rate; this curve also indicates that a following chemical reaction regenerates the original redox species. Further-

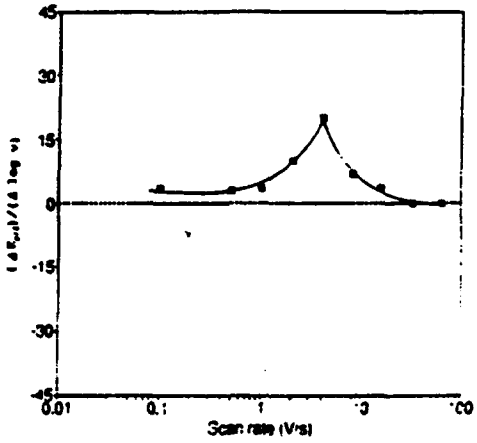

Fig. 3. Plot of the function $(\Delta E_{p/2})/(\Delta \log \upsilon)$ *vs.* the scan rate for the first reduction wave obtained by CV for Nb(V) in $AlCl_3$-$NaCl_{sat}$. The Nb(V) concentration was $2.91 \times 10^{-2}M$, the working electrode was a tungsten wire, the temperature was 178°C, and the scan rate ranged from 0.1 to 50 V/s. The dotted line represents the curve expected in the complete absence of complicating factors.

Table III. Voltammetric (CV) peak potentials for the last three waves of the Nb(V) reduction at 178°C.

Scan rate (V/s)	$E_{p,2}$ (V)	$E_{p,3}$ (V)	$E_{p,4}$ (V)	$E_{p,2} - E_{p,3}$ (V)
0.20	−0.293	−0.482	−0.809	0.189
2.0	−0.324	−0.504	(−0.830)	0.180
20.0	−0.395	−0.548	(−0.879)	0.153
40.0	−0.421	−0.568	(−0.919)	0.147

Table IV. Data for four main waves in SWV of $NbCl_5$.

ω (Hz)	$E_{p,1}$ (V)	$E_{p,2}$ (V)	$E_{p,3}$ (V)	$E_{p,4}$ (V)	$i_{p,2}/i_{p,1}$	$i_{p,3}/i_{p,1}$	$i_{p,4}/i_{p,1}$
60	0.172	−0.266	−0.442	−0.791	—	0.306	0.387
120	0.170	−0.266	−0.458	−0.804	0.292	0.304	0.719
240	0.167	−0.275	−0.464	−0.803	0.281	0.292	0.893
480	0.170	−0.278	−0.479	−0.807	0.282	0.298	0.938

more, the shapes of the curves observed in Fig. 2 and 3 exclude the occurrence of an EC mechanism, and do not support dimerization of the redox product.

The variations of peak potentials with scan rate for the second, third, and fourth waves in the CV are given in Table III. The peak potentials of the second and third waves shifted to more negative values as the scan rate was increased; the amount by which they were separated became smaller. At none of the scan rates studied were the two waves sufficiently resolved that peak current determination for the third wave could be accomplished. Complications from the shoulder preceding the second wave prevented the extraction of meaningful data for the second wave at low scan rates, and the proximity of the third wave caused similar difficulties at higher scan rates.

The most negative wave (E_p = −0.8 V) in the CV was small and broad at all scan rates studied. The potential of this wave, like those of the second and third waves, shifted to more negative values with increasing scan rates.

It was noted that a dark-colored film formed on the electrode surface as the potential was swept past the third wave. This film became more prominent at potentials corresponding to the fourth wave. Analysis of these films by x-ray diffraction were fruitless, yielding no definitive lines other than a broad band in the region of d-spacing.

Square wave voltammetry (SWV).—In general, the peak current for a SWV wave is given by the function in Eq. 3

$$i_p = [nFaC^*(\pi D)^{1/2}\omega^{1/2}]\psi_p \qquad [3]$$

i_p is the peak current, ω is the frequency in Hz, and ψ_p is a dimensionless current function which depends on the pulse height and the magnitude of the square wave excitation signal; other parameters are as given before.[b]

Figure 4 shows a SWV obtained in the 29 m*M* solution at a frequency of 60 Hz and a pulse height of 25 mV; Table IV lists some pertinent voltammetric data. As in CV, four definite waves are present, with the second wave having a prewave shoulder. Also as in CV, this shoulder disappeared as the speed (frequency) of the experiment was increased. The parameters $i_{p,2}/i_{p,1}$, $i_{p,3}/i_{p,1}$, and $i_{p,4}/i_{p,1}$ give the ratio of the peak current of waves 2, 3, and 4, respectively, to that of wave 1.

It is clear that the peak potential for the first reduction wave remains constant with increasing frequency, as is expected for a reversible process. All other peak potentials tend toward more negative values, just as in CV, but the shift is to a lesser extent. Of particular interest are the last three columns of Table IV. The values for $i_{p,2}/i_{p,1}$ and $i_{p,3}/i_{p,1}$ remain constant with changing frequency, but that for $i_{p,4}/i_{p,1}$ tends toward unity as the frequency is increased. Since the peak current of a SWV wave depends on *D*, *n*, and frequency, the ratio of peak heights can be considered to be a rough approximation of the relative number of electrons involved in each process, assuming other factors remain the same. Given that the first wave involves only one electron, these ratios provide an approximation of the apparent number of electrons transferred, assuming that possible complications, such as irreversibility and higher order reactions, are of lesser importance.

The SWV theory predicts[14] that the peak height should be linearly dependent upon $\omega^{1/2}$; *i.e.*, a plot of peak height *vs.* $\omega^{1/2}$ should be linear, and should have an intercept of zero. Figure 5 shows plots of i_p *vs.* $\omega^{1/2}$ for the four main waves observed in SWV. The plots for waves 1, 2, and 3 are indeed linear, and have intercepts near zero; this is not the case for wave 4, probably due to the change in its relative peak height with frequency, as demonstrated in Table IV. The slopes of the plots for waves 1, 2, and 3 are 0.351, 0.099, and 0.102, respectively; normalized to the slope of the first wave plot, these values are 1.00, 0.282, and 0.290, respectively. These are in good agreement with the values of $i_{p,2}/i_{p,1}$ and $i_{p,3}/i_{p,1}$ presented in Table IV.

Controlled potential coulometry (CPC).—A potential of 0.05 V was applied to a stirred melt containing $NbCl_5$; after the measured current had decayed to less than 1% of the initial value, the charge passed was determined and an *n* value of 0.974 was calculated, indicating that the first wave in the reduction of Nb(V) involves one electron, in agreement with voltammetric results. It should be noted that some portions of the aluminum counter- and quasi-reference electrodes above the level of the melt were considerably blackened, probably by a reaction with gas-phase

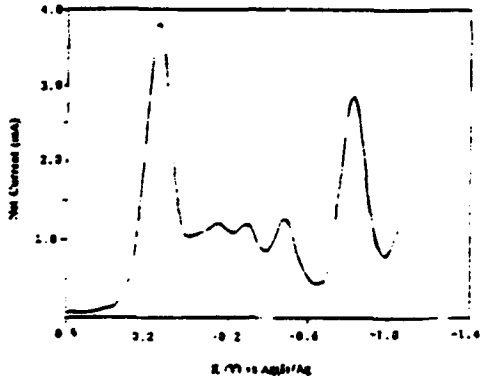

Fig. 4. Square wave voltammogram obtained for Nb(V) in $AlCl_3$-$NaCl_{sat}$. The Nb(V) concentration was 2.91 × 10^{-2}*M*, the working electrode was a tungsten wire, the temperature was 178°C, the frequency was 60 Hz, and the pulse height was 25 mV.

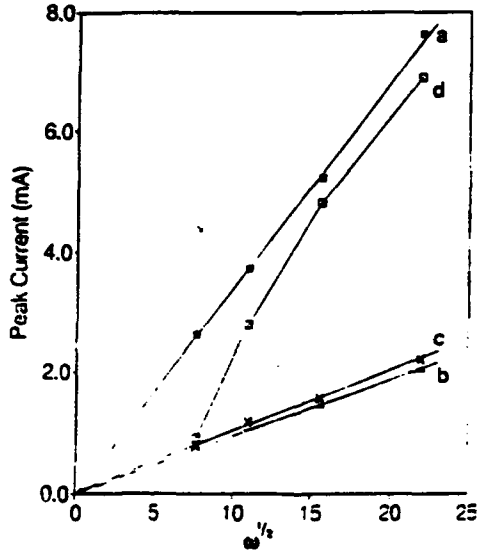

Fig. 5. Plots of peak current *vs.* $\omega^{1/2}$ for the four primary waves in SWV for Nb(V) in $AlCl_3$-$NaCl_{sat}$ (2.91 × 10^{-2}*M*) at 178°C. The plots are for the a, first; b, second; c, third; and d, fourth waves.

Table V. Values for *n* determined by CPC.

Voltammetric wave	Apparent *n*
1	0.974
2′ (prewave)	1.46
2	2.19
3	2.44

$NbCl_4$; this reaction could partially account for the fact that the calculated *n* value was slightly less than unity.

Controlled potential coulometry experiments were carried out at potentials corresponding to those of the subsequent waves observed in voltammetry, including that of the shoulder to the second wave, using a fresh $NbCl_5$ solution each time. Table V lists the apparent *n* values determined for each wave.

In each CPC experiment, the aluminum electrodes became blackened. Although these electrodes were separated from the bulk melt using medium porosity frits, it was necessary to have a small hole (≈4 mm diam) in the counter- and reference electrode compartments, above the melt level, for pressure equilibration. It was in the region of this hole that blackening of the electrode occurred. It is probable that this reaction diminished the total amount of $NbCl_5$ available for experimental evaluation of the *n* values.

UV-visible spectroelectrochemistry (SEC).—(These experiments were carried out at 200°C.) UV-visible spectra were acquired in a thin-layer cell containing a solution of $NbCl_4$ in $AlCl_3$-$NaCl_{SAT}$ while stepping the potential of the electrode to those corresponding to the peaks of the CV reduction waves. The electrode potential was held constant for at least 10 min to allow sufficient time to monitor the thin-layer solution and observe any following chemical reactions. After stepping to the potential of wave 4 (E = −0.92 V), in Fig. 1a, a new band was observed at 410 nm (Fig. 6); the intensity of this band increased with time. Figure 7 shows the spectra acquired after the electrode potential was returned to the initial value (E = 0.60 V). An isosbestic point, arising from the shift in the maximum from 410 to 431 nm, is observed. At longer times, the maximum continued to shift to 444 nm, followed by a decrease in the absorbance at this latter wavelength; after 110 min, no significant absorbance beyond 400 nm was observed.

Hussey and coworkers[15] reported a shift in a band at 423 nm (attributed to a metal-metal electronic transition) to lower energy when they oxidized a fresh solution of $[(Nb_6Cl_{12})Cl_4]^{4-}$, *i.e.*, $Nb^{2.33+}$, in 44.4/55.6 m/o $AlCl_3$-MEICl at 100°C. The final product was believed to be $[(Nb_6Cl_{12})Cl_4]^{2-}$, or $Nb^{2.67+}$.

The behavior of the band attributed to the $Nb^{2.33+}$ cluster in the $AlCl_3$-MEICl melt at 100°C [15] is similar to that observed for the band at 410 nm in $AlCl_3$-$NaCl_{SAT}$ at 200°C. In the $AlCl_3$-MEICl solvent, the band shifted from 423 to 458 nm during oxidation, whereas in the $AlCl_3$-$NaCl_{SAT}$ solvent, a band shift from 410 to 444 nm occurs during oxidation.

At the completion of the experiment, black particles were observed on the platinum screen working electrode. The UV-visible spectrum of a solution of these particles in HCl-saturated ethanol matched those reported for the $Nb_{2.67}$ and $Nb^{2.33+}$ clusters reported by Hussey and coworkers.[15,16]

It is interesting to note that the band at 410 nm was also seen when the electrode was stepped to a potential corresponding to any of the first three waves in the CV, although the increase in absorbance was significantly less than that observed when stepping to the potential of the fourth wave. The formation of the $Nb^{2.33+}$ cluster at more positive potentials is evidence for the slow disproportionation of Nb^{4+}, formed during the first reduction wave, to Nb^{3+} and Nb^{2+}, the latter of which likely decomposes to form the subvalent cluster. The formation of the $Nb^{2.33+}$ cluster in solutions containing Nb(IV) was confirmed by observing the increase with time in the UV-visible bands at 415, 480, and 580 nm, in spectra acquired using a 30 m*M* $NbCl_4$ solution in $AlCl_3$-$NaCl_{SAT}$ at 175°C. These bands decreased as the temperature of the solution was increased to 350°C, indicating that this species is less stable at higher temperatures.

Discussion of Low Temperature Results

The first wave in the reduction of $NbCl_5$ in $AlCl_3$-$NaCl_{SAT}$ at 178°C is essentially a reversible one-electron charge-transfer process. Values for *n* near unity were determined by CV, NPV, and CPC. Reversibility was indicated by CV, NPV, CA, and SWV results.

The diffusion coefficient for the Nb(V) species in $AlCl_3$-$NaCl_{SAT}$ at 178°C was determined by CV, CA, and CC experiments to be 1.8×10^{-6} cm²/s (average). The $E_{1/2}$ of the redox process was found to be 0.169 V (average) *vs.* Ag(I)/Ag via CV, SWV, and NPV experiments.

Unfortunately, studies as comprehensive as those conducted on the first wave could not be extended to the waves occurring at more negative potentials. However, several characteristics were noted. In the voltammetric (CV, NPV, and SWV) experiments, the shoulder preceding the second wave was most prominent at long times (slow scan rate, long pulse widths, and low frequencies); it tended to disappear entirely at very short times or in fast experiments. This behavior indicates that the shoulder was due to the reduction of some species being generated by a rather slow chemical reaction following the first reduction. As explained below, the following chemical reaction is believed to be one which competes with, but which results in the same product as the second reduction step. The fact that there was no gross effect on the characteristics of the first reduction wave indicates that the chemical reaction was slow, or did not proceed to a great extent. It was possible, however, to perform CPC in the rising portion of the shoulder and determine a cumulative *n* value of 1.46 electrons; subtracting the one electron due to the first reduction yields an *n* value for this reduction of 0.46 electrons. Analysis of the

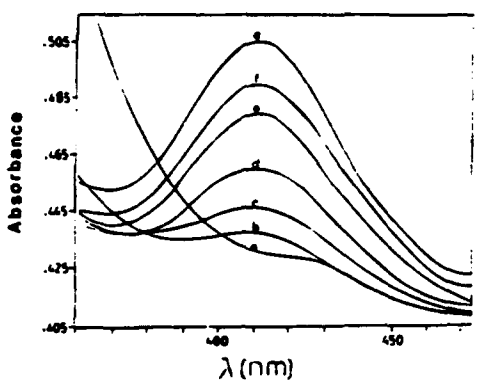

Fig. 6. Absorbance *vs.* wavelength at E = −0.92 V. Spectra acquired at (a) *t* = 0, (b) 1, (c) 2, (d) 4, (e) 8, (f) 12, and (g) 14 min.

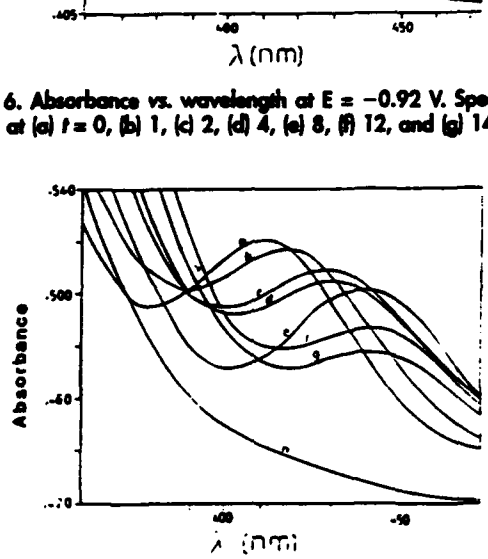

Fig. 7. Absorbance *vs.* wavelength after returning to the initial potential of 0.60 V. Spectra acquired at (a) *t* = 0, (b) 2, (c) 7, (d) 16, (e) 25, (f) 53, (g) 59, and (h) 110 min.

voltammetric data from the first reduction wave using additional Nicholson/Shain criteria[14] revealed that some complications were involved. These analyses indicated that the following chemical reaction involved partial regeneration of the initial redox species [Nb(V), in this case]. Spectroscopic results supported the electrochemical results; UV-visible spectra of an $NbCl_4$ solution showed bands attributed to the $Nb^{2.33+}$ cluster, which was likely the decomposition product of Nb^{3+} formed from the disproportionation of Nb^{4+}. Similar phenomena were observed by Mamantov and coworkers for the oxidation of U(IV) in $LiF-BeF_2-ZrF_4$[16] and the reduction of U(IV) in FLiNaK.[17] These workers proposed schemes involving the disproportionation of the redox product [U(V) and U(III), respectively] to regenerate U(IV).

Studies of the second wave were hindered by the appearance of the shoulder discussed above, as well as the close proximity of the third wave. The peak potential tended to shift to more negative values as the rate of the experiment (CV, SWV) increased. Also, CPC at the potential corresponding to the second wave provided a value of n of 2.19 electrons cumulative from the initial potential. When the potential was stepped past the shoulder and into the second wave, the process which gave rise to the shoulder would have little effect if it were due to the product of a slow chemical reaction. Therefore, it is likely that the n value for the second wave is 1.19 electrons. It should be stressed again, however, that the time scale of the coulometric experiments was as much as three orders of magnitude greater than that of the voltammetric experiments. This could be an important factor in the differences observed between the relative n values obtained for the first and second waves in the two types of experiments.

The third wave suffered from analysis problems similar to those discussed above for the second wave. In brief, it was noted that the peak potential for this wave tended towards more negative values as the experiment rate increased; this was less obvious in the SWV studies than in the CV studies. Coulometry yielded a cumulative n value of 2.44 electrons for this wave.

The fourth wave proved to be the most difficult to analyze using only the electrochemical results. Its appearance in CV was generally broad and small, making it difficult to measure properly the peak potential, much less any other voltammetric parameters. In SWV, the wave appeared to have some reversible character, especially at high frequencies, when the intensity of this wave tended to be higher than that of the first wave. As mentioned above, time in an experiment is an important factor. It is possible that the film formed on the electrode surface during the third and fourth waves could have caused some passivation over the long experimental times, whereas at short times (high frequencies), passivation was minimized. Nevertheless, spectroelectrochemical results supported the generation of the $Nb^{2.33+}$ cluster following this reduction.

Proposed reaction sequence.—At fast rates (short times), only four reduction waves were observed in CV, NPV, and SWV. Based on the results presented and discussed above, and previous results from the literature cited below, the reaction sequence for the reduction of $NbCl_5$ in $AlCl_3$-$NaCl_{SAT}$ at 178°C is proposed to be as given in Eq. 4-7

$$Nb^{5+} + e^- \rightleftharpoons Nb^{4+} \quad (E1) \qquad [4]$$

$$3Nb^{4+} + 4e^- \rightleftharpoons Nb_3^{8+} \quad (E2) \qquad [5]$$

$$2Nb_3^{8+} + e^- \rightleftharpoons Nb_6^{15+} \quad (E3) \qquad [6]$$

$$Nb_6^{15+} + ne^- \rightleftharpoons Nb_6^{(15-n)+} \quad (E4) \qquad [7]$$

Since the n value of the first wave was found definitively to be unity, it follows that step (E1) in the reduction scheme for $NbCl_5$ is the reduction of Nb^{5+} to Nb^{4+}.

An apparent n value of 2.19 was obtained by CPC for the second wave. Reduction of Nb^{5+} to Nb_3^{8+} (Eq. 4 + Eq. 5) would be expected to exhibit an n value of 2.33 per niobium atom. However, as noted previously, some reaction of $NbCl_5$ with the aluminum electrodes present in the cells as indicated, which would effectively diminish the concentration. The species Nb_3Cl_8 is known and has been characterized,[18] and evidence of its existence in chloroaluminate melts has been reported.[11b,13]

The total number of electrons passed per mole of $NbCl_5$ in CPC at the potential of the third wave was determined to be 2.44. The direct reduction of Nb^{5+} to Nb_6^{15+} would require 2.5 electrons per mole of $NbCl_5$ in solution. The substance Nb_6Cl_{14} is known and has been characterized,[18] and evidence for the $[Nb_6Cl_{12}]^{2+}$ moiety in chloroaluminates has been reported.[13]

No direct electrochemical evidence for the reduction represented in Eq. 7 was found; the apparent n value could not be determined reliably in any case, but an apparent n value close to unity can be inferred from the SWV data (Table IV) at high frequencies. As with the third wave, the fourth wave results in the deposition of a film on the electrode surface. The identity of this film could not be determined using x-ray diffraction, but it is unlikely that it is metallic Nb, as indicated by the lack of any definitive lines in the x-ray diffraction pattern. UV-visible spectra of the HCl-saturated ethanol solution of this deposit showed bands attributable to the $Nb^{2.67+}$ and $Nb^{2.33+}$ clusters, while the SEC clearly showed that $Nb^{2.33+}$ could be generated when the potential was held at a value corresponding to this reduction wave.

At long times, or slow experiment rates, an additional wave was observed as a shoulder to the second wave. Some of the voltammetric results suggest that the product of the first reduction undergoes some chemical reaction to regenerate the initial species (although the extent of this reaction must be small on the voltammetric time-scale, since no gross effects were seen). McCurry[11b] suggested that solutions of Nb^{4+} undergo disproportionation to Nb^{3+} and Nb^{5+} at temperatures above 200°C; also, current spectroscopic studies have shown that this reaction occurs at temperatures below 200°C. Given sufficient time, the Nb^{4+} generated in the initial reduction probably disproportionates to produce an additional species, Nb^{3+}.

The Nb^{3+} produced by Nb^{4+} disproportionation subsequently undergoes a higher order reduction to a stable cluster species (Nb_3^{8+}), involving a net of one-third electrons per atom of Nb^{3+}. The excess charge exhibited by the n value of 0.46 obtained by CPC for this step may be attributed to reduction in the second wave, since it was impossible to truly isolate the shoulder from this wave. Support for such a proposal is provided by prior studies by Lantelme *et al.*[3] and Suzuki and coworkers.[19,20] Studies involving the formation of subvalent niobium species in chloride media by reduction of Nb(V)[3] and anodization of niobium metal[19,20] indicated that the species produced had a valence of less than 3; the studies by Suzuki and coworkers indicated that the predominant species was Nb_3Cl_8. The Nb^{3+} produced by disproportionation of Nb(IV) would be less stable than Nb_3^{8+}, and would be apt to be reduced at a potential more positive than that of Nb_3^{8+} (Eq. 6). Further evidence for this step was provided by SEC experiments in which the UV-visible bands due to subvalent niobium chloride species were observed, and increased with time, when the potential of the electrode was held at a potential just negative of the first reduction wave.

It follows, then, that the reaction which gives rise to the shoulder competes for reactant with that which gives rise to the second wave, but that the products of the reactions are identical; this product is further reduced in the third wave. Based on these criteria, the steps given in Eq. 8 and 9 are proposed to occur between those given in Eq. 4 and 5, at long experimental times

$$Nb^{4+} \rightleftharpoons Nb^{3+} + Nb^{5+} \quad (C) \qquad [8]$$

$$3Nb^{3+} + e^- \rightleftharpoons Nb_3^{8+} \quad (E2') \qquad [9]$$

Effect of Increased Temperature and Added Fluoride

Previous studies[3,6,11b] indicated that at low temperatures (<300°C), niobium metal was not produced when Nb(V) was

Table VI. Peak potentials[a] for CV waves at various temperatures.

Temp. (°C)	$E_{p,1}$ (V)	$(E_{p,2})^b$ (V)	$E_{p,2}$ (V)	$E_{p,3}$ (V)	$E_{p,4}$ (V)	$E_{p,5}$ (V)
160	0.11	−0.18	−0.29	−0.49	−0.80	—
180	0.13	−0.15	−0.24	−0.44	−0.78	—
200	0.13	→ −0.17 ←[c]		−0.42	−0.75	—
240	0.14	−0.19		(−0.40)[d]	−0.75	—
280	0.10	(−0.20)		→ (−0.45) ←		
325	0.088	→ −0.50 ←				(−1.2)
375	—	(−0.30)				−1.2
425		(−0.30)				−1.13
460		(−0.26)				−1.04
500		(−0.25)				−0.98

[a]All potentials given in V *vs.* the Ag(I)/Ag reference.
[b]This column refers to the shoulder preceding the second wave.
[c]Arrows indicate a merging of two waves into one.
[d]Parentheses indicate that the given value is approximate due to difficulty in determining peak potential.

reduced in $AlCl_3$-$NaCl_{SAT}$ due to the formation of stable niobium chloride clusters. Results of present studies support that conclusion. However, attempts to electrodeposit niobium in chloroaluminates at higher temperatures have not been reported. This section deals with the studies of the electrochemical behavior of Nb(V) in $AlCl_3$-$NaCl_{SAT}$ and $AlCl_3$-$NaCl_{SAT}$-NaF melts, and attempts to electrodeposit niobium in these melts at elevated temperatures.

Temperature effects.—Studies on the electrochemistry of Nb(V) in $AlCl_3$-$NaCl_{SAT}$ were conducted in the temperature range of 160 to 500°C. Table VI lists the peak potentials of the waves observed in the CV as the temperature was increased. Some general trends can be distinguished. As the temperature was increased from 160 to 240°C, all observed waves shifted in the positive direction; at 240°C and above, the first wave began to broaden and shift negatively. While the observed shifts may be in part related to a change in the junction potential of the glass bulb of the reference electrode, the lack of significant variation in the cathodic limit demonstrates that the shifts were, to some extent, real. At 325°C and above, no distinction between the second, third, and fourth waves could be seen: rather, only a large, broad wave was observed. The first wave ceased to be peak-shaped at temperatures above 325°C, as it became simply a broad, low plateau preceding the larger wave into which the second, third, and fourth waves had merged.

At temperatures ≥325°C, a new wave was observed near the cathodic limit of the melt. At temperatures below 400°C, this wave was generally difficult to resolve from the melt limit, but it became markedly observable above 400°C. This new wave was much larger than any observed in the more positive region of the CV, and it tended to shift to more positive values with increasing temperature.

Figure 8 shows a CV obtained at a temperature of 500°C. The primary features are a broad wave at approximately −0.25 V, and a large, sharper wave nearer the cathodic melt limit (−0.98 V). Also seen, beginning near +0.1 V, is the broad plateau which incorporates the initial wave in Fig. 1a. Associated with the reduction wave at −0.25 V is an anodic wave observed at approximately 0.27 V. The two anodic waves observed at −0.92 and −0.06 V are associated with the more cathodic reduction wave.

When the electrode was observed during the process of a slow linear scan at 500°C, a black film was seen to form on its surface as the potential was swept past −0.25 V, where the first peak appears in Fig. 8.

The decrease in the UV-visible bands due to the Nb_6^{+12} cluster as the temperature was increased from 175 to 350°C supports the lower stability of this cluster at elevated temperatures.

Effect of adding fluoride.—No significant differences were observed between CVs obtained from $AlCl_3$-$NaCl_{SAT}$ and $AlCl_3$-$NaCl_{SAT}$-NaF solutions of Nb(V), even with a NaF composition as high as 10 m/o. Two main reduction waves were seen at −0.27 and −0.97 V. As in the $AlCl_3$-$NaCl_{SAT}$ melt, a film was formed on the electrode surface at the first reduction wave, and no changes in the appearance of the electrode surface were observed upon reaching the second wave. The film disappeared during the anodic scan after reaching the most positive anodic wave.

Electrolysis of Nb(V).—Attempts were made to produce niobium metal by constant current electrolysis of a Nb(V) solution in $AlCl_3$-$NaCl_{SAT}$ and $AlCl_3$-$NaCl_{SAT}$-NaF melts. Several parameters were varied, including the temperature, the Nb(V) concentration, the fluoride content of the melt, the current density, and the cathode substrate material. The range of parameters was by no means exhausted, and much work remains in this area before definitive results can be reported. We report here some preliminary observations made in the process of attempting to reduce Nb(V) to the metal. In all but a few cases, no metal was obtained, at least none that could be observed using electron spectroscopy for chemical analysis and x-ray diffraction analysis. In all cases, at the end of an experiment the cathode was found to be covered with a thick coating of undissolved, dark-green colored material; UV-visible spectra of an aqueous solution of this material had the appearance of a combination of the spectra reported for niobium chloride cluster species of the form $[Nb_6Cl_{12}]^{m+}$, with m = 2, 3, 4.

Current densities ranging from 5 to 250 mA/cm² were studied, and in some cases, the current was pulsed between cathodic and anodic values, in an attempt to minimize the accumulation of nonmetallic deposit on the electrode surface. These experiments seemed to indicate that, when niobium metal was produced at all, it was only at low current densities (<50 mA/cm²); in such cases, the coating of undissolved material on the cathode was thinner and more evenly distributed. The pulsed method had no observable effect.

The fluoride content of the melt was varied from R = 0 to R = 1.0.[c] The variation of R appeared to have no significant effect on deposition. In fact, the best deposit was obtained from a melt containing no fluoride.

The temperature at which deposition was attempted was varied from 525 to 625°C. It was apparent that temperatures higher than 525°C were needed to allow the deposition of niobium metal. No distinct advantage to using temperatures higher than 550°C was seen, although it is likely that extending the studies to temperatures higher than 700°C will produce better results, due to the lower stability and possibly higher solubility of cluster species at such temperatures.

[c]The value of R is given by the molar ratio of fluoride to aluminum, *e.g.*, a 10 m/o NaF melt would have $R = F/Al = 10/90 = 0.11$.

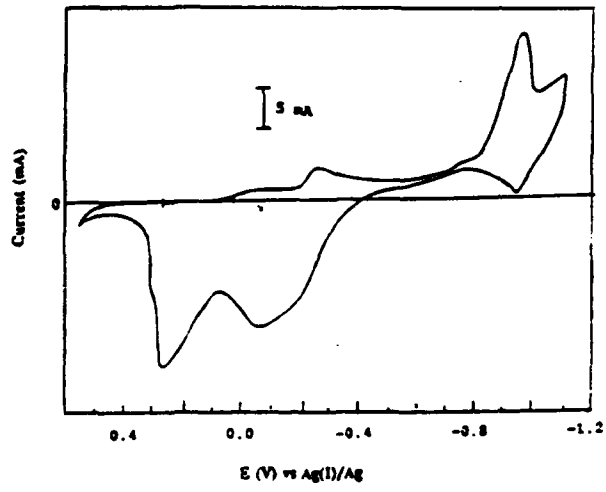

Fig. 8. Cyclic voltammogram obtained for a 3.2×10^{-2} *M* Nb(V) solution in $AlCl_3$-$NaCl_{SAT}$ at 500°C. The working electrode was a tungsten wire, and the scan rate was 0.1 V/s.

Tungsten foil and nickel plates were used as cathode materials. The smoothest deposit was obtained using a tungsten foil cathode, but experiments that produced niobium were sufficiently few that no definite conclusion concerning the cathode material can be put forth.

The thickness of the deposits was estimated to be less than 10 μm, due to the fact that x-ray diffraction patterns for niobium deposits invariably showed strong lines due to the substrate material; niobium lines generally had intensities of about 1 to 2% of that of the strongest substrate line.

Conclusions

Results are presented which demonstrate that previous reports from our laboratory[4,6] on the electrochemistry of Nb(V) in $AlCl_3$-$NaCl_{SAT}$ melt were in error. We previously proposed a reaction sequence for the reduction of Nb(V) based on the assumption that the reacting species was $NbCl_4$. It is shown here that the previous studies were conducted in melts which contained quite high concentrations of oxide impurities, and that the species under study was in fact niobium(V) oxychloride.

The electrochemical and spectroelectrochemical behavior of $NbCl_4$ in $AlCl_3$-$NaCl_{SAT}$ was reinvestigated using melts which were treated with phosgene or CCl_4 to remove oxide impurities. It was determined that the reduction of Nb(V) at 178°C involved four steps in the simplest case, which was when the experiment rate was fast or experiment times were short. At long experimental times (slow rates), a complication was observed in the form of an additional wave between the first and second reduction waves. It was postulated, based on the analysis of experimental data, that this wave was due to the reduction of Nb(III), produced by the disproportionation of Nb(IV) formed in the first step.

An examination of the effect of temperature on the electrochemical behavior of Nb(V) in $AlCl_3$-$NaCl_{SAT}$ and $AlCl_3$-$NaCl_{SAT}$-NaF melts was undertaken. No significant difference in the Nb(V) electrochemistry in these two melts was observed, but variations in temperature produced dramatic changes in the voltammetric response. In general, as the temperature was increased from <200 to 500°C, the first wave broadened and became almost indistinguishable, except as a broad, flat plateau. The final three (four) waves in the low-temperature voltammogram merged into a single large wave. Also, as the temperature was increased, a new wave was observed near the melt cathodic limit: the peak potential of this new wave shifted to more positive values as the temperature was increased.

Some constant current electrolysis experiments were conducted in sodium chloroaluminate and fluorochloroaluminate melts at temperatures >400°C in attempts to electrochemically produce Nb metal from Nb(V) solutions. It was possible to produce smooth coatings of Nb metal on both nickel and tungsten substrates. Although these deposits were rather thin, this represents the first successful production of metallic niobium from sodium chloroaluminate melts.

Acknowledgments

This work was supported by the U.S. Air Force Office of Scientific Research, Grants No. 88-0307 and No. F49620-93-1-0129. We would like to acknowledg useful discussions with Professor Roberto Marassi, University of Camerino.

Manuscript submitted Oct. 16, 1993; revised manuscript received March 2, 1994.

The University of Tennessee assisted in part in meeting the publication costs of this article.

REFERENCES

1. V. I. Konstantinov, E. G. Polyakov, and P. T. Stangrit. *Electrochim. Acta*, **26**, 445 (1981).
2. L. P. Polyakova, E. G. Polyakov, A. I. Sorokin, and P. T. Stangrit, *J. Appl. Electrochem.*, **22**, 628 (1992).
3. F. Lantelme, A. Barhoun, and J. Chevalet, *This Journal*, **140**, 324 (1993).
4. I-W. Sun and C. L. Hussey, *Inorg. Chem.*, **28**, 2731 (1989).
5. G. Ting, Ph.D. Thesis, The University of Tennessee, Knoxville, TN (1973).
6. G. Ting, K. W. Fung, and G. Mamantov, *This Journal*, **123**, 624 (1976).
7. H. Linga, Z. Stojek, and R. A. Osteryoung, *J. Am. Chem. Soc.*, **103**, 3754 (1981).
8. K. D. Sienerth, Ph.D. Thesis, The University of Tennessee, Knoxville, TN (1992).
9. I-W. Sun, K. D. Sienerth, and G. Mamantov, *This Journal*, **138**, 2850 (1991).
10. G-S. Chen, I-W. Sun, K. D. Sienerth, A. G. Edwards, and G. Mamantov, *ibid.*, **140**, 1523 (1993).
11. (a) P. A. Flowers, Ph.D. Thesis, The University of Tennessee, Knoxville, TN (1988); (b) L. E. McCurry, Ph.D. Thesis, The University of Tennessee, Knoxville, TN (1978).
12. A. J. Bard and L. R. Faulkner, *Electrochemical Methods: Fundamentals and Applications*, Wiley, New York (1980).
13. R. S. Nicholson an I. Shain, *Anal. Chem.*, **36**, 706 (1964).
14. J. Osteryoung and J. J. O'Dea, in *Electroanalytical Chemistry: A Series of Advances*, Vol. 14, A. J. Bard, Editor, Marcel Dekker, Inc., New York (1989).
15. R. Quigley, P. A. Barnard, C. L. Hussey, and K. R. Seddon, *Inorg. Chem.*, **31**, 1255 (1992).
16. D. L. Manning and G. Mamantov, *J. Electroanal. Chem.*, **17**, 137 (1968).
17. F. R. Clayton, G. Mamantov, and D. L. Manning, *This Journal*, **121**, 86 (1974).
18. J. H. Canterford and R. Colton, in *Halides of the Transition Elements*, D. Brown, Editor, pp. 145-205, Wiley, New York (1969).
19. Y. Saeki and T. Suzuki, *J. Less Common Metals*, **9**, 362 (1965).
20. T. Suzuki, *Electrochim. Acta*, **15**, 127 (1970).

Spectroelectrochemical Investigation of the Behavior of Tetra-chloro-*p*-benzoquinone in Molten Sodium Chloroaluminates

E. M. HONDROGIANNIS, J. C. COFFIELD, D. S. TRIMBLE, A. E. EDWARDS, and G. MAMANTOV*

Department of Chemistry, University of Tennessee, Knoxville, Tennessee 37996-1600

The Raman, UV-visible, electron spin resonance spectroscopic, and spectroelectrochemical (SEC) behavior of tetrachloro-*p*-benzoquinone (chloranil) in molten aluminum chloride/sodium chloride mixtures has been examined. The results support previous findings suggesting that the chloranil is complexed by $AlCl_3$ or $Al_2Cl_7^-$ in acidic melts [>50 mole percent (m/o) $AlCl_3$], while in basic melts (<50 m/o $AlCl_3$) the chloranil remains uncomplexed. The results further support the previously proposed stepwise one-electron reductions in the acidic melt to produce the radical anion and the dianion. The present work, however, reveals that chloranil is also reduced through two closely spaced one-electron reductions in the basic melt.

Index Headings: **Molten salts; Sodium alkali chloroaluminates; Chloranil; UV-visible; Raman; Electron spin resonance; Spectroelectrochemistry; FT-IR; Infrared spectroscopy.**

INTRODUCTION

The electrochemistry of tetrachloro-*p*-benzoquinone (chloranil or *Q*) was first studied by Mamantov and coworkers[1] for its use as a cathode material for high-energy molten salt batteries. Bartak and Osteryoung[2] employed voltammetric methods to study the behavior of chloranil in $AlCl_3$–NaCl melts and concluded that the reduction proceeds via the following mechanism:

$$Q + e^- \rightleftharpoons Q^- \quad (1)$$

$$Q^- + A \rightarrow QA^- \quad (2)$$

$$QA^- + e^- \rightleftharpoons QA^{2-} \quad (3)$$

$$QA^{2-} + A \rightarrow QA_2^{2-} \quad (4)$$

where *A* is a Lewis acid species, i.e., either $AlCl_3$ or $Al_2Cl_7^-$. The complexed radical anion QA^- is reduced at potentials similar to that of *Q* (Eq. 1); thus only one cathodic wave corresponding to an overall two-electron reduction is observed. Only when the complexation is "outrun" at very fast scan rates are two waves, corresponding to the stepwise reduction of *Q* to Q^{2-}, observed.

Cheek and Osteryoung[3] used electrochemical and infrared spectroscopic methods to study chloranil in the $AlCl_3$–butyl pyridinium chloride (BPC) solvent system. Only slight differences in the electrochemical behavior were observed in comparison with the $AlCl_3$–NaCl melts. These differences were attributed to the greater Lewis acidity of the alkali chloroaluminate system. Infrared spectroscopy using the acidic melt showed that only one of the two carbonyl oxygens was complexed by $AlCl_3$.

Infrared and Raman spectroscopic and spectroelectrochemical results for chloranil in sodium chloroaluminate melts[4,5] show that in acidic melts ($AlCl_3$/NaCl mole ratio >1) chloranil is complexed with $AlCl_3$ (or $Al_2Cl_7^-$) at one of the carbonyl oxygens and at the carbon–carbon double bonds. The infrared spectroelectrochemical results suggest stepwise one-electron reductions to produce the complexed radical anion and the complexed dianion. No evidence for complexation of neutral chloranil was found in the basic melt ($AlCl_3$/NaCl mole ratio <1), where spectroelectrochemical results showed an overall two-electron reduction.

In this paper, Raman, electron spin resonance (ESR), and UV–visible spectroscopic and spectroelectrochemical (SEC) results for chloranil in molten sodium chloroaluminates are presented. These techniques were successful in identifying the radical anion intermediate which had not been observed in the basic melt previously. The UV–visible spectrum for this species and the Nernst plot support the transfer of one electron to generate the anion intermediate. Raman and ESR spectroelectrochemical results support the stepwise reduction scheme in basic chloroaluminate melts.

EXPERIMENTAL

Materials. Sodium chloride (Mallinckrodt, reagent grade) was dried under vacuum at 450°C for several days. Aluminum chloride (Fluka, puriss grade, >99%) was purified by distillation in a three-bulb Pyrex® tube containing a small amount of aluminum metal (Aesar, 99.9999%) and NaCl as described previously.[6] Chloranil (Fluka >99%) was purified by sublimation at 150°C. Melts were prepared by adding the desired amounts of $AlCl_3$ and NaCl to a Pyrex® tube inside a nitrogen-filled glove box, evacuating, sealing the tube, and then fusing the mixture in a rocking furnace at 180°C overnight.

Spectroelectrochemical Cells. The SEC cell used for both the Raman and the UV–visible studies has been described previously.[7] The thin-layer working electrode, contained in the quartz cuvette, was either a platinum screen or a reticulated vitreous carbon (RVC) electrode. The reference electrode was an aluminum spiral immersed in an $AlCl_3$–$NaCl_{sat}$ melt and separated from the bulk solution by a fine Pyrex® frit. The counter electrode was platinum foil (~1.0 cm^2) separated from the bulk solution by a coarse Pyrex® frit. The ESR spectroelectrochemical cell, constructed in-house, is similar to the cell used for the UV–visible and Raman spectroelectrochemistry except that the quartz cell was flattened. This

Received 10 August 1993; revision received 13 December 1993.
* Author to whom correspondence should be sent.

0003-7028/94/4803-0406$2.00/0
© 1994 Society for Applied Spectroscopy

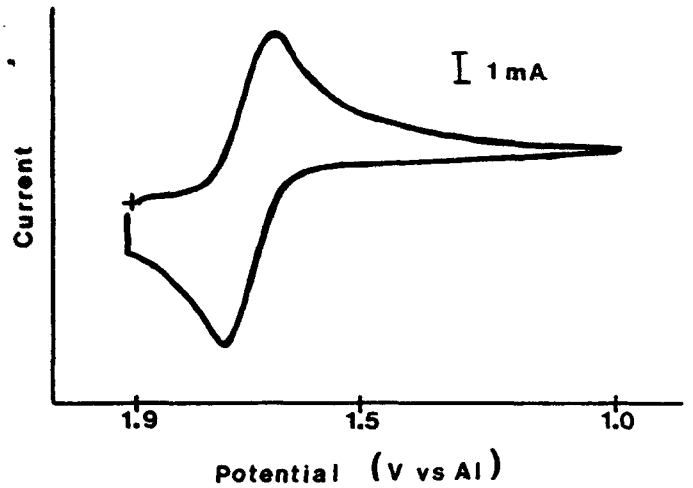

FIG. 1. Cyclic voltammogram for 20.7 mM chloranil in $AlCl_3$–$NaCl_{sat}$ at 175°C obtained in the thin-layer cell. Experimental parameters: RVC working electrode, Pt flag auxiliary electrode, Al reference, 50 mV/s.

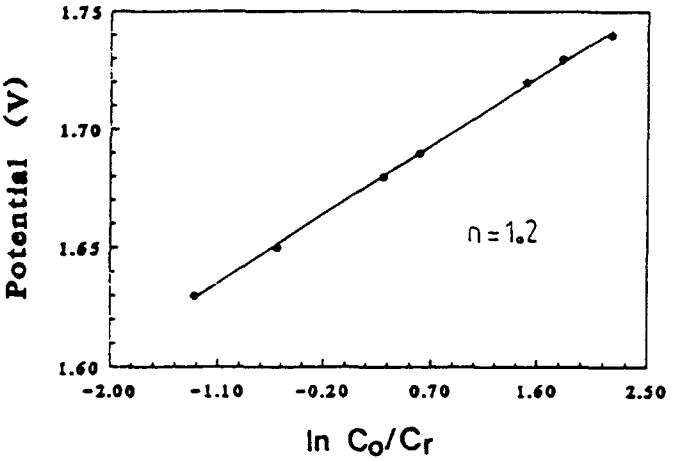

FIG. 2. Nernst plot for the generation of chloranil anion in $AlCl_3$–$NaCl_{sat}$ at 175°C.

flattened quartz end was placed perpendicular to the electric field. The quartz part was in turn joined to the bulk of the Pyrex® cell via a quartz-to-Pyrex® graded seal. The cell employed a platinum flag thin-layer working electrode and a tungsten wire counter electrode. The platinum was in turn welded to a tungsten wire which served as the electrical contact at the top of the cell. The electrodes were sheathed with Pyrex® to avoid exposure of the metals to the solution. The solution was added to the cell through a sidearm which was then sealed after evacuating the cell.

Instrumentation. Electrochemical measurements were carried out with the use of a Princeton Applied Research (PAR) Model 174A polarographic analyzer in conjunction with a PAR Model 175 universal programmer and a Houston Omnigraphic X-Y recorder. Raman measurements were made with the use of the 363.8-nm line (power typically between 50 and 125 mW) from a Coherent Innova 100-15 argon–ion laser, a Spex 1877 triple monochromator, and a Tracor Northern (TN)-6133 intensified 512-element photodiode array. UV–visible spectra were acquired with a TN-6500 photodiode array rapid scanning spectrophotometer employing deuterium and tungsten halogen lamps. The experimental arrangement for the ESR spectroscopy has been described.[8]

RESULTS AND DISCUSSION

UV-Visible Spectroelectrochemistry in Basic Melts. A cyclic voltammogram for 20.7 mM chloranil in the $AlCl_3$–$NaCl_{sat}$ melt is shown in Fig. 1. A reduction wave at 1.65 V and an oxidation wave at 1.73 V at a scan rate of 50 mV/s are observed. The UV–visible spectrum of a solution containing 1.2 mM chloranil in the $AlCl_3$-$NaCl_{sat}$ melt shows a broad band with a maximum at 305 nm; no other features are present out to 750 nm. Electrolysis at a potential of 0.8 V for 30 min generates the chloranil dianion which gives a spectrum showing a broad band with a maximum at 302 nm; no other features are present out to 750 nm.

Spectra acquired during this potentiostatic electrolysis revealed a weak transient band at 515 nm. This band reached a maximum absorbance and then decreased back to "zero" when the electrode potential was stepped negative with respect to the Q/Q^{2-} reduction potential. This band is not present at potentials corresponding to that of either the chloranil parent or the dianion. The plot of absorbance with time for the parent band at 305 nm shows the expected decrease in the band due to the parent as it is reduced to the dianion.

According to the Nernst equation, the ratio for the equilibrium concentrations of the oxidized to reduced forms at the electrode is determined by the applied potential

$$E = E^{0\prime} + RT/nF \ln(C_o/C_r) \qquad (5)$$

where E is the applied potential, $E^{0\prime}$ is the formal potential, R is the molar gas constant, T is the temperature, n is the number of electrons transferred, and F is the Faraday constant. In thin-layer spectroelectrochemistry, C_o/C_r can be defined as[9]

$$C_o/C_r = A_o/(A_{oi} - A_o) = (A_{ri} - A_r)/A_r \qquad (6)$$

where A_x ($x = r$ or o) is the absorbance of species x at any given potential, and A_{xi} is the absorbance of species x at a potential where it is the only form of the redox couple present. A plot of E versus $\ln C_o/C_r$ yields a straight line in which the $E^{0\prime}$ is obtained from the y-intercept, and the number of electrons is obtained from the slope of the plot.

Figure 2 shows such a Nernst plot constructed with the use of the chloranil intermediate and parent bands. An n value of 1.2 electrons was calculated from the slope of this plot. This result is consistent with the one-electron reduction of the chloranil parent to produce the radical anion intermediate.

UV-Visible Spectroelectrochemistry in Acidic Melts. The spectrum obtained for a 1.1 mM chloranil solution in the $AlCl_3$–NaCl (63/37 mol %) melt at its rest potential shows two bands at 515 and 330 nm. The band with its maximum absorbance at 515 nm is due to the chloranil radical anion. This is the same wavelength at which the radical anion absorbs in the basic melt. The band at 330 nm is attributed to the complexed chloranil parent, since both Raman and infrared data[4,5] previously showed this species to be present along with the radical anion at the

solution rest potential. The presence of the radical anion in the acidic melt in the absence of any applied potential supports the spontaneous formation of this species via reduction of chloranil by the solvent. The spectrum obtained at electrode potentials negative of the Q/Q^{2-} reduction potential matches that observed for the same conditions in the basic melt. At intermediate potentials, the band at 515 nm rises to a maximum and then decreases, as expected.

Flowers and Mamantov[4] previously showed that the chloranil parent is complexed, with $AlCl_3$ or $Al_2Cl_7^-$, in the acidic melt and that it is reduced to the complexed radical anion and then to the complexed dianion. The fact that the absorbance maximum for the anion intermediate occurs at 515 nm in both the acidic and the basic melts supports the formation of the complexed anion intermediate in both melts.

Raman Spectroelectrochemistry in Basic Melts. The Raman spectrum of a 20.7 mM solution of chloranil in the $AlCl_3$–$NaCl_{sat}$ melt shows two bands at 1602 and 1700 cm^{-1}. When the electrode potential is held at 0.8 V for 30 min to generate the chloranil dianion, these two bands disappear as expected, since the electrode potential is negative with respect to the Q/Q^{2-} potential. No new bands are observed due to the dianion. This outcome is not surprising, since previous results support the observation that the parent and the radical anion bands are due to a resonance Raman effect. Both the parent and the radical anion absorb at the 363.8-nm wavelength used for the Raman excitation; the dianion, however, does not absorb at that wavelength. At potentials intermediate to those which produce the parent and the dianion, the bands at 1602 and 1700 cm^{-1} have decreased in intensity, as expected. In addition, two weak bands are present at 1071 and 1350 cm^{-1}. These bands appear at approximately the same Raman shifts (1076 and 1338 cm^{-1}) as those present in spectra of acidic melts under the same conditions.[5] Electrolysis at increasingly negative potentials shows that the intensities of these bands decrease after reaching a maximum. This behavior is indicative of the generation of the anion intermediate from reduction of chloranil and its subsequent reduction to the dianion. When the potential is sufficiently negative, these bands are no longer present. A similar transient behavior is observed upon stepping the electrode potential anodically to regenerate neutral chloranil.

It should be noted that the choice of the 363.8-nm line for excitation was made only after attempts to use both the 514.5- and the 488.0-nm lines failed due to a large background fluorescence which prohibited the observation of the chloranil bands. An attempt was also made to use a greater chloranil concentration in the melt to increase the intensity of the Raman signals. It was, however, limited to only ~40 mM, since this concentration was determined to be the solubility limit of chloranil.

ESR Spectroelectrochemistry in Basic Melts. ESR spectroelectrochemistry revealed no signal at the solution rest potential, where it has been shown that only the chloranil parent is present. When the platinum foil working electrode is stepped negative with respect to the Q/Q^{2-} reduction potential, a weak signal grows in and then decreases. Likewise, when the electrode potential is stepped back to the original value, the signal grows back in to a maximum and then decreases, clearly indicating the dependence of the species giving rise to the ESR signal on the electrode potential. Since it was thought that the low signal intensity might be the result of the platinum foil working electrode decreasing the electric field strength inside the cell cavity, a new cell was constructed with the use of a platinum mesh working electrode, and the spectroelectrochemistry was repeated as described above. The same behavior was observed but with a slight increase in the intensity of the signal. The average g-value obtained in the basic solution is 2.0044 ± 0.003.

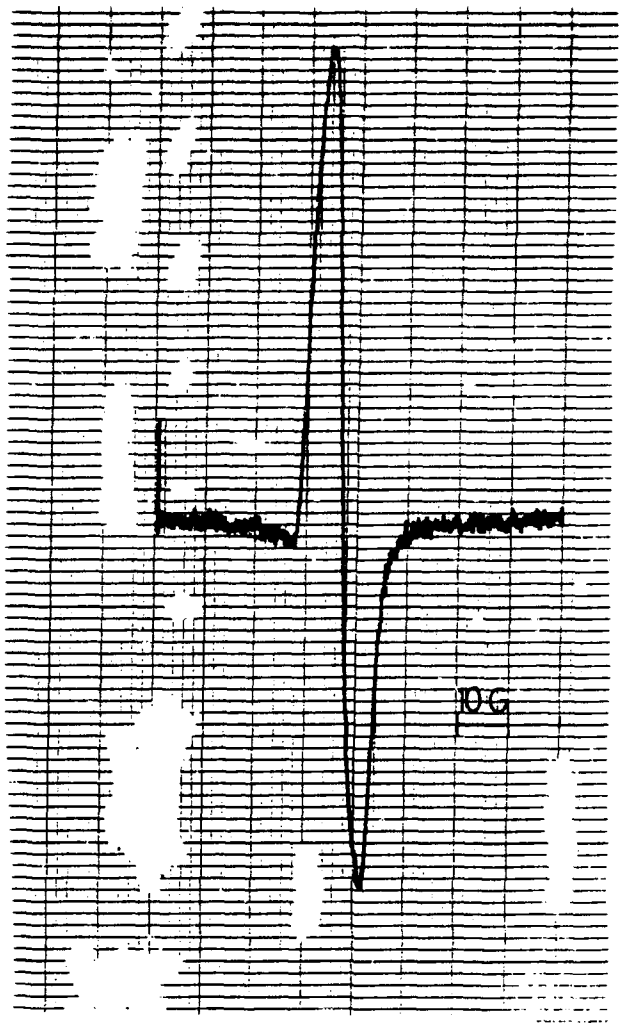

FIG. 3. ESR spectrum for chloranil radical anion in $AlCl_3$–NaCl (63/37 mol % $AlCl_3$) melt at 175°C.

ESR Spectroelectrochemistry in Acidic Melts. A solution containing 9.5 mM chloranil in the $AlCl_3$–NaCl (63/37 mol %) melt gave a weak ESR signal with no applied potential, supporting the spontaneous formation of the radical anion. Stepping the working electrode to a value negative of the Q/Q^{2-} reduction potential resulted in an increase of this signal. Since it was believed that the working electrode was decreasing the electric field strength in the cell cavity, a new cell was prepared without a working electrode. A solution of Q^- was prepared *ex situ* by bulk electrolysis and transferred to the ESR cell. The resulting ESR signal (Fig. 3) is significantly larger than that obtained in the presence of the working elec-

trode. The average g-value in the acidic melt is 2.0051 $\pm$ 0.0001. The difference between the g-values for the anion intermediate in the acidic and the basic melts is not expected, since both UV–visible and Raman spectroelectrochemical results support the existence of the complexed radical anion in both melts. One likely explanation is the uncertainty in reading line positions from the spectra recorded of the basic solution, since those spectra exhibit a low signal-to-noise ratio.

CONCLUSIONS

Other investigators previously identified the radical anion in the acidic melt using Raman and infrared spectroscopies. The UV–visible and ESR spectroelectrochemical results discussed here support their findings. Furthermore, the presence of radical anion bands in the Raman and UV–visible spectra at the same frequencies for both the acidic and the basic melts suggests that the radical anion is complexed in each medium. On the basis of the new spectroelectrochemical evidence presented here, it is apparent that the reduction of chloranil in the basic melt occurs not by a single two-electron process but through the stepwise reduction of chloranil to the radical anion and dianion.

It is not surprising that the anion intermediate was not observed in the saturated melt with the use of infrared spectroelectrochemistry.[4] Close examination of these spectra reveals a significantly larger potential step than that used in acquiring the UV–visible, Raman, and ESR spectra. Furthermore, each infrared spectrum was acquired two minutes after the potential step, which would give the transient species enough time to be reduced to the dianion.

In a final note, the above results exemplify the utility of combining spectroscopy and electrochemistry for the characterization of electrochemical systems. In this particular case, cyclic voltammetry in the basic melt showed only one wave due to the overall two-electron reduction of the chloranil to the dianion. Only from the spectroelectrochemical results was the formation of the radical anion intermediate detected.

ACKNOWLEDGMENTS

The authors wish to express their appreciation to Dr. A. C. Buchanan of Oak Ridge National Laboratory for obtaining the ESR spectra, Elder Mellon of UTK for construction of the spectroelectrochemical cells, and Dr. Paul Flowers for useful discussions aiding in preparation of this paper. This research was supported by the Air Force Office of Scientific Research, Grants No. 88-0307 and No. F49620-93-0129.

1. G. Mamantov, R. Marassi, and J. Q. Chambers, in "High Energy Cathodes for Fused Salt Batteries," Final Report, Contract DAABO7-73-7-0060 (1974), ECOM-0060-F.
2. D. E. Bartak and R. A. Osteryoung, J. Electroanal. Chem. **74**, 69 (1976).
3. G. Cheek and R. A. Osteryoung, J. Electrochem. Soc. **129**, 2739 (1982).
4. P. A. Flowers and G. Mamantov, J. Electrochem. Soc. **136**, 2944 (1989).
5. D. S. Trimble, Ph.D. Dissertation, University of Tennessee, Knoxville (1989).
6. R. Marassi, J. Q. Chambers, and G. Mamantov, J. Electroanal. Chem. **69**, 345 (1976).
7. V. E. Norvell and G. Mamantov, Anal. Chem. **47**, 1470 (1977).
8. R. Livingston and H. Zeldes, J. Chem. Phys. **44**, 1245 (1966).
9. T. P. DeAngelis and W. R. Heineman, J. Chem. Ed. **53**, 594 (1976).

Reprinted from the Journal of the American Chemical Society, 1993, 115.
Copyright © 1993 by the American Chemical Society and reprinted by permission of the copyright owner.

Novel Photochemical Behavior of Anthracene in a Room Temperature Molten Salt

George Hondrogiannis, Carlos W. Lee, Richard M. Pagni,* and Gleb Mamantov*

Department of Chemistry
University of Tennessee
Knoxville, Tennessee 37996-1600

Received July 19, 1993

There are now available ionic mixtures which are liquid at or near room temperature.[1] The most widely studied of these consists of mixtures of 1-ethyl-3-methyl-1*H*-imidazolium chloride (EMIC) and $AlCl_3$ which are liquid at room temperature over a wide range of EMIC:$AlCl_3$ ratios (R).[2] By adjusting R, liquids are

EMIC

created which are basic ($R > 1$; Cl^- = base), neutral ($R = 1$; $[EMI^+] = [AlCl_4^-]$), and acidic ($R < 1$; $Al_2Cl_7^-$ = acid) and have vastly different pCl (i.e., –log $[Cl^-]$) values.[3] Basic and acidic melts also have significantly different electrochemical windows[4] and chemical properties. HCl, for example, is a powerful Brønsted acid in acidic media, but a much weaker one in basic ones.[4,5] We wish to report the first example of a photochemical reaction in a molten salt and to show how altering the composition of this molten salt profoundly influences photochemical behavior.

Photolysis of a 0.140 M solution of anthracene (1) in a basic EMIC/$AlCl_3$ melt (55.0 mol % EMIC; pale yellow solution) under vacuum in a Pyrex vessel[6] afforded dimer 2 exclusively.[7] This behavior is identical to that seen for 1 in a wide variety of more traditional solvents.[8] This dimerization, in fact, is the paradigm for a photochemically allowed [4 + 4] cycloaddition reaction.[8,9] Photolysis of a 0.148 M solution of anthracene in an acidic melt containing proton (55.0 mol % $AlCl_3$; green solution), on the other hand, is quite different, yielding at least 16 oxidized, neutral, and reduced monomeric and dimeric products (analytical HPLC).[10] The major products were identified as 2–7, with trace amounts of 9,9′-bianthracene and 1,2,3,4-tetrahydroanthracene also being formed, as well as a fused dimer of unknown structure (8) but similar spectroscopically to 7.[11] No chlorinated products or those which incorporated the EMI ring (uncharged or cationic)[12] were formed in the photoreaction.

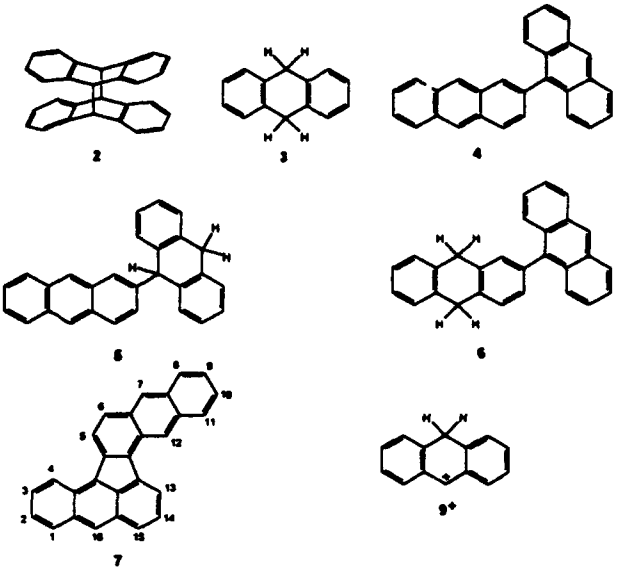

Product yields were followed as a function of time (Table I, entries 1–3). The photoreaction is rapid initially but much slower at longer reaction times, due likely to an internal filter effect of the highly conjugated 4, 7, and 8 and quenching of excited states by these same species. Most of the products are also reactive as their yields go down as the reaction progresses. Only the yield of the highly oxidized 7 (and 2) goes up as the reaction proceeds. The mass balance also decays as a function of time, suggesting the formation of oligomeric and polymeric compounds at longer reaction times. The hydrogen balance, which is a measure of the excess of reduction or oxidation in the characterized products, is small but not 0, also demonstrating the formation of missing products.

This unusual photochemistry must be initiated by an electron-transfer reaction. One possible electron acceptor is EMI^+, but this is not correct. First of all, EMI^+ did not function as an electron acceptor in the photochemistry of 1 in the basic melt, nor does it in the photoreaction of 1 in CH_3CN saturated with EMIC, where 2 is formed quantitatively. The electron acceptor is, in fact, the anthracenium ion 9^+,[13] formed by protonation of 1 with trace amounts of HCl in the melt,[14] and it is more easily reduced electrochemically than is EMIC (eqs 1–3).[14] Even the

$$1 + HCl \rightleftharpoons 9^+ \qquad (1)$$

$$1 + 9^+ \xrightarrow{h\nu} 1^{\bullet+} + 9^{\bullet} \qquad (2)$$

$$1^{\bullet+} + 9^{\bullet} \longrightarrow \text{products} \qquad (3)$$

most rigorously purified melts contain traces of HCl. In the first three photoreactions described in Table I, there is approximately 3% of 9^+ present in each solution. When the HCl content of the melt is deliberately increased by the addition of EMIC·HCl,[14] the content of 9^+ increases to 26% (Table, entry 4). When this solution is irradiated, the photochemistry is somewhat different than the previously described cases, but it is exclusively redox in

(1) Hussey, C. H. In *Advances in Molten Salt Chemistry*; Mamantov, G., Mamantov, C., Eds.; Elsevier: Amsterdam, 1983; Vol. 5, p 185.
(2) (a) Wilkes, J. S.; Levisky, J. A.; Wilson, R. A.; Hussey, C. L. *Inorg. Chem.* **1982**, *21*, 1263. (b) Fannin, A. A., Jr.; Floreani, D. A.; King, L. A.; Landers, J. S.; Piersma, B. J.; Stech, D. J.; Vaughn, R. L.; Wilkes, J. S.; Williams, J. L. *J. Phys. Chem.* **1984**, *88*, 2614.
(3) Hussey, C. L.; Scheffler, T. B.; Wilkes, J. S.; Fannin, A. A., Jr. *J. Electrochem. Soc.* **1986**, *133*, 1389.
(4) Smith, G. P.; Dworkin, A. S.; Pagni, R. M.; Zingg, S. P. *J. Am. Chem. Soc.* **1989**, *111*, 525.
(5) Smith, G. P.; Dworkin, A. S.; Pagni, R. M.; Zingg, S. P. *J. Am. Chem. Soc.* **1989**, *111*, 5075.
(6) A Rayonet reactor with 3500-Å lamps was used as the light source.
(7) The reaction mixtures were quenched with water under argon and products extracted into methylene chloride.
(8) (a) Cowan, D. O.; Drisco, R. L. *Elements of Organic Photochemistry*; Plenum: New York, 1976; Chapter 2. (b) Becker, H.-D. *Chem. Rev.* **1993**, *93*, 145 and references cited therein.
(9) Woodward, R. B.; Hoffmann, R. *The Conservation of Orbital Symmetry*; Verlag: Weinheim, Germany, 1970.
(10) An uncharacterized condensation chemistry also occurs in the absence of light, but the reaction is much slower than the photochemical reaction.
(11) The products were separated by column chromatography, prep TLC, and prep HPLC and characterized spectroscopically. Known samples of 2, 9,9′-bianthracene, and 1,2,3,4-tetrahydroanthracene were available. The spectra of some other products were available in the literature. 2,3-Dichloro-5,6-dicyanobenzoquinone (DDQ) oxidation of the reduced products gave the corresponding aromatic hydrocarbons.
(12) The aqueous solution formed during reaction workup, which contains EMI^+ and other ionic organic compounds, was evaporated and the residue subjected to SIMS. Only EMI^+ was detected.
(13) The electron transfer from arene excited states including that of anthracene to diaryl- and triarylmethyl carbocations is known and is very fast: Johnston, L. J.; Kanigan, T. *J. Am. Chem. Soc.* **1990**, *112*, 1271. Samanta, A.; Gopidas, K. R.; Das, P. K. *Chem. Phys. Lett.* **1993**, *204*, 269.
(14) Carlin, R. T.; Trulove, P. C.; Osteryoung, R. A. *Electrochim. Acta* **1992**, *37*, 2615.

0002-7863/93/1515-9828$04.00/0 © 1993 American Chemical Society

Table I. Product Distributions from the Photolysis of Anthracene in Acidic Melts[a]

entry	reaction time (h)	ratio of 1 to protonated 1[b]	% of 1 consumed	yield[c] (%)							material balance (%)[e]	hydrogen balance (%)[f]
				3	4	5	6	7	8[d]	2		
1	0.5	29:1	12.7	24.5	19.4	12.1	2.3	0	13.7	0	72.0	4
2	24	29:1	60.4	7.3	6.8	2.3	1.5	1.0	1.8	2.0	22.7	8
3	48	29:1	64.2	6.2	4.6	2.4	1.3	3.1	1.3	2.4	21.3	–4
4	48	2.9:1[g]	73.6	2.5 (2.8)[h]	0	0	0	9.0	0	0	14.2	–6
5	24	1:0[i,j]	15.4	1.9	0	0	0	0	0	2.5	44.4	

[a] 0.148 M solution (2.35 mmol of 1 in 21.0 g of melt (55.0 mol % $AlCl_3$) which has a density of 1.32 g/mL[20] photolyzed in Pyrex under argon. [b] Based on the extinction coefficient of protonated anthracene (Zingg, S. P.; Dworkin, A. S.; Sølie, M.; Chapman, D. M.; Buchanan, A. C., III; Smith, G. P. *J. Electrochem. Soc.* **1984**, *31*, 1602 and ref 4–5) and the equilibrium constant for the reversible protonation of anthracene[14] using dilute solutions of anthracene in the melt. [c] For monomeric products: (mmol of product/mmol of consumed 1) × 100. For dimeric products: (mmol of product × 2/mmol of consumed 1) × 100. [d] An unknown fused product similar to 7. [e] [(Σmmol of monomeric products + 2Σmmol of dimeric products)/mmol of consumed 1] × 100. [f] (mmol of H added to reduced products – mmol of H lost from oxidized products)/(mmol of H added to reduced products + mmol of H lost from oxidized products) × 100. [g] HCl in the melt increased by the addition of EMIC-HCl.[14] [h] Yields of 1,2,3,4-tetrahydroanthracene. [i] HCl removed from the melt by addition of excess methylaluminum sesquichloride.[14] [j] GC/MS of the product mixture revealed the presence of methylanthracene(s) (8%), 9,10-dimethylanthracene (1%), and chloroanthracene(s) (2%).

nature, giving largely the highly oxidized and reduced products 7 and 1,2,3,4-tetrahydroanthracene. This reaction is clearly farther along the cascade of oxidation and reduction reactions than are the previous three examples. When the HCl is deliberately removed by addition of excess methylaluminum sesquichloride,[14] the overall reaction is slower than when HCl is present, and the redox chemistry is largely suppressed (Table I, entry 5).[15]

The essential difference in the photochemistry of 1 in the basic and acidic molten salts is due to the different in acidity of HCl in the two media. In the basic melt, HCl is insufficiently acidic to protonate 1, and the photochemistry proceeds in the normal manner. In the acidic medium, however, HCl, now a powerful Brønsted acid, protonates 1 to form a small amount of 9^+, which function as an electron acceptor, thus diverting the chemistry of 1 into an entirely new channel. Photolysis of 1 in H_2O also generates $1^{\bullet+}$,[16] which reacts rapidly with the nucleophilic H_2O.[16,17] In the acidic molten salt, there are no good nucleophiles with which $1^{\bullet+}$ can react. Only 1 or products or transients derived from 1 can serve this purpose. As a result, the chemistry is dominated by bimolecular electron transfer, hydrogen transfer, and coupling reactions. The present chemistry is reminiscent of that described by Smith *et al.* for 1 in molten $SbCl_3$, which is also poorly basic, at elevated temperatures.[18] In that case, the electron transfer is driven thermally by the reversible reduction of Sb(III). Thermally and photochemically driven electron-transfer reactions in poorly basic solvents should yield other unusual chemical transformations.

Acknowledgment. The authors thank the Air Force Office of Scientific Research for support, Dr. Michael Sigman of the Oak Ridge National Laboratory for giving us selected hydrocarbons, and Professor David Baker for allowing us to use his analytical HPLC.

Supplementary Material Available: Experimental details and characterization of the products (4 pages). Ordering information is given on any current masthead page.

(15) The interpretation of this fact is complicated by the fact that products are formed here which contain Cl and CH_3 (from excess $Me_3Al_2Cl_3$).

(16) Sigman, M. E.; Zingg, S. P.; Pagni, R. M.; Burns, J. H. *Tetrahedron Lett.* **1991**, 5737.

(17) Wirz, J., unpublished results.

(18) (a) Poutsma, M. L.; Dworkin, A. S.; Brown, L. L.; Benjamin, B. M.; Smith, G. P. *Tetrahedron Lett.* **1978**, 873. (b) Dworkin, A. S.; Poutsma, M. L.; Brynestad, J.; Brown, L. L.; Gilpatrick, L. O.; Smith, G. P. *J. Am. Chem. Soc.* **1979**, *101*, 5299. (c) For a related case, see also: Keszthelyi, C. P. *Electrochim. Acta* **1981**, *26*, 1261.